People's Democratic Republic of Algeria
Ministry of Higher Education and Scientific Research

Setif 1 University Ferhat Abbas
Faculty of Sciences
Department of Mathematics

جامعـــة سطيف 1 فرحـــــات عباس
كـليـــة العلـــــــوم
قســـــم الرياضيـــــــات

Doctoral Thesis

Submitted in Fulfillment of the Requirements
for the Degree of Doctor in Mathematics

Option : Analyse Numérique, EDPs et Applications

Theme:

THEORETICAL AND NUMERICAL STUDY OF SOME INTERACTION PROBLEMS IN CONTINUUM MECHANICS

Presented by

Mr. **BOUKELIA AHMED AYOUB**

Supervisor: **Dr. MOHAMED KARA**

Thesis defended on February 16th, 2026, in front of the jury composed of:

Mr.	Salim MESBAHI	Prof.	Setif 1 University Ferhat Abbas	President
Mr.	Mohamed KARA	MCA.	Setif 1 University Ferhat Abbas	Supervisor
Mr.	Hamid BENSERIDI	Prof.	Setif 1 University Ferhat Abbas	Co- supervisor
Mr.	Salah ZITOUNI	MCA.	Souk Ahras University Mohamed Cherif Messadia	Examiner
Mr.	Sofiane DEHILIS	MCA.	Oum el Bouaghi University Larbi Ben M'Hidi	Examiner
Mr.	Nasserdine KECHKAR	Prof.	Oum el Bouaghi University Larbi Ben M'Hidi	Examiner
Mr.	Nadhir Chougui	MCA.	Setif 1 University Ferhat Abbas	Guest

2026

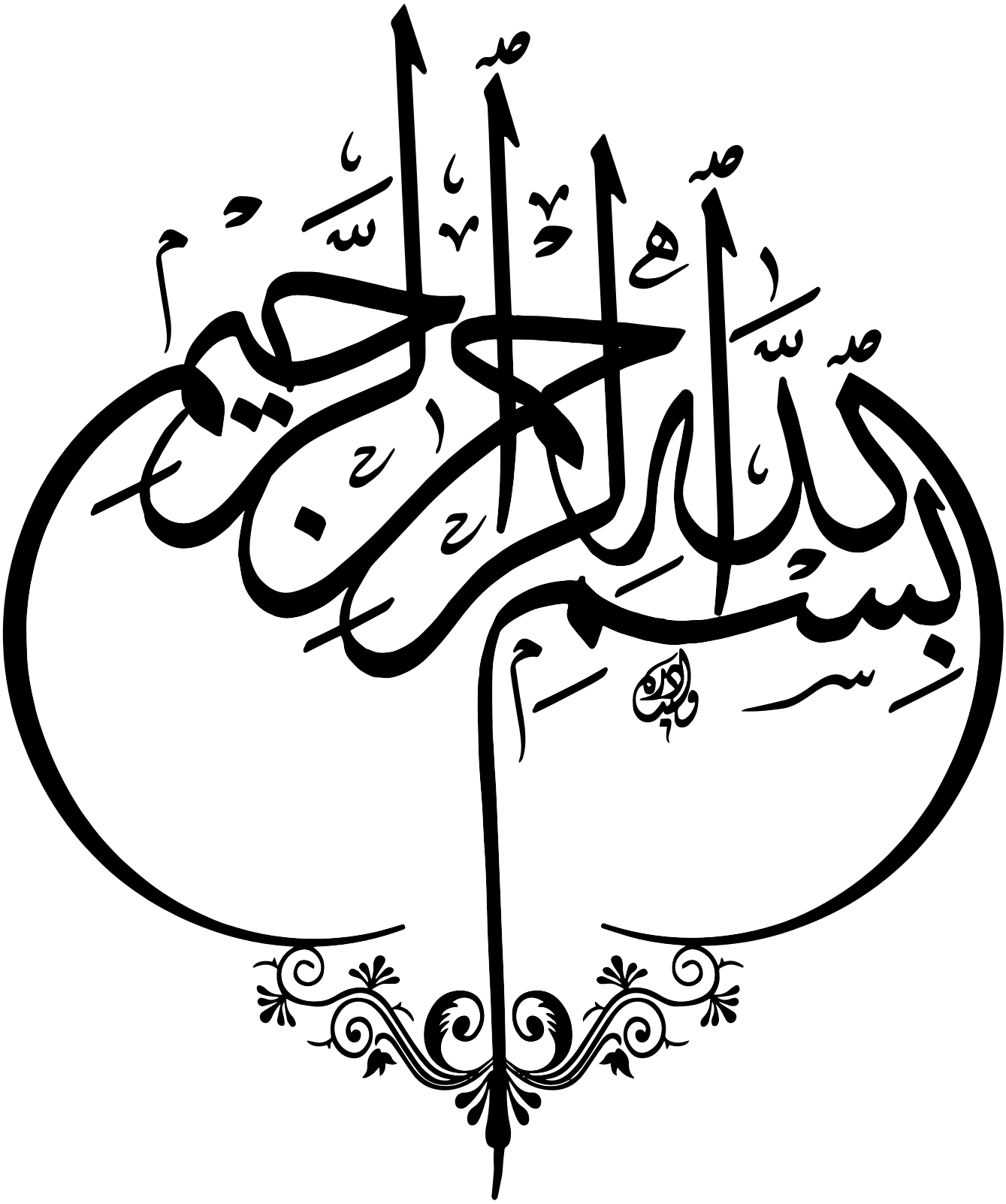
بسم الله الرحمن الرحيم

I dedicate this work to my **parents**, whose guidance and unwavering belief in me have been a constant source of inspiration and strength. Their values and lessons have shaped my journey in ways for which I will be forever grateful.

To my **wife**, whose patience, support, and unconditional love have been my greatest source of comfort and motivation. Her presence has given me balance, courage, and the determination to move forward.

To my **sister** and my **brothers**, I owe my deepest thanks for their unconditional love, encouragement, and support, which have carried me through every challenge and triumph. Their presence in my life has been a true blessing in moments of both difficulty and joy.

Finally, I extend my heartfelt gratitude to my dear **friends** and **colleagues**, whose constant encouragement, understanding, and companionship have provided me with the resilience to pursue this path. Their invaluable friendship and unwavering belief in me have been a true pillar of strength throughout this remarkable journey.

Acknowlegement

All praise is due to Allah, to whom belongs all gratitude and thanks. We seek His help in times of ease and hardship and place our trust in Him in all matters. May peace and blessings be upon the best of creation, our beloved Prophet Muhammad, and upon his family and companions.

I would like first and foremost to express my profound gratitude to my supervisor, Doctor **Mohamed Kara**, for his exceptional guidance, continuous support, and insightful advice. His scientific rigor, generosity with his time, and constant encouragement have been invaluable throughout the preparation of this thesis. Working under his supervision has been a privilege and an inspiring experience that has deeply shaped my academic path.

I wish also to extend my sincere appreciation to Professor **Nasserdine Kechkar**, who provided me with valuable assistance, advice, and encouragement. His generosity, open-mindedness, and readiness to help deserve my utmost respect and gratitude. My thanks are likewise addressed to my co-supervisor, Professor **Hamid Benseridi**, for his involvement in the supervision of this work and for his contribution to the academic framework of this research.

I also gratefully acknowledge the support of the directors of the laboratory of Applied Mathematics (LaMA), Professor **Ahmed Bendjeddou** and Doctor **Abdelbaki Merouani**, whose guidance and valuable advices have been of great help during the course of my doctoral studies.

I would like to thank Professor **Salim Mesbahi**, who is responsible for the doctoral cycle, for his support, for ensuring the smooth progression of this academic journey, and for kindly accepting to serve as the president of the jury for my thesis defense. I would also like to express my sincere gratitude to the members of the jury, Professor **Salah Zitouni**, Doctor **Sofiane Dehilis** and Doctor **Nadhir Chougui**, for kindly accepting my invitation to participate in the defense of this thesis.

Finally, I would like to thank all my professors, each by his name, for every piece of advice, and guidance they have generously given me throughout my academic journey.

Contents

List of Figures

List of Tables

Notations

Symbol	**Meaning**
Ω_s, Ω_f	Structure and fluid domains of $\mathbb{R}^d$ $(d = 2, 3)$, respectively.
Ω_T	$= (0, T) \times \Omega$ with $T > 0$ a real number.
Γ_s, Γ_f	Boundaries of Ω_s and Ω_f, respectively.
Γ_s^D, Γ_f^D	Parts of Γ_s, Γ_f where Dirichlet conditions are applied.
Γ_s^N, Γ_f^N	Parts of Γ_s, Γ_f where Neumann conditions are applied.
Σ	Interface between the two domains Ω_f and Ω_s.
$mes(\Omega)$	Lebesgue measure of the domain Ω.
$mes(\Gamma)$	Lebesgue surface measure of the boundary Γ.
ρ	Density.
μ_s, λ	Lamé coefficients.
μ_f	Fluid viscosity.
$\boldsymbol{\sigma}_s, \boldsymbol{\sigma}_f$	Elasticity and fluid stress tensors, respectively.
$\boldsymbol{\varepsilon}, \boldsymbol{d}$	Elastic and Fluid strain tensors, respectively.
$D(\Omega)$	Space of infinitely differentiable functions in Ω with compact support.
$D'(\Omega)$	Topological dual of $D(\Omega)$.
$\mathscr{D}(\Omega)$	Space of divergence-free functions in $D(\Omega)$.
$\mathscr{D}(\Omega_T)$	Space of divergence-free functions in $D(\Omega^T)$.
$tr(\cdot)$	Trace of a matrix operator.
$L^p(\Omega)$	Lebesgue space for $1 \leq p \leq \infty$.
$W^{m,p}(\Omega),\ H^m(\Omega)$	Sobolev spaces for $1 \leq p \leq \infty$, $m \in \mathbb{Z}$.
$H_{\mathscr{D}}(\Omega)$	Discrete finite volume space.
$\mathscr{D}$	Finite Volume Admissible mesh.
$\mathscr{M}$	A finite sequence of convex subsets of Ω.
$\mathscr{E}$	The set of control volumes edges.
$\mathscr{P}$	The set of centre points of finite volume cells.

Symbol	**Meaning**
∇	Gradient operator.
$\nabla\cdot$ or $div(\cdot)$	Divergence operator.
Δ	Laplacian operator.
Δ_K	Discrete Delta operator.
∇_K	Discrete Gradient operator.
div_K	Discrete Divergence operator.
δ_a	Dirac distribution at point a.
$\hookrightarrow$	Continuous embedding.
$\hookrightarrow_c$	Compact continuous embedding.
$A : B$	Hadamard (element-wise) product of matrices A and B.
a.e.	Almost everywhere.
i.e.	That is.
e.g.	For example.

Introduction

The interaction between fluids and solids is a topic that arises naturally in many areas of science and engineering. One can think of examples as diverse as bridges and tall buildings subjected to wind, aircraft wings vibrating under aerodynamic forces, or blood circulating in arteries and deforming their walls. In all of these cases, the underlying mathematical model consists of coupling the equations of fluid mechanics with those of elasticity through suitable interface conditions. What makes these problems particularly challenging is not only the different physical nature of the two systems, but also the fact that they are linked through a moving boundary where time scales and regularity properties do not match in a simple way. Classical references such as Temam's work on the Navier–Stokes equations [87] and Ciarlet's treatise on elasticity [30] provide the mathematical foundation for each subsystem in isolation, but the coupling of both is still the subject of active research.

Among the different application domains, cardiovascular mechanics has been a major driving force for the development of fluid–structure interaction (FSI) models. Blood flow is inherently pulsatile, vessel walls are heterogeneous and anisotropic, and geometries are highly patient-specific. These features demand accurate but also efficient models, since simulations are expected to be predictive and robust enough to be used in clinical or industrial practice. The work of Quarteroni, Formaggia, and collaborators [40, 78, 79] has played a central role in establishing both the mathematical and computational tools needed to deal with these situations.

The mathematical aspect of FSI has advanced significantly, focusing on theoretical foundations. Classical FSI formulations typically impose standard interface conditions, such as no-slip velocity continuity and stress balance. Rigorous studies have established the existence of weak solutions for incompressible, viscous flows coupled with deformable structures [13,72,93], as well as local existence of strong solutions for nonlinear FSI systems [54, 55, 69]. These contributions provide a solid theoretical framework that supports both the existence and uniqueness of solutions for a wide range of FSI configurations [18].

From the computational point of view, the way the fluid and the structure exchange

information across the interface is critical. The classical approach is to impose continuity of velocity and balance of stresses as in most of the literature [13,16–18]. While physically natural, this approach is not always sufficient to guarantee numerical stability, especially in the case of loosely coupled algorithms. A phenomenon known as the *added-mass effect* illustrates this difficulty: the inertia of the surrounding fluid may destabilize the structural response if not treated carefully. This issue has been extensively studied in the literature, and it remains a central concern in the design of efficient coupling strategies [25, 38].

The study of interaction problems between different physical media has its roots in classical continuum mechanics, where coupling across an interface was originally modeled by enforcing perfect transmission conditions—namely, continuity of velocity or displacement and balance of normal stresses [13, 16–18]. These classical laws were sufficient for many idealized configurations, but as applications became more complex—particularly in porous media, multiphysics coupling, and imperfect contact phenomena—it became clear that more flexible interface descriptions were needed.

A decisive development occurred with the introduction of jump embedded boundary conditions within fictitious domain frameworks by Angot in [3], where discontinuities in primary variables were incorporated in a mathematically consistent way for Stokes/Brinkman coupling problems. This idea was further formalized in [4], where generalized, matrix-valued interface operators were introduced and the well-posedness of the coupled system was rigorously established. More recently, the framework was extended to elasticity systems through a sharp fictitious domain approach by Kara in [50], showing that operator-based jump conditions provide a unified and robust methodology for a broad class of interaction problems.

Today, these generalized interface laws constitute a powerful alternative to classical transmission conditions, offering enhanced modeling capabilities together with improved analytical and numerical stability properties.

On the discretization side, finite element methods have been the tool of choice in most of the literature. Nevertheless, finite volume methods (FVM) offer important advantages, especially for problems where local conservation is crucial. Their flux-based formulation makes them particularly suitable for incompressible flows and for heterogeneous media where sharp transitions occur. The framework introduced by Eymard, Gallouët, and Herbin [36] provides a solid mathematical basis for finite volume schemes on admissible meshes, and this perspective motivates part of the present work.

In summary, the motivation for this thesis arises from the need to combine a rigorous mathematical analysis of generalized interface conditions within the framework of the fictitious domain approach, together with numerical methods designed to ensure conservation and stability. By integrating theoretical analysis and numerical discretization in the finite

volume context, we aim to advance the development of robust and reliable methodologies for coupled fluid–structure problems. This fictitious domain strategy enables the treatment of both fluid and solid subdomains within a single computational domain, thereby simplifying the management of complex interface geometries while preserving accuracy and physical consistency.

The numerical and analytical literature on fluid–structure interaction (FSI) has developed along several complementary directions, driven both by mathematical questions (well-posedness, stability, error estimates) and by practical needs in engineering and biomedical applications. From a modeling and analysis viewpoint, the Navier–Stokes equations for viscous incompressible fluids and the linear elasticity equations for solids are classical; however, their coupling at a moving interface creates subtle mathematical issues that do not occur when the two systems are considered in isolation. In particular, the incompressibility constraint and the disparity of physical time scales can introduce strong coupling effects that must be accounted for in both continuous analysis and discrete schemes [25].

Algorithmically, two broad classes of methods dominate modern FSI practice: monolithic solvers, which discretize and solve the coupled fluid–structure system simultaneously, and partitioned (or staggered) schemes, which reuse separate fluid and structure solvers and exchange interface data at each time step. Partitioned schemes offer software modularity and lower implementation cost, but they can suffer from robustness and stability problems in the presence of the so-called added-mass effect, especially when a light structure is coupled with an incompressible fluid. This observation motivated a long stream of work that analyzes the added-mass phenomenon and proposes remedies—implicit coupling, sub-iterations, optimized transmission conditions (Robin/impedance), and preconditioners tuned to the FSI spectrum [9, 10, 25].

Another major strand of research focuses on interface modeling itself. Beyond the classical kinematic continuity (no slip) and equality of tractions, more general interface laws have been proposed to represent realistic physical layers, imperfect contact, or numerical stabilization. Impedance or generalized Robin conditions—often motivated by reduced models or by domain decomposition theory—have proved effective both as a modeling tool (to represent interfacial stiffness and damping) and as a numerical device (to stabilize partitioned schemes and to accelerate monolithic preconditioners). Foundational contributions in this direction have shown how suitable choices of Robin parameters can dramatically improve both stability and accuracy [42, 75].

The choice of spatial discretization is also crucial. Finite element methods have long been the standard in FSI because of their flexibility for complex geometries and high-order approximations; nevertheless, finite volume (FV) approaches remain attractive in

many contexts due to their exact local conservation properties and natural flux-balancing formulations. Recent works have explored both Eulerian fully coupled FV formulations and hybrid approaches that combine FV for fluids with stiffness solvers for solids, while comparative studies report trade-offs between conservation, stability, and ease of handling moving boundaries. The finite volume literature also supplies a rigorous framework of admissible meshes and discrete operators that is well suited to the conservative treatment of interface fluxes [16, 64, 67].

Immersed and unfitted methods (immersed boundary, fictitious domain, immersed finite element, cut-cell and related techniques) offer a different strategy: they avoid body-fitted remeshing by embedding the structure in a fixed background mesh and enforcing interface conditions by penalization, regularized delta forces, or Lagrange multipliers. These methods simplify mesh management for large structural deformations, but they raise their own analysis and implementation challenges—consistency of force spreading, conditioning of the coupled linear systems, and the precise enforcement of interface balance laws. The diverse families of immersed methods have been reviewed extensively and remain an active research area [46].

Despite these advances, several persistent challenges remain. On the theoretical side, proving well-posedness and deriving a priori energy estimates for FSI systems with generalized interface laws (matrix-valued impedance, spring–dashpot layers, etc.) requires carefully designed function spaces and coercivity arguments that capture the interplay between bulk operators and boundary/interface terms. On the numerical side, designing discretizations that (i) are consistent with the generalized continuous interface model, (ii) preserve discrete energy balances that mirror continuous stability, and (iii) remain efficient for large three-dimensional problems is still nontrivial. Moreover, the simultaneous demands of local conservation (important for incompressible flow), accurate traction transfer across nonconforming meshes, and robustness with respect to physical parameters (density ratios, stiffness contrasts, Reynolds number) create conflicting design objectives that must be balanced in any practical scheme [77].

From a computational perspective, large-scale FSI simulations confront additional issues: the added-mass effect imposes tight coupling or costly sub-iterations unless impedance-based stabilization or fully implicit coupling is used; moving and deforming geometries motivate either expensive mesh updates or the adoption of unfitted/immersed approaches with attendant numerical subtleties; and flow regimes with high Reynolds numbers or turbulence demand stabilization techniques that interact nontrivially with structure coupling and interface conditions. These challenges motivate continued research on theory-informed discretizations, parameter-robust transmission conditions, and solver technology (block preconditioners, optimized Schwarz/Robin methods) tailored to the coupled spec-

trum [9, 10, 77].

In this context, there is a clear niche for a thesis that combines rigorous analysis of generalized interface conditions (including elastic–elastic variants and matrix-valued Robin laws) with finite volume discretizations designed to respect conservation and discrete energy estimates. The remainder of this work develops this program: we formulate continuous FSI models with abstract impedance operators, prove existence and energy stability results under appropriate hypotheses, design cell-centered FV schemes on admissible meshes that approximate the interface terms consistently, and validate the approach through numerical experiments that probe the penalized limits, interface parameter sensitivity, and robustness across mesh families.

The purpose of this thesis is to advance both the theoretical and numerical understanding of problems in which an elastic solid interacts with a viscous incompressible fluid through generalized interface conditions. The study is motivated by the observation that classical coupling laws, although physically natural, are not always sufficient to guarantee stability or to capture the richness of real interface phenomena. Introducing generalized, matrix-valued conditions offers a more flexible description, but it also raises new questions concerning analysis and discretization. The thesis is organized around three main objectives.

The first objective is of theoretical nature. We aim to provide a rigorous functional framework for elastic–elastic and fluid–structure interaction problems with generalized interface conditions. This includes the formulation of appropriate weak problems, the identification of the natural energy spaces, and the derivation of existence and stability results. In particular, the goal is to understand how the additional interface terms modify the balance laws and what conditions are needed to ensure well-posedness.

The second objective is numerical. The work develops finite volume schemes that are consistent with the continuous models while retaining the essential features of local conservation and discrete stability. The construction of the discrete operators must account for the presence of the interface, and the schemes are designed on admissible meshes so that the discrete analogues of the continuous estimates remain valid. An important point is to show that the penalized or regularized versions of the problem converge to the original formulation as the penalization parameter vanishes.

The third objective is to validate the theoretical and numerical results through computational experiments. The simulations are used not only to confirm convergence and stability but also to explore the influence of the interface parameters on the coupled dynamics. By comparing the numerical outcomes with the theoretical predictions, we can assess the robustness of the proposed framework and highlight its potential advantages over more classical formulations.

Taken together, these objectives define a program that combines rigorous mathematical analysis with the construction and testing of practical numerical schemes. The thesis therefore seeks to make a contribution on two complementary levels: clarifying the role of generalized interface conditions from the analytical point of view, and providing finite volume discretizations that make these models accessible to computation.

The methodology adopted in this thesis combines analytical techniques from functional analysis with numerical strategies based on the finite volume method. The guiding principle is to develop a framework where theoretical results and computational schemes support and complement each other.

On the analytical side, the work relies on a number of well-established tools. Sobolev spaces provide the natural functional setting, and compactness arguments such as the Aubin–Lions lemma are essential to deal with nonlinear terms and time-dependent problems [87]. Trace theorems and inequalities like those of Poincaré and Korn play a central role in deriving energy estimates and in handling the coupling across the interface [30]. These techniques allow us to prove existence and stability of weak solutions, even when generalized interface conditions are introduced into the model.

On the numerical side, the approach is centered on cell-centered finite volume schemes constructed on admissible meshes. This choice ensures local conservation, which is particularly important for incompressible flow. The construction of discrete operators—gradient, divergence, and Laplacian—follows the systematic framework developed by Eymard, Gallouët, and Herbin, which provides both consistency and convergence guarantees [36]. Particular care is devoted to the discretization of the interface terms, since they represent the novelty of the model and must reflect the continuous balance laws as closely as possible.

A further methodological ingredient is the use of penalization strategies. Instead of imposing the generalized interface conditions in their exact form from the outset, the problem is first approximated by penalized formulations. It is then shown that solutions of these approximate problems converge to those of the original formulation as the penalization parameter vanishes. This approach simplifies implementation and provides a natural bridge between theory and computation, a strategy also adopted in earlier works on interface problems [42, 75].

In summary, the methodology rests on a continuous dialogue between analysis and computation. The analytical framework guides the design of discrete schemes, ensuring stability and conservation properties at the numerical level. In return, computational experiments confirm the theoretical predictions and help explore the influence of the interface parameters on the dynamics of the coupled system. The contributions of this thesis can be viewed from both the theoretical and the numerical perspective. They are closely connected: the analytical results motivate the design of the numerical schemes,

and the computational experiments in turn validate the theoretical findings.

From the theoretical point of view, the work develops a framework for elastic–elastic and fluid–structure interaction problems in which the coupling is expressed through generalized interface conditions. Unlike the standard case, where only velocity continuity and stress balance are enforced, here the interface laws include additional terms that can be interpreted as impedance, stiffness, or damping effects. These terms are represented by positive definite operators, and they modify the natural energy balance of the system. The thesis provides weak formulations for these problems, establishes existence results, and derives stability estimates that highlight the role of the interface parameters. In this way, the analysis clarifies under what conditions the generalized coupling is mathematically well posed and energetically consistent.

On the numerical side, the thesis introduces finite volume schemes tailored to these generalized models. The discretization is carried out on admissible meshes and follows the systematic construction of discrete operators described by Eymard, Gallouët, and Herbin [36]. A particular emphasis is placed on the interface terms, which are approximated in a conservative way so that the discrete scheme mirrors the energy estimates of the continuous problem. In addition, penalized formulations are employed as a practical tool to enforce the generalized interface laws, and convergence of the penalized solutions to the original model is demonstrated. This approach provides both an effective numerical technique and a bridge between theory and computation.

Finally, the thesis includes a set of numerical experiments designed to test the proposed schemes. These simulations illustrate the convergence properties of the finite volume discretization, confirm the stability predicted by the analysis, and provide insight into the influence of the interface parameters. In particular, the results show how the choice of the impedance terms affects the dynamic response of the coupled system, an aspect that is relevant both from the mathematical and from the physical point of view.

In summary, the thesis makes contributions on three levels: (i) it establishes well-posedness for elastic–elastic and fluid–structure interaction problems with generalized interface laws, (ii) it develops finite volume schemes that are consistent, conservative, and stable for these problems, and (iii) it validates the framework through computational experiments that connect theory with practice. The manuscript is organized in four main chapters, each of which builds on the previous one and contributes to the overall objective of combining rigorous analysis with practical discretization techniques.

The first chapter recalls the mathematical background needed for the work. It introduces the main functional spaces, compactness results, and inequalities that are repeatedly used in the analysis, together with the basic ingredients of the finite volume method. The aim of this chapter is not to present new results, but to establish a consistent framework

and notation that will be employed throughout the thesis.

The second chapter is devoted to the physical models that form the basis of the study. It reviews the equations of linear elasticity and the incompressible Navier–Stokes system, with particular attention to their variational formulations and boundary conditions. This chapter also highlights the mathematical similarities and differences between the two models, and sets the stage for their coupling.

The third chapter focuses on the interaction between two elastic bodies. It introduces generalized interface conditions of the spring–dashpot type, establishes well-posedness results, and analyzes penalized formulations. The finite volume discretization is then constructed, and numerical tests are presented to illustrate the convergence of the scheme and the role of the interface parameters.

The fourth and final chapter extends the analysis to the fluid–structure interaction problem. The model couples the Navier–Stokes equations with elasticity through generalized interface laws expressed in terms of positive definite operators where a weak formulation is derived, and existence and uniqueness are discussed.

The thesis concludes with a short summary of the main results and a discussion of possible extensions. In particular, attention is drawn to future work on more complex interface laws, nonlinear structures, and large-scale three-dimensional simulations.

Chapter 1

Functional Analysis and Elementary Concepts

1.1 Functional Analysis

1.1.1 Functional Spaces

Let Ω be an open set of $\mathbb{R}^d$ ($d = 2$ or 3 in application) equipped with the Lebesgue measure. Let us define some essential functional spaces.

Lebesgue spaces constitute a cornerstone in modern mathematical analysis, exerting a profound influence on diverse fields such as functional analysis, measure theory, integration, and approximation theory. They establish a comprehensive framework for investigating the integrability and qualitative properties of measurable functions. In particular, the notions of integration and convergence developed within the setting of L^p spaces admit natural generalizations that play a decisive role in numerous mathematical contexts.

For any $1 \leq p < \infty$, the Lebesgue space $L^p(\Omega, \mu)$ is defined as the collection of all measurable functions $g : \Omega \to \mathbb{R}$ for which the p-th power of the absolute value is integrable with respect to the measure μ. These spaces provide fundamental tools for analyzing convergence, continuity, and related properties of functions, and they serve as indispensable instruments in harmonic analysis, the theory of partial differential equations, and probability theory, among many other areas.

Formally, the application

$$g \mapsto \|g\|_{\mathscr{L}^p(\Omega)} = \left(\int_\Omega |u(x)|^p \, dx \right)^{1/p},$$

defines a semi-norm on the space $\mathscr{L}^p(\Omega,\mu)$, since distinct functions may admit the same value whenever they coincide almost everywhere. More precisely, one has

$$\|g\|_{\mathscr{L}^p(\Omega)} = 0 \quad \Rightarrow \quad g = 0 \ \text{ a.e. on } \Omega.$$

Accordingly, for two measurable functions $f, g : \Omega \to \mathbb{R}$, we write $f \sim g$ if $f(x) = g(x)$ for μ-almost every $x \in \Omega$. It is clear that $\sim$ defines an equivalence relation on the class of measurable functions. The quotient space of $\mathscr{L}^p(\Omega,\mu)$ with respect to this relation is precisely the Lebesgue space $L^p(\Omega,\mu)$.

Definition 1.1 (Lebesgue spaces L^p)**.** *For any $1 \le p < \infty$ the space of functions p-th power absolutely Lebesgue integrable $L^p(\Omega)$, i.e.:*

$$L^p(\Omega) = \left\{ u : \Omega \to \mathbb{R} \text{ measurable such that } \int_\Omega |u(x)|^p \, dx < \infty \right\}. \tag{1.1}$$

For $p = \infty$ the Lebesgue space $L^\infty(\Omega)$ of essentially bounded functions is defined by

$$L^\infty(\Omega) = \left\{ u : \Omega \to \mathbb{R} \text{ measurable such that } ess\sup_{x\in\Omega} |u(x)| < \infty \right\}. \tag{1.2}$$

The spaces $L^p(\Omega)$ and $L^\infty(\Omega)$ are equipped, respectively, with the norms

$$\|u\|_{L^p(\Omega)} = \left(\int_\Omega |u(x)|^p \, dx \right)^{1/p}, \qquad \text{for all } 1 \le p < \infty, \tag{1.3}$$

$$\|u\|_{L^\infty(\Omega)} = ess \sup_{x\in\Omega} |u(x)|, \qquad \text{for } p = \infty. \tag{1.4}$$

For $0 < q < 1$, the space $L^q(\Omega,\mu)$ is defined by (1.1), and for $f \in L^q(\Omega,\mu)$, we define

$$\|f\|_{L^q} = \left(\int_\Omega |f|^q \, d\mu \right)^{1/q}.$$

The mapping $\|\cdot\|_{L^q}$ is called a quasi-norm.

Proposition 1.1.

- *For $1 \le p \le \infty$, $\left(L^p(\Omega), \|\cdot\|_{L^p(\Omega)}\right)$ are Banach spaces.*
- *For $p = 2$, we denote the norm of $L^2(\Omega)$ by $\|\cdot\|_{0,\Omega} := \|\cdot\|_{L^2(\Omega)}$, and the space $L^p(\Omega)$ equipped with the inner product $(u,v)_{0,\Omega} = \int_\Omega u(x)v(x)\,dx$ is a Hilbert space.*
- *For $0 < q < 1$, $L^q(\Omega)$ is not a normed space, not locally convex and is called a quasi-Banach space.*

Definition 1.2 (Zero-mean Lebesgue spaces L_0^p)**.** *For $1 \leq p < \infty$, we define the subspace of $L^p(\Omega)$ consisting of functions with zero mean value over Ω:*

$$L_0^p(\Omega) = \left\{ u \in L^p(\Omega) \ : \ \int_\Omega u(x)\, dx = 0 \right\}.$$

Remark 1.1.

- *$L_0^p(\Omega)$ is a closed subspace of $L^p(\Omega)$.*
- *The condition $\int_\Omega u(x)\, dx = 0$ implies that the average value of u on Ω vanishes.*
- *For $p = 2$, $L_0^2(\Omega)$ is a Hilbert subspace of $L^2(\Omega)$ equipped with the same inner product*

$$(u, v)_{0,\Omega} = \int_\Omega u(x)v(x)\, dx.$$

- *This space often arises in problems with Neumann boundary conditions or in Stokes and Navier-Stokes problem, where solutions (for example the pressure in fluid flows) are determined up to an additive constant. Restricting to $L_0^p(\Omega)$ ensures uniqueness.*

Definition 1.3 (Sobolev spaces $W^{m,p}$)**.** *Let m be a non-negative integer and let $1 \leq p \leq \infty$). The space $W^{m,p}(\Omega)$ is the space of $L^p(\Omega)$-functions with derivatives of order less than or equal to m also in $L^p(\Omega)$, called Sobolev space. i.e.:*

$$W^{m,p}(\Omega) = \{u \in L^p(\Omega) \text{ such that } D^\alpha u \in L^p(\Omega), [\alpha] \leq m\} \tag{1.5}$$

where $\alpha = (\alpha_1, \ldots, \alpha_d)$, $[\alpha] = \alpha_1 + \ldots + \alpha_d$ and $D^\alpha = \dfrac{\partial^{[\alpha]}}{\partial^{\alpha_1} \ldots \partial^{\alpha_d}}$.
For $p = 2$, the Sobolev space is denoted by $H^m(\Omega) := W^{m,2}(\Omega)$.

Proposition 1.2.

- *The spaces $W^{m,p}(\Omega)$ equipped with the usual norm*

$$\|u\|_{m,p,\Omega} = \left(\sum_{[\alpha] \leq m} \|D^\alpha u\|_{p,\Omega}^p \right)^{1/p},$$

  are Banach spaces.

- *For $p = 2$, the space $H^m(\Omega)$ equipped with the usual inner product*

$$(u, v)_{m,\Omega} := \sum_{[\alpha] \leq m} (D^\alpha u, D^\alpha u)_{0,\Omega},$$

is a Hilbert space.

Let $D(\Omega)$ (or $D(\bar{\Omega})$) be the space of C^∞ functions with compact support contained in Ω (or $\bar{\Omega}$). We define the closure of $D(\Omega)$ in $W^{m,p}(\Omega)$

Definition 1.4 (The space $W_0^{m,p}$)**.** *Let m be a non-negative integer. We denote by $W_0^{m,p}(\Omega)$ (resp. H_0^m) the closure of $D(\Omega)$ in $W^{m,p}(\Omega)$ (resp. H^m), i.e.:*

$$\overline{D(\Omega)}^{W^{m,p}} = W_0^{m,p}(\Omega).$$

Remark 1.2.

1. *If $m = 0$, and $1 \leq p < \infty$ then $W^{0,p}(\Omega) = L^p(\Omega)$.*
2. *Generally, $W_0^{m,p}(\Omega) \neq W^{m,p}(\Omega)$.*
3. *If $\Omega = \mathbb{R}^d$, then $W_0^{m,p}(\mathbb{R}^d) = W^{m,p}(\mathbb{R}^d)$.*

We shall often be concerned with d-dimentional vector functions with components in one of these spaces. We shall use the notation

$$\boldsymbol{X(\Omega)} = (X(\Omega))^d, \tag{1.6}$$

where X play the role of L^p (with $1 \leq p \leq \infty$), D, $W^{m,p}$ or H^m, equipped with the usual product norm or an equivalent norm (except $D(\Omega)$ and $D(\bar{\Omega})$ which are not normed spaces).

These spaces will later be the natural settings for solutions of partial differential equations (Stokes, Navier–Stokes, elasticity). The Sobolev embeddings and inequalities ensure compactness and stability properties needed in variational formulations and numerical schemes.

1.1.2 Spaces of Banach-valued functions

When we study functional analysis, it is often natural to move beyond real- or complex-valued functions to functions that take values in a Banach space X. These are called *Banach-valued functions* [26], and they arise in areas such as partial differential equations, numerical analysis, stochastic processes, and control theory.

A typical framework is to consider a measure space $(\Omega, \mathscr{F}, \mu)$ where Ω is the underlying set, $\mathscr{F}$ is a σ-algebra and a measure μ, and define spaces of X-valued measurable functions.

The most important families are the *Bochner spaces* $L^p(\Omega; X)$, where $1 \leq p \leq \infty$. They consist of measurable functions $f : \Omega \to X$ such that

$$\|f\|_{L^p(\Omega;X)} = \left(\int_\Omega \|f(\omega)\|_X^p \, d\mu(\omega) \right)^{1/p} < \infty, \quad (1 \leq p < \infty),$$

and for $p = \infty$,

$$\|f\|_{L^\infty(\Omega;X)} = \operatorname*{ess\,sup}_{\omega \in \Omega} \|f(\omega)\|_X.$$

These spaces generalize classical L^p spaces and remain Banach spaces themselves. Notably:

- If X is a Hilbert space, then $L^2(\Omega; X)$ is also a Hilbert space with inner product

$$\langle f, g \rangle = \int_\Omega \langle f(\omega), g(\omega) \rangle_X \, d\mu(\omega).$$

- Many familiar properties of scalar L^p spaces extend to the vector-valued setting, such as Hölder's inequality and duality, although duality requires additional assumptions (e.g. reflexivity of X).

Another important class is given by *Sobolev spaces of Banach-valued functions*, denoted $W^{k,p}(\Omega; X)$, where derivatives are understood in the weak sense and values lie in X. These spaces play a central role in the analysis of PDEs with vector- or function-valued unknowns, for example in fluid-structure interaction models.

Such spaces make it possible to formulate time-dependent PDEs as abstract evolution equations in Banach spaces, for instance

$$\frac{du}{dt}(t) + Au(t) = f(t), \qquad u(t) \in X.$$

This perspective connects functional analysis, operator theory, and applied mathematics in a powerful way.

1.1.3 General properties

We present a collection of classical inequalities and embedding results. Each of these results will play a specific role: norm estimates (Young, Hölder), compactness (Rellich, Kondrachov, Aubin–Lions), PDE estimates (Poincaré, Korn), and stability arguments (Grönwall).

Proposition 1.3 (Young's Inequality [21]). *Let $n \geq 2$ and let $x_1, \ldots, x_n$ be the nonnegative real numbers. Then, for all $p_1, \ldots, p_n > 0$ such that*

$$\frac{1}{p_1} + \ldots + \frac{1}{p_n} = 1, \tag{1.7}$$

the following inequality holds

$$x_1 \ldots x_n \leq \frac{x_1^{p_1}}{p_1} + \ldots + \frac{x_n^{p_n}}{p_n}. \tag{1.8}$$

Remark 1.3. *In Young's inequality, we note that because of hypothesis (1.7) not all coefficients p_i, $i = 1, \ldots, n$ should be fixed (meaning, one can always be written depending of all the others).*

An immediate result of Young's inequality is Holder's inequality

Corollary 1 (Holder's inequality [21]). *Let Ω be an open set of $\mathbb{R}^d$, and let $p_1, \ldots, p_n > 0$ possibly infinite and let $r \in [1, \infty]$ such that*

$$\frac{1}{r} = \frac{1}{p_1} + \ldots + \frac{1}{p_n}. \tag{1.9}$$

Then, for all functions $u_i \in L^{p_i}(\Omega)$ $(i = 1, \ldots, n)$, we have

$$u_1 \times \ldots \times u_n \in L^r(\Omega).$$

Furthermore,

$$\|u_1 \times \ldots \times u_n\|_{L^r(\Omega)} \leq \|u_1\|_{L^{p_1}(\Omega)} \ldots \|u_n\|_{L^{p_n}(\Omega)}. \tag{1.10}$$

Proposition 1.4 (Minkowski's and reverse Minkowski's inequalities [21]). *Let $0 < q < 1 \leq r \leq \infty$ and Ω an open bounded set of $\mathbb{R}^d$. Then, for any nonnegative measurable functions f and g, we have*

$$f, g \in L^r(\Omega) \implies \|f + g\|_{L^r(\Omega)} \leq \|f\|_{L^r(\Omega)} + \|g\|_{L^r(\Omega)}. \tag{1.11}$$

$$f, g \in L^q(\Omega) \implies \|f + g\|_{L^q(\Omega)} \geq \|f\|_{L^q(\Omega)} + \|g\|_{L^q(\Omega)}. \tag{1.12}$$

Theorem 1.1 (Lax–Milgram [24,35]). *Let V be a real Hilbert space with norm $\|\cdot\|_V$. Let $a : V \times V \to \mathbb{R}$ be a bilinear form and $L : V \to \mathbb{R}$ a linear functional.*

Assume:

1. ***Continuity of** $a(\cdot, \cdot)$: There exists a constant $M > 0$ such that*

$$|a(u, v)| \leq M\|u\|_V\|v\|_V, \quad \forall u, v \in V$$

2. ***Coercivity:*** *There exists a constant* $\alpha > 0$ *such that*

$$a(v, v) \geq \alpha \|v\|_V^2 \quad \forall v \in V.$$

Then, for every $L \in V'$*, there exists a unique element* $u \in V$ *such that*

$$a(u, v) = L(v) \quad \forall v \in V.$$

Moreover, the solution satisfies the estimate

$$\|u\|_V \leq \frac{1}{\alpha} \|L\|_{V'}.$$

Theorem 1.2 (Rellich–Kondrachov Compactness Theorem)**.** *Let* $\Omega \subset \mathbb{R}^d$ *be a bounded open set with Lipschitz boundary, and let* $1 \leq p < d$*. Then the Sobolev space* $W^{1,p}(\Omega)$ *is compactly embedded into* $L^q(\Omega)$ *for every* q *such that*

$$1 \leq q < p^* := \frac{dp}{d-p}.$$

That is,

$$W^{1,p}(\Omega) \hookrightarrow_c L^q(\Omega), \qquad 1 \leq q < p^*.$$

Equivalently, every bounded sequence in $W^{1,p}(\Omega)$ *admits a subsequence that converges strongly in* $L^q(\Omega)$*.*

Theorem 1.3 (Rellich Theorem [74])**.** *Let* Ω *be an open bounded domain in* $\mathbb{R}^d$*,* $(d = 2, 3)$ *with continuous boundary* $\partial\Omega$*, then*

$$H^m(\Omega) \hookrightarrow_c H^{m-1}(\Omega), \quad \forall m \in \mathbb{N}^*, \tag{1.13}$$

where $\hookrightarrow_c$ *denotes the compact embedding. In particular,*

$$H^m(\Omega) \hookrightarrow_c L^2(\Omega), \quad \forall m \in \mathbb{N}^*. \tag{1.14}$$

Corollary 2 ([27])**.** *If* Ω *is a regular open bounded set of* $\mathbb{R}^d$*, then the injection of* $H^1(\Omega)$ *into* $L^2(\Omega)$ *is compact. i.e.:*
From any bounded sequence of $H^1(\Omega)$*, one can always extract a subsequence that converges in* $L^2(\Omega)$*.*

This result is essential to establish the Poincaré inequality in $H_0^1(\Omega)$ and to define the trace of a function in $H_0^1(\Omega)$.

Theorem 1.4 (Sobolev Embedding Theorem [74]). *Let Ω be an open bounded domain in $\mathbb{R}^d$, $(d = 2, 3)$ with lipschitizien boundary $\partial\Omega$, then*

$$H^m(\Omega) \hookrightarrow L^p(\Omega), \forall m \in \mathbb{N}^* \quad \text{such that } m - \frac{d}{2} \geq -\frac{d}{p}. \tag{1.15}$$

$$H^m(\Omega) \hookrightarrow \mathscr{C}(\bar{\Omega}), \quad \text{such that } m - \frac{d}{2} > 0. \tag{1.16}$$

Theorem 1.5 (Kondrasov compactness theorem [74]). *Let Ω be an open bounded domain in $\mathbb{R}^d$, $(d = 2, 3)$ with lipschitizien boundary $\partial\Omega$, then*

$$H^m(\Omega) \hookrightarrow_c L^p(\Omega), \forall m \in \mathbb{N}^* \quad \text{such that } m - \frac{d}{2} > -\frac{d}{p}. \tag{1.17}$$

Theorem 1.6 (Poincaré-Friedrichs Inequality [74]). *Let Ω be a connected open bounded domain with lipschitzien boundary. Let V be a closed subspace of $H^m(\Omega)$ such that*

$$V \cap \mathbb{P}_{m-1}(\Omega) = \{0\},$$

where $\mathbb{P}_{m-1}(\Omega) = \left\{p : \Omega \to \mathbb{R} \ : \ p(x) = \sum_{|\alpha| \leq m-1} a_\alpha x^\alpha\right\}$ is space of polynomials of total degree less than or equal to $m-1$ on Ω. Then, there exists a positive constant $C > 0$ such that

$$\|u\|_{m,\Omega} \leq C|u|_{m,\Omega}, \quad \forall u \in V, \tag{1.18}$$

where

$$|u|_{m,\Omega} := \left(\sum_{[\alpha]=m} \int_\Omega |D^\alpha u(x)|^{\,2} dx\right)^{1/2},$$

is a semi-norm in $H^m(\Omega)$.

Proposition 1.5. *The seminorm $|\cdot|_{m,\Omega}$ and the norm $\|\cdot\|_{m,\Omega}$ are equivalents in $H_0^m(\Omega)$. where*

$$|\boldsymbol{u}|_{m,\Omega} := \left(\sum_{|\alpha|=m} \int_\Omega |D^\alpha \boldsymbol{u}(x)|^2\right)^{1/2}. \tag{1.19}$$

i.e.: there exists $C_l, C_2 > 0$ such that, for all $u \in H_0^m(\Omega)$

$$C_1\|\boldsymbol{u}\|_{m,\Omega} \leq |\boldsymbol{u}|_{m,\Omega} \leq C_2\|\boldsymbol{u}\|_{m,\Omega}. \tag{1.20}$$

Lemma 1.1 (Korn's Inequality [63]). *Let Ω be an open bounded lipschitzien set of $\mathbb{R}^d$. There exists $C_K > 0$ (Korn constant) such that, for all $u \in H_0^1(\Omega)$ the following inequality*

holds

$$\|u\|_{0,\Omega} \leq C_K \|\varepsilon(u)\|_{0,\Omega}. \tag{1.21}$$

where $\varepsilon(u)$ is the strain rate tensor.

Lemma 1.2 ([23]). *Let Ω be an open bounded lipschitzien set of $\mathbb{R}^d$. For any p and q such that $1 \leq q \leq p < \infty$, there exists $c > 0$ such that $\forall u \in W^{1,n}(\Omega)$*

$$\|u\|_{L^p(\Omega)} \leq c\|u\|^{1-a}_{L^q(\Omega)} \|u\|^a_{1,n,\Omega}, \quad \text{with } a = 1 - \frac{q}{p}. \tag{1.22}$$

The often used case is for $n = 2$, $p = 4$, $q = 2$ and $a = \dfrac{1}{2}$. i.e.:

$$\|u\|_{L^4(\Omega)} \leq c\|u\|^{1/2}_{0,\Omega} \|u\|^{1/2}_{1,\Omega}. \tag{1.23}$$

Lemma 1.3 ([1] p.141). *Let Ω be an open set of $\mathbb{R}^d$. For any $v \in H^1_0(\Omega)^d$, we have*

$$\|\nabla v\|_{0,\Omega} \leq \sqrt{2}\|\varepsilon(v)\|_{0,\Omega}. \tag{1.24}$$

where $\varepsilon(v) = \dfrac{1}{2}\left(\nabla v + (\nabla v)^T\right)$ is the symmetric part of the strain tensor

Proof. [1] page 141 □

Lemma 1.4 (Korn Inequality in H^1 [1]). *Let Ω be an open $\mathscr{C}^1-$regular and bounded domain of $\mathbb{R}^d$. There exist a constant $C > 0$ such that, for every $v \in H^1(\Omega)^d$, the following inequality holds*

$$\|v\|_{1,\Omega} \leq C\left(\|v\|^2_{0,\Omega} + \|e(v)\|^2_{0,\Omega}\right)^{1/2}. \tag{1.25}$$

Let us now present the well used integral identity, divergence theorem (also known as Gauss' theorem)

Theorem 1.7 (Divergence Theorem [71], p. 35). *Let $\Omega \subset \mathbb{R}^d$ be a bounded domain with Lipschitz boundary $\partial\Omega$, and let $\mathbf{n}$ denote the outward unit normal vector to $\partial\Omega$.*

For any vector field $\boldsymbol{v} \in C^1(\overline{\Omega})^d$, we have

$$\int_\Omega \nabla \cdot \boldsymbol{v}\, dx = \int_{\partial\Omega} \boldsymbol{v} \cdot \mathbf{n}\, dS. \tag{1.26}$$

Theorem 1.8 (Crandall–Liggett [34]). *Let X be a Banach space and let $A : \mathscr{D}(A) \subset X \to 2^X$ be an m-accretive operator. Then A generates a unique strongly continuous nonlinear semigroup $\{S(t)\}_{t\geq 0}$ of contractions on $\overline{\mathscr{D}(A)} \subset X$.*

Moreover, for every $u_0 \in \overline{\mathscr{D}(A)}$, *the function* $u(t) = S(t)u_0$ *is the unique mild solution of the evolution problem*

$$\begin{cases} \dfrac{du}{dt}(t) + Au(t) \ni 0, & t > 0, \\ u(0) = u_0, \end{cases}$$

and the semigroup is given by the exponential formula

$$S(t)u_0 = \lim_{n\to\infty} \left(I + \frac{t}{n}A\right)^{-n} u_0, \quad \text{uniformly for } t \text{ in bounded intervals.}$$

Theorem 1.9 (Crandall–Liggett for ω-m-accretive operators [34])**.** *Let* X *be a Banach space and let* $A : \mathscr{D}(A) \subset X \to 2^X$ *be an* ω*-m-accretive operator, that is,* $A + \omega I$ *is m-accretive for some* $\omega \in \mathbb{R}$. *Then* A *generates a unique strongly continuous nonlinear semigroup* $\{S(t)\}_{t\geq 0}$ *on* $\overline{\mathscr{D}(A)} \subset X$ *satisfying*

$$\|S(t)u - S(t)v\|_X \leq e^{\omega t}\|u - v\|_X, \quad \forall\, u, v \in \overline{\mathscr{D}(A)},\ \forall\, t \geq 0.$$

Moreover, for every $u_0 \in \overline{\mathscr{D}(A)}$, *the function* $u(t) = S(t)u_0$ *is the unique mild solution of*

$$\begin{cases} \dfrac{du}{dt}(t) + Au(t) \ni 0, & t > 0, \\ u(0) = u_0, \end{cases}$$

and the semigroup admits the exponential representation

$$S(t)u_0 = \lim_{n\to\infty} \left(I + \frac{t}{n}A\right)^{-n} u_0, \quad \text{uniformly for } t \text{ in bounded intervals.}$$

Theorem 1.10 (Grönwall's Inequality [35, 82])**.** *Let* $y : [0, T] \to \mathbb{R}$ *be a continuous and non-negative function. Suppose there exist constants* $\beta \geq 0$ *and* $C \geq 0$, *and a non-negative, integrable function* $F \in L^1(0, T)$, *such that for all* $t \in [0, T]$,

$$y(t) \leq C + \int_0^t F(s)\, ds + \beta \int_0^t y(s)\, ds.$$

Then $y(t)$ *satisfies the estimate*

$$\boxed{y(t) \leq \left(C + \int_0^t F(s)\, ds\right) \exp(\beta t) \quad \text{for all } t \in [0, T].}$$

Lemma 1.5 (Aubin–Lions Lemma [62])**.** *Let* X, B, *and* Y *be three Banach spaces such*

that the embedding

$$X \hookrightarrow_c B \hookrightarrow Y$$

is compact from X into B, and continuous from B into Y.

Let $1 \leq p, q \leq \infty$. Then the set

$$\left\{ u \in L^p(0,T;X) \;\middle|\; \frac{\partial u}{\partial t} \in L^q(0,T;Y) \right\}$$

is relatively compact in $L^p(0,T;B)$ if:

- *$p < \infty$, or*
- *$p = \infty$ and $q > 1$.*

Proposition 1.6 (Local Lipschitz and hemicontinuity)**.** *Let V be a Banach space and let $L : V \to V'$ be a locally Lipschitz operator. Then L is hemicontinuous, i.e., for all $u, v, w \in V$, the mapping*

$$t \longmapsto \langle L(u + tv), w \rangle$$

is continuous on $\mathbb{R}$.

Theorem 1.11 (Browder–Minty [24, 83])**.** *Let X be a real reflexive Banach space and let $A : X \to X^*$ be a bounded, hemicontinuous, coercive and monotone operator. Then A is surjective.*

1.1.4 Trace Operator

The functional framework developed in the previous sections provides the continuous mathematical setting for partial differential equations arising in fluid mechanics and elasticity. In particular, Sobolev spaces allow us to define weak solutions, while inequalities such as Poincaré and Korn ensure stability and uniqueness. However, for practical computations, one must approximate these continuous operators and function spaces with discrete counterparts. In this spirit, we now turn to the finite volume method (FVM), a numerical scheme that preserves the integral conservation laws at the discrete level.

Theorem 1.12 (Trace operator [27, 61, 63, 86])**.** *Let Ω be a regular open bounded set of $\mathbb{R}^d$ with boundary $\Gamma = \partial\Omega$. The trace map γ_0 defined as*

$$\begin{array}{rccc} \gamma_0 & : & H^1(\Omega) & \to & L^2(\Gamma), \\ & & u & \mapsto & \gamma_0 u \equiv u_{|\Gamma}, \end{array} \tag{1.27}$$

is linear and continuous, i.e.:

$$\exists C > 0 \text{ such that } \forall u \in H_0^1(\Omega), \quad \|\gamma_0 u\|_{L^2(\Gamma)} \leq C\|u\|_{H^1(\Omega)}. \tag{1.28}$$

Remark 1.4.

- *Althought a function of* $H^1(\Omega)$ *is not neccesarily continuous, one can always define its trace on* Γ.
- $H_0^1(\Omega) = ker(\gamma_0)$.
- $Im(\gamma_0) = \gamma_0(H^1(\Omega)) = H^{1/2}(\Gamma)$.
- $H^{1/2}(\Gamma)$ *in dense in* $L^2(\Gamma)$.

The space $H^{1/2}(\Gamma)$ can be equipped with the norm carried from $H^1(\Gamma)$ by γ_0.

Theorem 1.13 (Extension of trace operator)**.** *Let* Ω *be a regular open bounded set of* $\mathbb{R}^d$ *and* $\Gamma = \partial\Omega$ *its boundary. For all functions* $\omega \in L^2(\Gamma)$*, there is an extension* $u \in H^1(\Omega)$ *to* ω *such that* $\gamma_0 u = u_{|\Gamma} = \omega$.

Theorem 1.14 ([44])**.** *Let* Ω *be an open* $\mathscr{C}^1-$*regular, connected and bounded set of* $\mathbb{R}^d$. *Let* L *be a linear continuous form of* $H_0^1(\Omega)^d$. *Then,* L *vanish in* V *if and only if there exists a function* $p \in L^2(\Omega)$ *such that*

$$L(\boldsymbol{v}) = \int_\Omega p\nabla \cdot \boldsymbol{v}\, dx \quad \forall \boldsymbol{v} \in H_0^1(\Omega)^d. \tag{1.29}$$

Furthermore, p *is unique up to an additive constant.*

Proof. see [44] □

1.2 Finite volume method

The finite volume method (FVM) is a numerical technique for the approximation of partial differential equations, particularly those expressing conservation laws. Its fundamental principle is to integrate the governing equations over a family of control volumes covering the computational domain, and then apply the divergence theorem in order to transform volume integrals into surface integrals. In this way, the fluxes across the boundaries of the control volumes become the essential quantities that are approximated numerically. As a consequence, the FVM ensures that conservation properties, which are crucial in fluid mechanics and elasticity problems, are preserved at the discrete level.

The discrete finite volume space $H_{\mathscr{D}}(\Omega)$ can be regarded as a discrete analogue of the Sobolev and Hilbert spaces introduced earlier. Likewise, the discrete divergence, gradient, and Laplacian operators mimic their continuous counterparts, while preserving essential conservation properties. This parallel ensures that the finite volume framework is consistent with the functional analytic setting established in Section 1.1 and provides a rigorous bridge between the continuous theory and its numerical approximation.

In what follows, we introduce the basic notions of finite volume discretization. We begin by defining admissible meshes and associated notations, before presenting the discrete operators and the main properties that will be used throughout this work.

1.2.1 Admissible meshes

Let Ω be an open bounded polytopal subset of $\mathbb{R}^d$ ($d = 2$ or 3). We consider the admissible mesh $\mathscr{D} = (\mathscr{M}, \mathscr{E}, \mathscr{P})$ in the sense of [36], that is:

- Ω is partitioned into a finite sequence of convex subsets $\mathscr{M}$ of $\mathbb{R}^d$ (polygons for $d = 2$ or polyhedrons for $d = 3$). The elements of $K \in \mathscr{M}$ are called control volumes of nonzero measure m_K. Let M be the numbert of control volumes in $\mathscr{M}$, i.e. $M = Card(\mathscr{M})$.

- Each control volume $K \in \mathscr{M}$ has the set $\mathscr{E}_K$ of edges (segments for $d = 2$ and polygons for $d = 3$) σ of size m_σ and each edge σ of K has a unit normal vector $\mathbf{n}_\sigma$ outward to K. The set of all edges is denoted $\mathscr{E} = \bigcup_{K\in\mathscr{M}} \mathscr{E}_K = \mathscr{E}_{int} \bigcup \mathscr{E}_{ext}$, where $\mathscr{E}_{int}$ include the interior edges (edges that does not coincide with $\Gamma = \partial\Omega$) and $\mathscr{E}_{ext}$ contains the exterior edges ($\sigma \in \mathscr{E} \bigcap \Gamma$).

- We refer with $\mathscr{P}$ to the set of points $(\mathbf{x}_K)_{K\in\mathscr{M}}$ satisfying the orthogonality condition. The Euclidean distance $d(\mathbf{x}_K, \sigma_K)$ is denoted $d_{K,\sigma}$.

- For any $K \in \mathscr{M}$ and $L \in \mathscr{N}_K$ ($\mathscr{N}_K$ the neighboring control volumes of K), we denote by $K|L \in \mathscr{E}_K \bigcup \mathscr{E}_L$ the common edge between K and L we then abbreviate $\mathbf{n}_{KL} := \mathbf{x}_{K,K|L}$, we also set $d_{K|L} = d_{K,K|L} + d_{L,K|L}$ the Euclidean distance $d(\mathbf{x}_K, \mathbf{x}_L)$

1.2.2 Discrete spaces and operators

In finite volume method, the functions are approximated by a piecewise functions which are constant on each control volume $K \in \mathscr{M}$, the space containing these functions is denoted by $H_{\mathscr{D}}(\Omega)$. For any function ϕ, the term $\phi_{\mathscr{D}}$ is the piecewise interpolation of ϕ

in $H_{\mathscr{D}}(\Omega)$ and ϕ_K is the constant value of $\phi_{\mathscr{D}}$ in the control volume $K \in \mathscr{M}$.

In order to determine the discrete form of the usual operators (Δ, ∇, $\nabla\cdot$) we integrate the continuous operator over a control volume $K \in \mathscr{M}$ and then using the finite difference techniques to approximate the value of the continuous operator in K by a constant value. For example, we give the discrete operators of some usual continuous operators discretized by the finite volume method.

Laplacian operator

Integrating Δu over a control volume K and applying the fact that $\Delta u = \nabla \cdot (\nabla u)$ as well as the divergence theorem, we get

$$\begin{aligned} \int_K \Delta u(x) \mathrm{d}\boldsymbol{x} &= \int_K \nabla \cdot (\nabla u(x)) \mathrm{d}\boldsymbol{x} \\ &= \int_{\partial K} \nabla u(x) \cdot \boldsymbol{n}_K(x) \mathrm{d}\gamma(\boldsymbol{x}), \end{aligned} \tag{1.30}$$

and for each face $\sigma = K|L$ of the cell K, the flux is approximated as

$$\int_\sigma \Delta \boldsymbol{u}(\boldsymbol{x}) \cdot \boldsymbol{n}_{K,\sigma}(\boldsymbol{x}) \mathrm{d}\gamma(\boldsymbol{x}) \approx |\sigma| \frac{\boldsymbol{u}_L - \boldsymbol{u}_K}{d_{K|L}}. \tag{1.31}$$

Summing the normal components of the flux across the faces of the control volume K gives $\Delta_K \boldsymbol{u}_{\mathscr{D}}$ the discretization of Laplacian $\Delta \boldsymbol{u}$ over the control volume K, that yields the following identities based on the placement of the control volume (internal cells, Dirichlet boundary cells or Neumann boundary cells)

1. **<u>Internal Cells:</u>**

   The discrete Laplace operator for the control volume K is obtained by summing the contributions from all faces $\sigma \subset \partial K$ by:

$$\Delta_K u_{\mathscr{D}} = \frac{1}{\mathrm{m}_K} \left(\sum_{L \in \mathscr{N}_K} \frac{\mathrm{m}_{K|L}}{d_{K|L}} (u_L - u_K) + \sum_{\sigma \in \mathscr{E}_K \cap \mathscr{E}_{\mathrm{ext}}} \frac{\mathrm{m}_\sigma}{d_{K,\sigma}} (0 - u_K) \right). \tag{1.32}$$

$$\int_K \Delta \boldsymbol{u}(\boldsymbol{x}) \mathrm{d}\boldsymbol{x} = \sum_{\sigma \in \mathscr{E}_K} \int_\sigma \nabla \boldsymbol{u}(\boldsymbol{x}) \cdot \boldsymbol{n}_{K,\sigma} \mathrm{d}\gamma(\boldsymbol{x}). \tag{1.33}$$

Now applying the finite difference approximation we get the discrete Laplacian operator (corresponding to the homogeneous Dirichlet boundary conditions) defined for all $K \in \mathscr{M}$ by

$$\Delta_K u_{\mathscr{D}} = \frac{1}{\mathrm{m}_K}\left(\sum_{L\in\mathscr{N}_K}\frac{\mathrm{m}_{K|L}}{d_{K|L}}\left(u_L-u_K\right)+\sum_{\sigma\in\mathscr{E}_K\cap\mathscr{E}_{\mathrm{ext}}}\frac{\mathrm{m}_\sigma}{d_{K,\sigma}}\left(0-u_K\right)\right). \tag{1.34}$$

Following the continuous framework, we define the following inner product of two elements v, w of the space $H_{\mathscr{D}}(\Omega)$:

$$\begin{aligned}[v,w]_{\mathscr{D}} &= -\int_\Omega w(\boldsymbol{x})\Delta_{\mathscr{D}}v(\boldsymbol{x})\mathrm{d}\boldsymbol{x} = -\int_\Omega v(\boldsymbol{x})\Delta_{\mathscr{D}}w(\boldsymbol{x})\mathrm{d}\boldsymbol{x}\\ &= \frac{1}{2}\sum_{K\in\mathscr{M}}\sum_{L\in\mathscr{N}_K}\frac{\mathrm{m}_{K|L}}{d_{K|L}}\left(v_L-v_K\right)\left(w_L-w_K\right)+\sum_{K\in\mathscr{M}}\sum_{\sigma\in\mathscr{E}_K\cap\mathscr{E}_{\mathrm{ext}}}\frac{\mathrm{m}_\sigma}{d_{K,\sigma}}v_K w_K.\end{aligned}$$

The corresponding norm of $w\in H_{\mathscr{D}}(\Omega)$, denoted by

$$\|w\|_{\mathscr{D}} = \left([w,w]_{\mathscr{D}}\right)^{1/2}.$$

Theorem 1.15 (Discrete $H_{\mathscr{D}}(\Omega)$ Poincaré inequality [36])**.** *Let Ω be a bounded set of $\mathbb{R}^d$, and let $\mathscr{D}=(\mathscr{M},\mathscr{E},\mathscr{P})$ be an admissible mesh in the sense defined above. Then*

$$\|w\|_{0,\Omega}\leq \mathrm{diam}(\Omega)\|w\|_{\mathscr{D}}, \forall w\in H_{\mathscr{D}}(\Omega). \tag{1.35}$$

Similarly, for $\boldsymbol{u}=\left(u^{(i)}\right)_{i=1,\dots,d}, \boldsymbol{v}=\left(v^{(i)}\right)_{i=1,\dots,d}, \boldsymbol{w}=\left(w^{(i)}\right)_{i=1,\dots,d}\in \boldsymbol{H}_{\mathscr{D}}(\Omega):=H_{\mathscr{D}}(\Omega)^d$, we define:

$$[\boldsymbol{v},\boldsymbol{w}]_{\mathscr{D}}=\sum_{i=1}^d\left[v^{(i)},w^{(i)}\right]_{\mathscr{D}},\quad \|\boldsymbol{u}\|_{\mathscr{D}}=\left(\sum_{i=1}^d\left[u^{(i)},u^{(i)}\right]_{\mathscr{D}}\right)^{1/2}.$$

Divergence operator and stabilization

Next, we aim to introduce a discrete divergence operator that approximates the continuous divergence term $\nabla\cdot(\bar{z}\overline{\boldsymbol{u}})$, where $\bar{z}$ is a scalar function from Ω to $\mathbb{R}$ (density viscosity,concentration, temperature, etc...) and $\bar{u}$ is a vector function, from Ω to $\mathbb{R}^d$ (typically a velocity).
Integrating once again over K and using the divergence theorem, we get

$$\begin{aligned}\int_K \mathrm{div}(\bar{z}\overline{\boldsymbol{u}}) &= \int_{\partial K}\bar{z}\overline{\boldsymbol{u}}\cdot\boldsymbol{n}_K\,\mathrm{d}\gamma(\boldsymbol{x})\\ &= \sum_{\sigma\in\mathscr{E}_K}\int_\sigma \bar{z}\overline{\boldsymbol{u}}\cdot\boldsymbol{n}_{K,\sigma}\mathrm{d}\gamma(\boldsymbol{x}).\end{aligned} \tag{1.36}$$

Assuming the homogeneous Dirichlet boundary condition for $\overline{\boldsymbol{u}}$, the centred finite

volume approximation of $div(\overline{z}\overline{\boldsymbol{u}})$ is therefore $\mathrm{div}^0_{\mathscr{D}}(z,\boldsymbol{u}) \in H_{\mathscr{D}}(\Omega)$, such that $\mathrm{div}^0_{\mathscr{D}}(z,\boldsymbol{u}) = \left(\mathrm{div}^0_K(z,\boldsymbol{u})\right)_{K\in\mathscr{M}}$ and for all $K \in \mathscr{M}$,

$$\mathrm{div}^0_K(z,\boldsymbol{u}) = \frac{1}{\mathrm{m}_K}\sum_{L\in\mathscr{N}_K}\frac{\mathrm{m}_{K|L}}{d_{K|L}}\boldsymbol{n}_{KL}\cdot\left(d_{L,K|L}\boldsymbol{u}_K + d_{K,K|L}\boldsymbol{u}_L\right)\frac{z_K+z_L}{2}. \tag{1.37}$$

where $z \in H_{\mathscr{D}}(\Omega)$ and $\boldsymbol{u} \in \boldsymbol{H}_{\mathscr{D}}(\Omega)$ are the desired approximations of $\bar{z}$ and $\bar{\boldsymbol{u}}$.

We highlight here that in the well-known Stokes and Navier-Stokes equations, there are two unknowns to be determined pressure p and velocity vector $\mathbf{u}$, and because of the choice of collocating the approximations of velocity and pressure fields (meaning the approximations p and $\mathbf{u}$ are made both in the center of each control volume K), defining a modified discrete divergence operator is inevitable. This operator involves a family of stabilization parameters, denoted by λ, and the pressure field p. Hence, for a velocity field $\boldsymbol{u} \in \boldsymbol{H}_{\mathscr{D}}(\Omega)$, for a pressure field $p \in H_{\mathscr{D}}(\Omega)$, for a scalar field $z \in H_{\mathscr{D}}(\Omega)$, we define the discrete divergence operator $\mathrm{div}_{\mathscr{D}}(z,\boldsymbol{u},\lambda,p) \in H_{\mathscr{D}}(\Omega)$, such that $\mathrm{div}_{\mathscr{D}}(z,\boldsymbol{u},\lambda,p) = \left(\mathrm{div}^0_K(z,\boldsymbol{u},\lambda,p)\right)_{K\in\mathscr{M}}$ and is given for all $K \in \mathscr{M}$ by

$$\mathrm{div}_K(z,\boldsymbol{u},\lambda,p) = \frac{1}{\mathrm{m}_K}\sum_{L\in\mathscr{N}_K}\Phi_{KL}(\boldsymbol{u},\lambda,p)\frac{z_K+z_L}{2},$$

with

$$\Phi_{KL}(\boldsymbol{u},\lambda,p) = \frac{\mathrm{m}_{K|L}}{d_{K|L}}\left(\mathbf{n}_{KL}\cdot\left(d_{L,K|L}\boldsymbol{u}_K + d_{K,K|L}\boldsymbol{u}_L\right) - \lambda_{K|L}\left(p_L - p_K\right)\right), \forall L \in \mathscr{N}_K, \tag{1.38}$$

where $\lambda = (\lambda_\sigma)_{\sigma\in\mathscr{E}_{\mathrm{int}}}$ is a given family of nonnegative real numbers.

However, the choice of stabilization is not unique or optimal. One can apply a global stabilization where every two touching volumes has a stabilization parameter. Another approach is to use a local stabilization (clusters), for more details see [19, 20, 28, 52] and references therein.

Convection-Advection operator

As it is known, the Navier-Stokes equations has the nonlinear term (Convection-Advection term) $(\boldsymbol{u}\cdot\nabla)\boldsymbol{u}$, and as our framework include only incompressible flows, which yields the

continuity equation (incompressibility equation)

$$\nabla \cdot \boldsymbol{u} = 0. \tag{1.39}$$

For incompressible flows, we get

$$\begin{aligned} \nabla \cdot (\boldsymbol{u} \otimes \boldsymbol{v}) &= (\boldsymbol{v} \cdot \nabla)\boldsymbol{u} + (\nabla \cdot \boldsymbol{u})\boldsymbol{v} \\ &= (\boldsymbol{v} \cdot \nabla)\boldsymbol{u}. \end{aligned} \tag{1.40}$$

For all $\boldsymbol{v} \in \boldsymbol{H}_{\mathscr{D}}(\Omega)$, the approximation $\mathrm{div}_{\mathscr{D}}(\boldsymbol{v}, \boldsymbol{u}, \lambda, p)$ of $\mathrm{div}(\overline{\boldsymbol{v}} \otimes \overline{\boldsymbol{u}})$ (in incompressible flows) is obtained by replacing in (1.38) the scalars z_K and z_L by the vectors $\boldsymbol{v}_K$ and $\boldsymbol{v}_L$, that is:

$$\mathrm{div}_K(\boldsymbol{v}, \boldsymbol{u}, \lambda, p) = \frac{1}{\mathrm{m}_K} \sum_{L \in \mathscr{N}_K} \Phi_{KL}(\boldsymbol{u}, \lambda, p) \frac{\boldsymbol{v}_K + \boldsymbol{v}_L}{2}. \tag{1.41}$$

Gradient operator

Finally, let us define a discrete gradient operator. It is fimiliar that the gradient operator is the adjoint of the non stabilized divergence operator, this implies that for any discrete field $p \in H_{\mathscr{D}}(\Omega)$, $\nabla_{\mathscr{D}} p \in \boldsymbol{H}_{\mathscr{D}}(\Omega)$ and satisfies

$$\int_\Omega \nabla_{\mathscr{D}} p(\boldsymbol{x}) \cdot \boldsymbol{v}(\boldsymbol{x}) \mathrm{d}\boldsymbol{x} = -\int_\Omega p(\boldsymbol{x}) \, \mathrm{div}^0_{\mathscr{D}}(1, \boldsymbol{v})(\boldsymbol{x}) \mathrm{d}\boldsymbol{x}, \forall \boldsymbol{v} \in H_{\mathscr{D}}(\Omega)^d.$$

This implies the following definition for $\nabla_{\mathscr{D}} p = (\nabla_K p)_K$ for all $K \in \mathscr{M}$:

$$\nabla_K p = \frac{1}{\mathrm{m}_K} \sum_{L \in \mathscr{N}_K} \frac{d_{L,K|L}}{d_{K|L}} \, \mathrm{m}_{K|L} \boldsymbol{n}_{KL} \left(p_L - p_K\right). \tag{1.42}$$

Defining p_σ as

$$p_\sigma = \begin{cases} \frac{d_{K,K|L}}{d_{K|L}} p_K + \frac{d_{L,K|L}}{d_{K|L}} p_L & , \sigma = K|L \\ p_K & , \sigma \in \mathscr{E}_e xt \bigcap \mathscr{E}_K \end{cases}, \tag{1.43}$$

and using the fact that (geometric property of polytopals)

$$\sum_{\sigma \in \mathscr{E}_K} \mathrm{m}_\sigma \boldsymbol{n}_{K,\sigma} = 0. \tag{1.44}$$

One notices that $\nabla_K p$ may also be rewritten as

$$\nabla_K p = \frac{1}{\mathrm{m}_K} \sum_{\sigma \in \mathscr{E}_K} \mathrm{m}_\sigma p_\sigma \boldsymbol{n}_{K,\sigma}. \tag{1.45}$$

Chapter 2

Fundamentals of Elasticity and Fluid Mechanics

Introduction

In the analysis of physical systems governed by partial differential equations, two paradigmatic physical media are most often encountered: elastic solids and incompressible fluids. Both types of media are captured under the scope of continuum mechanics, which assumes materials are continuously distributed within the domain of interest and ignores the distinct atomic structure of materials.

Understanding elastic solids and fluid dynamics separately is necessary before allowing for their interaction (cases that frequently occurs in real-world phenomena). For example, in many biological systems (blood vessels behave as elastic solids), the deformation of the blood vessel wall interacts dynamically with other inertial forces acting on the blood flow regarded as an incompressible fluid, see for example [12, 65, 68, 94]. Likewise, in civil engineering, soil-structure interaction [89, 90] typically results in coupled behavior between deformable solids and pore fluids. When studying this type of problem, the proper modeling of the solid domain and the fluid domain, along with their interaction, essential for ensuring accuracy and stability of numerical simulations.

This chapter is devoted to summarizing the essential concepts and governing equations associated with linear elasticity and the flows of incompressible fluids. The goal is to develop a common mathematical framework for each medium so we can refer back to it when discussing the coupled problems in later chapters. In particular, our interest is with the linear elastic model for solids and incompressible viscous flows governed by the Navier–Stokes or Stokes equations.

We begin by formulating linear elasticity, paying special attention to the definition

of stress and strain tensors, the constitutive equations, and the related boundary value problems. Next, we present the governing equations of fluid mechanics, with consideration of momentum balance, the incompressibility condition, as well as the form of the stress tensor for Newtonian fluids. Finally, we note how these two media differ both mathematically and physically, in preparation for the subsequent formulation of coupled interaction problems with solids and fluids.

2.1 Linear Elasticity

Elasticity theory describes how solid materials deform and recover under external forces. In this framework, the body is modeled as a continuous medium, where each point undergoes a small displacement in response to the applied loads. The *linear elasticity* model is valid under the assumption of small deformations and linear stress-strain behavior. This assumption is suitable for a wide range of engineering and physical applications. For readers interested in a more detailed treatment of elasticity, see e.g. [30–32, 56, 66] for detailed treatments.

2.1.1 Kinematics of Deformation

In continuum mechanics, a deformable solid body is described through its motion over time. Let $\Omega_0 \subset \mathbb{R}^d$ (with $d = 2$ or 3) be the *reference configuration* of the body, representing its shape at an initial time $t = 0$. A material point originally located at $\boldsymbol{X} \in \Omega_0$ moves to a new position $\boldsymbol{x} \in \Omega_t \subset \mathbb{R}^d$ at time $t > 0$, given by the mapping:

$$\boldsymbol{x} = \boldsymbol{\chi}(\boldsymbol{X}, t),$$

where

- $\boldsymbol{X} \in \Omega_0$ is the material (Lagrangian) coordinate,
- $\boldsymbol{x} \in \Omega_t$ is the spatial (Eulerian) coordinate in the current (deformed) configuration,
- $\boldsymbol{\chi} : \Omega_0 \times [0, T] \to \mathbb{R}^d$ is a smooth and invertible function called the *motion*.

The **displacement field** is defined as the difference between the current and reference positions:

$$\boldsymbol{u}(\boldsymbol{X}, t) = \boldsymbol{\chi}(\boldsymbol{X}, t) - \boldsymbol{X}. \tag{2.1}$$

This vector field describes the local deformation of the body. The displacement may vary in both space and time.

Deformation Gradient Tensor

To quantify local changes in length, area, and volume, we define the *deformation gradient tensor* $\boldsymbol{F}$ as:

$$\boldsymbol{F}(\boldsymbol{X}, t) = \frac{\partial \boldsymbol{\chi}}{\partial \boldsymbol{X}} = \boldsymbol{I} + \nabla_{\boldsymbol{X}} \boldsymbol{u}(\boldsymbol{X}, t), \tag{2.2}$$

where:

- $\boldsymbol{F} \in \mathbb{R}^{d \times d}$ measures the local linear transformation of vectors under the motion $\boldsymbol{\chi}$,
- $\nabla_{\boldsymbol{X}} \boldsymbol{u}$ is the gradient of the displacement with respect to the reference coordinates,
- $\boldsymbol{I}$ is the identity tensor.

The deformation gradient satisfies $\det(\boldsymbol{F}) > 0$ if the motion is locally invertible and orientation-preserving. In general, $\boldsymbol{F} = \boldsymbol{I}$ corresponds to a rigid body with no deformation.

Remark

The deformation gradient $\boldsymbol{F}$ is a fundamental quantity in nonlinear elasticity. However, in the context of small deformations, we will introduce a linearized strain tensor in the next subsection.

2.1.2 Strain Tensors and the Small Deformation Assumption

To characterize the internal deformation of a solid body, strain tensors are introduced. These tensors measure the relative displacement of nearby material points. In general (i.e., for large deformations), the appropriate strain measure is the *Green–Lagrange strain tensor*, defined by:

$$\boldsymbol{E} = \frac{1}{2} \left(\boldsymbol{F}^\top \boldsymbol{F} - \boldsymbol{I} \right), \tag{2.3}$$

where $\boldsymbol{F}$ is the deformation gradient, and $\boldsymbol{I}$ is the identity tensor.

However, in many practical problems such as those involving small displacements and small strains, we can assume that:

$$\nabla \boldsymbol{u} \ll 1 \quad \text{(i.e., the components of } \nabla \boldsymbol{u} \text{ are much less than 1)},$$

which justifies neglecting higher-order terms in the expansion of $\boldsymbol{F}^\top \boldsymbol{F}$. Under this **small deformation assumption**, the Green–Lagrange tensor reduces to its linearized form:

$$\boldsymbol{\varepsilon}(\boldsymbol{u}) = \frac{1}{2} \left(\nabla \boldsymbol{u} + (\nabla \boldsymbol{u})^\top \right),$$

known as the **infinitesimal strain tensor** or **linearized strain tensor**.

Properties of the Infinitesimal Strain Tensor

- $\boldsymbol{\varepsilon}(\boldsymbol{u})$ is symmetric: $\boldsymbol{\varepsilon}(\boldsymbol{u}) = \boldsymbol{\varepsilon}(\boldsymbol{u})^\top$.
- It vanishes for rigid body motions (translations and rotations).
- It measures local extension and shear.

This linearized strain tensor will be used throughout the rest of this work when formulating the equations of linear elasticity, as well as in numerical approximations where small deformations are assumed.

2.1.3 Stress Tensor and Hooke's Law

While strain tensors measure deformation, the internal mechanical response of a solid body is described by the **stress tensor**. Specifically, the *Cauchy stress tensor* $\boldsymbol{\sigma} \in \mathbb{R}^{d\times d}$ represents the force per unit area acting on an infinitesimal surface inside the body. For any oriented surface with unit normal vector $\boldsymbol{n}$, the force acting on the surface is given by:

$$\boldsymbol{t} = \boldsymbol{\sigma} \cdot \boldsymbol{n}, \tag{2.4}$$

where $\boldsymbol{t}$ is the traction vector.

To relate stress to strain, a **constitutive law** is required. In the context of small deformations and isotropic, homogeneous materials, the most common model is the *linear Hooke's law*, which states:

$$\boldsymbol{\sigma}(\boldsymbol{u}) = 2\mu_s\, \boldsymbol{\varepsilon}(\boldsymbol{u}) + \lambda_s\, \mathrm{tr}(\boldsymbol{\varepsilon}(\boldsymbol{u}))\, \boldsymbol{I}, \tag{2.5}$$

where:

- $\mu_s > 0$ and $\lambda_s \geq 0$ are the **Lamé coefficients** characterizing the elastic properties of the material,
- $\mathrm{tr}(\cdot)$ denotes the trace of a tensor,
- $\boldsymbol{I}$ is the identity tensor.

These coefficients are related to the more physically intuitive parameters:

$$\lambda_s = \frac{E\nu}{(1+\nu)(1-2\nu)}, \qquad \mu_s = \frac{E}{2(1+\nu)}, \tag{2.6}$$

where:

- E is the **Young's modulus**, measuring stiffness,
- ν is the **Poisson's ratio**, describing the lateral contraction under axial loading.

Properties of the Linear Elastic Law

- The stress-strain relation is linear.
- The model is valid only for small deformations.
- The tensor $\boldsymbol{\sigma}(\boldsymbol{u})$ is symmetric if no body couples or moments are present.
- Isotropy implies material response is direction-independent.

The linear elastic constitutive law, combined with the infinitesimal strain tensor, forms the core of the *linear elasticity model*, which is widely used in engineering and solid mechanics due to its simplicity and effectiveness in modeling small deformations.

2.1.4 Balance of Linear Momentum

The fundamental physical principle governing the motion or equilibrium of a solid body is the **balance of linear momentum**. In the context of linear elasticity, and under the small deformation assumption, this principle leads to the following differential equation for the displacement field.

Let $\boldsymbol{u} : \Omega_s \to \mathbb{R}^d$ denote the displacement field in the solid domain $\Omega_s \subset \mathbb{R}^d$. Then the momentum balance equation reads:

$$\rho_s \frac{\partial^2 \boldsymbol{u}}{\partial t^2} - \nabla \cdot \boldsymbol{\sigma}(\boldsymbol{u}) = \boldsymbol{f} \quad \text{in } \Omega_s, \tag{2.7}$$

where:

- ρ_s is the density of the solid material,
- $\boldsymbol{f}$ a given body-force density (e.g., gravity).
- $\boldsymbol{\sigma}(\boldsymbol{u})$ is the Cauchy stress tensor defined by Hooke's law.

In the **quasi-static** (or static) case, inertia is neglected, and the equation simplifies to:

$$-\nabla \cdot \boldsymbol{\sigma}(\boldsymbol{u}) = \boldsymbol{f} \quad \text{in } \Omega_s. \tag{2.8}$$

Boundary Conditions

To close the problem, suitable boundary conditions must be imposed on the boundary $\partial\Omega_s$. It is common to partition the boundary into two disjoint parts:

$$\partial\Omega_s = \Gamma_D^s \cup \Gamma_N^s, \quad \Gamma_D^s \cap \Gamma_N^s = \emptyset,$$

where:

- On the Dirichlet part Γ_D^s, the displacement is prescribed:

$$\boldsymbol{u} = \boldsymbol{u}_D \quad \text{on } \Gamma_D^s, \tag{2.9}$$

- On the Neumann part Γ_N^s, the traction (surface force) is prescribed:

$$\boldsymbol{\sigma}(\boldsymbol{u}) \cdot \boldsymbol{n} = \boldsymbol{t}_N \quad \text{on } \Gamma_N^s, \tag{2.10}$$

  with $\boldsymbol{n}$ the outward unit normal to the boundary, and $\boldsymbol{t}_N$ the applied traction vector.

This boundary value problem defines the linear elasticity model in either static or dynamic cases.

2.1.5 Time-discretization

For any time-step $\delta t > 0$ and any $n \in \mathbb{N}$ we set $t^n = n\delta t$ and denote by $\boldsymbol{u}^n(\boldsymbol{x})$ (or simply $\boldsymbol{u}^n$) the approximation of $\boldsymbol{u}(t^n, \boldsymbol{x})$.

We approximate the second time derivative $\dfrac{\partial^2 \boldsymbol{u}}{\partial t^2}$ by finite differences in time. Two common choices are:

1. **Centered (three-point) difference (second-order accurate).**

$$\frac{\partial^2 \boldsymbol{u}}{\partial t^2}(t_n, \boldsymbol{x}) \approx \frac{\boldsymbol{u}^{n+1} - 2\boldsymbol{u}^n + \boldsymbol{u}^{n-1}}{\delta t^2}. \tag{2.11}$$

   This formula is derived from a symmetric Taylor expansion and has a local truncation error $O(\delta t^2)$. Because it is time-centred and symmetric, it preserves the time-reversal symmetry of the continuous wave operator and, for undamped linear systems, is associated with favorable discrete energy behavior (subject to spatial discretization and mass-lumping).

2. **Backward (one-sided) multi-step difference (second-order accurate).**

$$\frac{\partial^2 \boldsymbol{u}}{\partial t^2}(t_n, \boldsymbol{x}) \approx \frac{2\boldsymbol{u}^n - 5\boldsymbol{u}^{n-1} + 4\boldsymbol{u}^{n-2} - \boldsymbol{u}^{n-3}}{\delta t^2}. \tag{2.12}$$

This is a consistent approximation with truncation error $O(\delta t^2)$. It is one-sided in time and therefore useful when future values cannot be accessed. However, unlike the centred scheme (2.11), it is not symmetric and does not inherit the discrete energy conservation properties of the centred scheme. In practice, when embedded in elastodynamics discretizations, one-sided multi-step formulas can produce spurious high-frequency responses or unphysical stress peaks unless additional numerical damping or filtering is introduced.

Remarks. The centred formula (2.11) is the standard choice in undamped transient elastodynamics when one desires second-order accuracy and favourable energy behaviour (subject to the spatial discretization and mass treatment). Its main drawback is conditional stability: an explicit implementation requires a timestep satisfying a CFL-type bound.

One-sided formulas such as (2.12) are sometimes used for their causal character or for multi-step implicit algorithms, but they break the time symmetry and may degrade the discrete energy balance; consequently they tend to amplify or misrepresent high-frequency modes unless combined with controlled numerical dissipation (e.g. filtering, upwinding in time, or algorithmic damping such as the generalized-α method).

Finite volume perspective (Jasak and Weller [49]). In the finite volume formulation for linear elasticity, the time derivative is treated in a manner consistent with the spatial flux discretization by integrating the momentum balance over each control volume. Jasak and Weller observed that the bounded backward approximation (2.13) while formally only first-order accurate in the sense of their implementation, provided enhanced robustness and boundedness on unstructured meshes and in strongly coupled problems.

$$\frac{\partial^2 \boldsymbol{u}}{\partial t^2} \approx \frac{\boldsymbol{u}^n - 2\boldsymbol{u}^{n-1} + \boldsymbol{u}^{n-2}}{\delta t^2}, \tag{2.13}$$

They observed that certain formally higher-order, time-symmetric schemes can produce unphysical stress peaks or instabilities on complex meshes; consequently they favored the more dissipative but bounded approximation (2.13) in their solver to ensure smooth convergence for large-scale transient elasticity simulations. The choice between (2.11) and (2.13) therefore depends on whether one prioritizes discrete energy fidelity (choose (2.11))

or robustness on highly unstructured/parallel computations (choose (2.13)).

2.1.6 Space-discretization

Let $\mathscr{D} = (\mathscr{M}, \mathscr{E}, \mathscr{P})$ denote an admissible mesh in the sense defined in Section 1.2 of Chapter 1. For each control volume $K \in \mathscr{M}$, the space-discretized elasticity equation can be expressed in compact form as

$$\rho \frac{\partial^2 \boldsymbol{u}_K}{\partial t^2} - \operatorname{div}_K\big(\boldsymbol{\sigma}(\boldsymbol{u})\big) = \boldsymbol{f}_K, \tag{2.14}$$

where ρ is the material density, $\boldsymbol{u}_K$ denotes the discrete displacement field, and $\boldsymbol{f}_K$ represents the external body force acting on the control volume K. The operator div_K refers to the discrete divergence operator, which is defined consistently with the discrete gradient ∇_K within the finite volume framework (see Section 1.2).

For a linear, homogeneous, and isotropic elastic material, the constitutive law (Hooke's law) relates the Cauchy stress tensor $\boldsymbol{\sigma}(\boldsymbol{u})$ to the displacement field $\boldsymbol{u}$ through

$$\boldsymbol{\sigma}(\boldsymbol{u}) = \lambda \,(\operatorname{div}_K \boldsymbol{u})\, \mathbf{I} + 2\mu\, \boldsymbol{\varepsilon}_K(\boldsymbol{u}), \tag{2.15}$$

where λ and μ are the Lamé coefficients, $\mathbf{I}$ is the identity tensor, and $\boldsymbol{\varepsilon}_K(\boldsymbol{u})$ denotes the discrete strain tensor defined by

$$\boldsymbol{\varepsilon}_K(\boldsymbol{u}) = \frac{1}{2}\Big(\nabla_K \boldsymbol{u} + (\nabla_K \boldsymbol{u})^T\Big). \tag{2.16}$$

To express the stress divergence explicitly, we substitute (2.15) into $\operatorname{div}_K(\boldsymbol{\sigma}(\boldsymbol{u}))$, yielding

$$\operatorname{div}_K\big(\boldsymbol{\sigma}(\boldsymbol{u})\big) = \lambda \operatorname{div}_K\Big((\operatorname{div}_K \boldsymbol{u})\, \mathbf{I}\Big) + \mu \operatorname{div}_K\Big(\nabla_K \boldsymbol{u} + (\nabla_K \boldsymbol{u})^T\Big). \tag{2.17}$$

Using the compatibility between the discrete gradient and divergence operators, the first term can be rewritten as $\nabla_K(\operatorname{div}_K \boldsymbol{u})$. Consequently, the discrete divergence of the stress tensor becomes

$$\operatorname{div}_K\big(\boldsymbol{\sigma}(\boldsymbol{u})\big) = \mu \operatorname{div}_K\Big(\nabla_K \boldsymbol{u} + (\nabla_K \boldsymbol{u})^T\Big) + \lambda\, \nabla_K\big(\operatorname{div}_K \boldsymbol{u}\big). \tag{2.18}$$

Substituting (2.18) into (2.14) gives the local discrete momentum equation

$$\rho \frac{\partial^2 \boldsymbol{u}_K}{\partial t^2} - \mu \operatorname{div}_K\Big(\nabla_K \boldsymbol{u} + (\nabla_K \boldsymbol{u})^T\Big) - \lambda\, \nabla_K\big(\operatorname{div}_K \boldsymbol{u}\big) = \boldsymbol{f}_K. \tag{2.19}$$

The complete stress-divergence operator involves both the symmetric gradient and volumetric strain terms. To ensure stability and matrix symmetry, Jasak and Weller [49] proposed splitting the stress divergence into an implicit Laplacian term and an explicit correction:

$$\nabla_K \cdot \boldsymbol{\sigma}(\boldsymbol{u}^{n+1}) \simeq (2\mu+\lambda)\nabla_K^2 \boldsymbol{u}^{n+1} + \Big[\nabla_K \cdot \big(\mu(\nabla_K \boldsymbol{u}^n)^T + \lambda \mathbf{I}\,(\nabla_K \cdot \boldsymbol{u}^n) - (\mu+\lambda)\nabla_K \boldsymbol{u}^n\big)\Big], \quad (2.20)$$

where the first term is treated implicitly, while the remainder is evaluated explicitly at the previous time level. This decomposition preserves diagonal dominance and significantly enhances the convergence of the iterative solver. The resulting discretized momentum equation forms a sparse, symmetric, and diagonally dominant linear system, well suited for iterative solvers such as the Incomplete Cholesky Conjugate Gradient (ICCG) method. The implicit–explicit splitting described in (2.20) yields robust convergence characteristics without the need for multigrid acceleration, as demonstrated by Jasak and Weller [49]. This finite volume formulation is therefore an efficient and accurate alternative to the classical finite element approach for large-scale structural analyses on unstructured meshes.

2.1.7 Numerical Simulation

In order to evaluate the computational performance and efficiency of the numerical FV scheme described and analyzed previously, we pick several test problems using known analytical solutions allows to calculate the convergence rates.
All computations and figure production were carried out using a selfmade Matlab program on an Intel(R) Core(TM) i5 Laptop @ 1.70GHz and 8GB of RAM.

To investigate the convergence rate, we define the relative error vector $\boldsymbol{e}_h^{(i)} = \left(\boldsymbol{e}_j^{(i)}\right)_{1,\dots,M}$ and its norm $\|\boldsymbol{e}_h\|_{\mathscr{D}}$ of approximate displacement $\boldsymbol{u}_{\mathscr{D}} = \left(\boldsymbol{u}_{\mathscr{D}}^{(1)}, \boldsymbol{u}_{\mathscr{D}}^{(2)}\right)$ with respect to the exact solution $\boldsymbol{u} = \left(\boldsymbol{u}^{(1)}, \boldsymbol{u}^{(2)}\right)$ given for $i = 1, 2$ by:

$$\|\boldsymbol{e}_h\|_{\mathscr{D}} = \sqrt{\sum_{j=1}^{M} \left(e_j^{(i)}\right)^2}, \qquad \boldsymbol{e}_j^{(i)} = \frac{\mathbf{u}_j^{(i)} - \mathbf{u}_j^{(i)}}{\mathbf{u}_j^{(i)}} \quad j = 1, \dots, M.$$

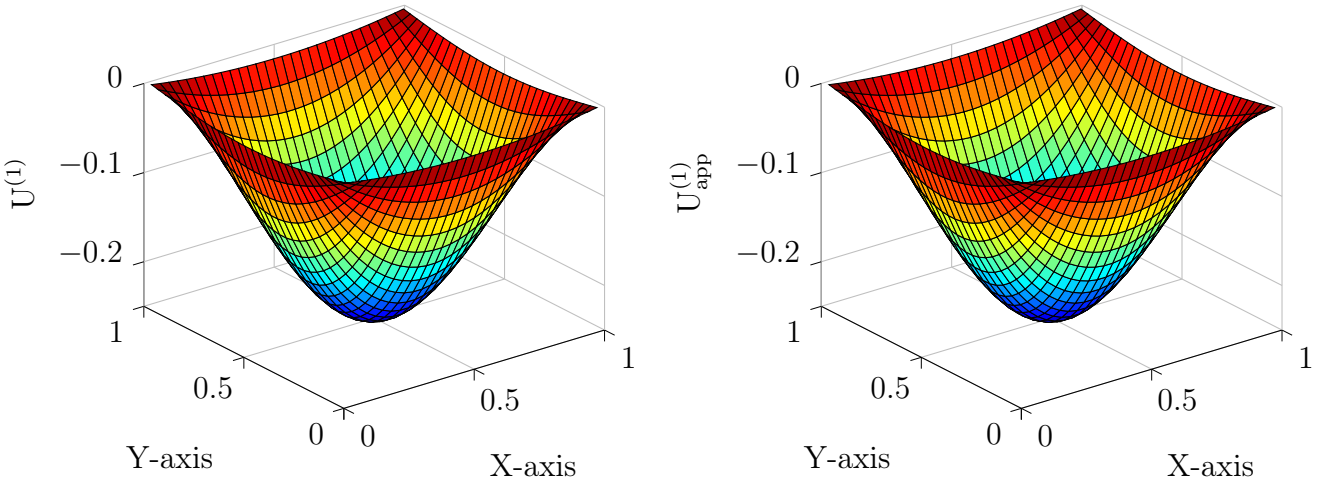

(a) Exact solution $u^{(1)}$

(b) Approximate solution $u_{\mathscr{D}}^{(1)}$

Figure 2.1: Test 1: Displacement graph : (a) Exact solution (b) Approximate solution for $M = 900$, $\mu = 6E + 5$ and $\lambda = 8E + 5$.

Test 1 For the first test case, a steady elasticity problem is solved in the computational domain $\Omega = (0,1) \times (0,1)$,

$$\begin{aligned} -\nabla \cdot \boldsymbol{\sigma}(\boldsymbol{u}) &= \boldsymbol{f} \quad in\ \Omega = (0,1) \times (0,1), \\ \boldsymbol{u} &= 0 \quad on\ \partial\Omega. \end{aligned}$$

The analytical solution of the problem is

$$\begin{pmatrix} u_1(x,y) \\ u_2(x,y) \end{pmatrix} = \begin{pmatrix} y(y-1)\sin(\pi x) \\ x(x-1)\sin(\pi y) \end{pmatrix}.$$

along side a constructed source function $\boldsymbol{f}$.

Since the domain work is squared, we choose a rectangular grid which gives $M = Mx \times My$ rectangular (possibly squared) control volumes.

Figures 2.1 and 2.2 illustrate, respectively, the 3D surface plot of the first displacement component and the 2D quiver plot representing the displacement vector field. As observed, the approximate solution exhibits a high level of smoothness and aligns closely with the exact solution.

To better elucidate the difference, table 2.1 present relative error norm for various step sizes. As the table shows, the relative error norm is decreasing as the step size is augmented, the convergence rate is close to 2, confirming second-order accuracy.

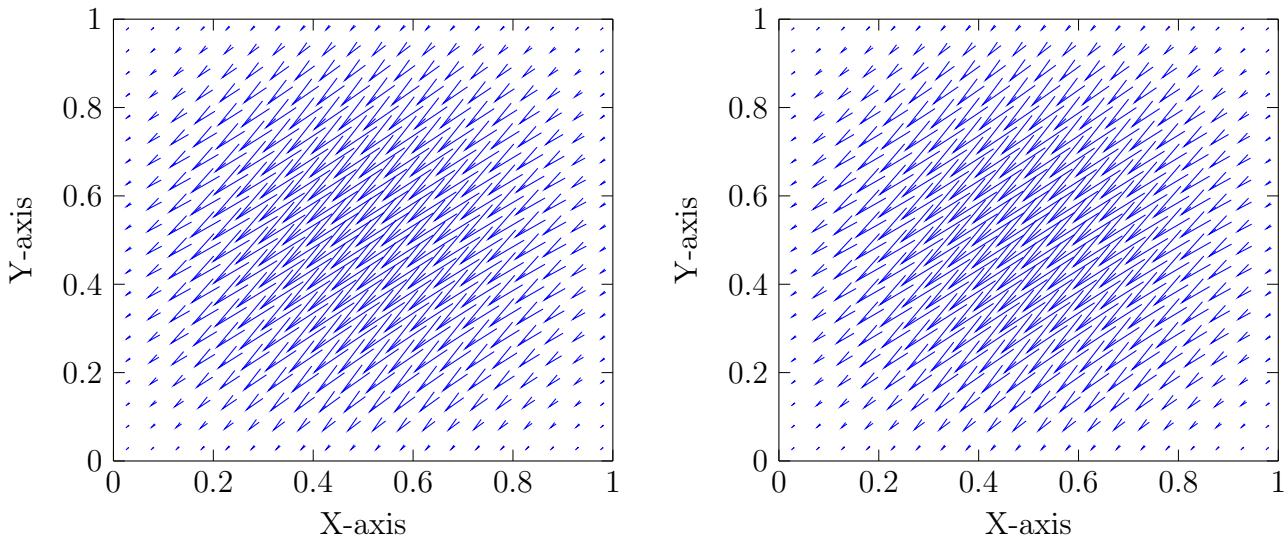

(a) Exact displacement

(b) Approximate displacement

Figure 2.2: Test 1: Displacement vector field : (a) Exact (b) Approximate for $M = 400$, $\mu = 6E + 5$ and $\lambda = 8E + 5$.

h	$\frac{1}{10}$	$\frac{1}{30}$	$\frac{1}{50}$	$\frac{1}{70}$	$\frac{1}{90}$
$\|e_h^1\|$	$1.4009E-2$	$1.5569E-3$	$5.6042E-4$	$2.8592E-4$	$1.7296E-4$
conv. rate	–	1.9998	2.0002	2.0001	2.0001

Table 2.1: Test 1: Relative error norms and convergence rates for $\nu = 0.1$ and $\lambda = 0.01$ using prediction-correction approach.

h	$\frac{1}{10}$	$\frac{1}{30}$	$\frac{1}{50}$	$\frac{1}{70}$	$\frac{1}{90}$
$\|e_h^1\|$	$5.9266E{-}2$	$6.6101E{-}3$	$2.3800E{-}3$	$1.2139E{-}3$	$7.3378E{-}4$
conv. rate	–	1.9966	1.9997	2.0008	2.0032

Table 2.2: Test 2: Relative error norms and convergence rates at $T = 1/5$ for different h values with $\delta t = 1/50$, $\mu = 7.6923E + 10$ and $\lambda = 6.5934E + 10$.

Test 2 The following test case is on an unsteady elasticity problem in the same computational domain $\Omega = (0,1) \times (0,1)$, with $\delta t = \frac{1}{50}$ and $T = \frac{1}{5}$.

$$\begin{aligned} \frac{\partial^2 \boldsymbol{u}}{\partial t^2} - \nabla \cdot \boldsymbol{\sigma}(\boldsymbol{u}) &= \boldsymbol{f} \quad in\ (0,T) \times \Omega \\ \boldsymbol{u} &= 0 \quad on\ (0,T) \times \partial\Omega \\ \boldsymbol{u}_{|t=0} = \boldsymbol{u}_0,\ \boldsymbol{u}_{|t=1/50} &= \boldsymbol{u}_1, \quad on\ \Omega \end{aligned}$$

the analytical solution of the problem is

$$\begin{pmatrix} u_1 \\ u_2 \end{pmatrix}(x,y,t) = \begin{pmatrix} y(y-1)\left(y-\frac{1}{4}\right)\sin(\pi x)\left(1-e^{-t}\right) \\ x(x-1)\left(x-\frac{3}{4}\right)\sin(\pi y)\left(1-e^{-t}\right) \end{pmatrix}.$$

along side the initial condition

$$\boldsymbol{u}_0(x,y) = \begin{pmatrix} 0 \\ 0 \end{pmatrix}, \qquad \boldsymbol{u}_1(x,y) = \begin{pmatrix} y(y-1)(y-1/4)\sin(\pi x)(1-e^{-1/50}) \\ x(x-1)(x-1/4)\sin(\pi y)(1-e^{-1/50}) \end{pmatrix},$$

and a constructed source function $\boldsymbol{f}$. The same domain and mesh configuration as in test 1 are adopted. We use the equation (2.19) instead of the usual elasticity equation, the semi-discretization in time is done using centered difference scheme to discretize the problem in time, and the a finite volume discretization in space

Figure 2.3 displays the 3D surface of the first displacement component, and Figure 2.4 depicts the 2D quiver plot of the displacement vector field at the final time step. The obtained results confirm the accuracy and robustness of the proposed numerical method, showing that the displacement evolves smoothly and consistently with the analytical solution throughout the simulation.

Similarly, Table 2.2 displays the computed relative error norms for different mesh refinements. It can be observed that as the mesh becomes finer, the error systematically decreases, and the estimated convergence rate remains near 2, which confirms the expected second-order precision of the proposed scheme.

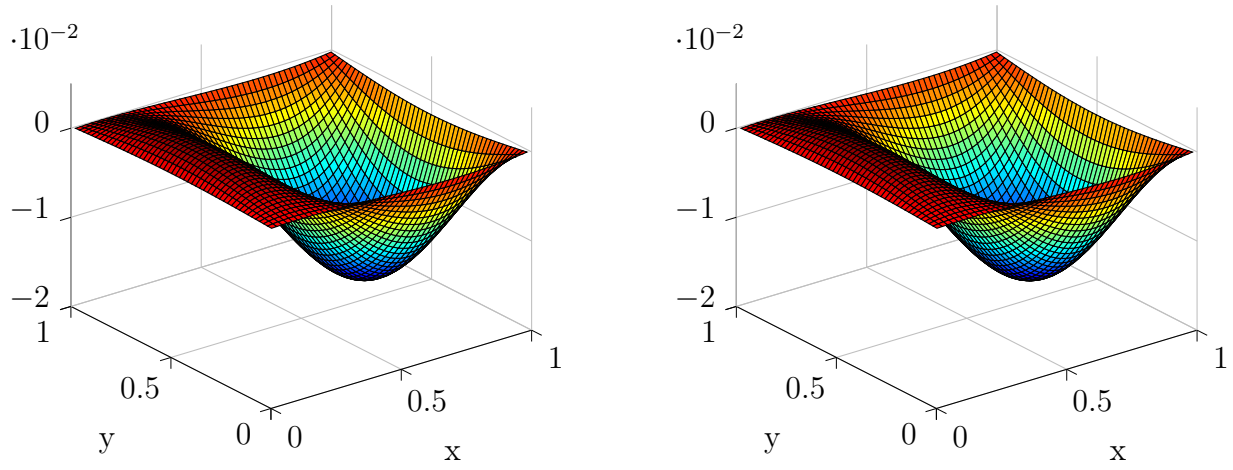

(a) Exact solution $u^{(1)}$

(b) Approximate solution $u_{\mathscr{D}}^{(1)}$

Figure 2.3: Test 2: Displacement graph : (a) Exact solution (b) Approximate solution at $T = 1/5$ for $M = 2500$, $\delta t = 1/50$, $\mu = 7.6923E + 10$ and $\lambda = 6.5934E + 10$.

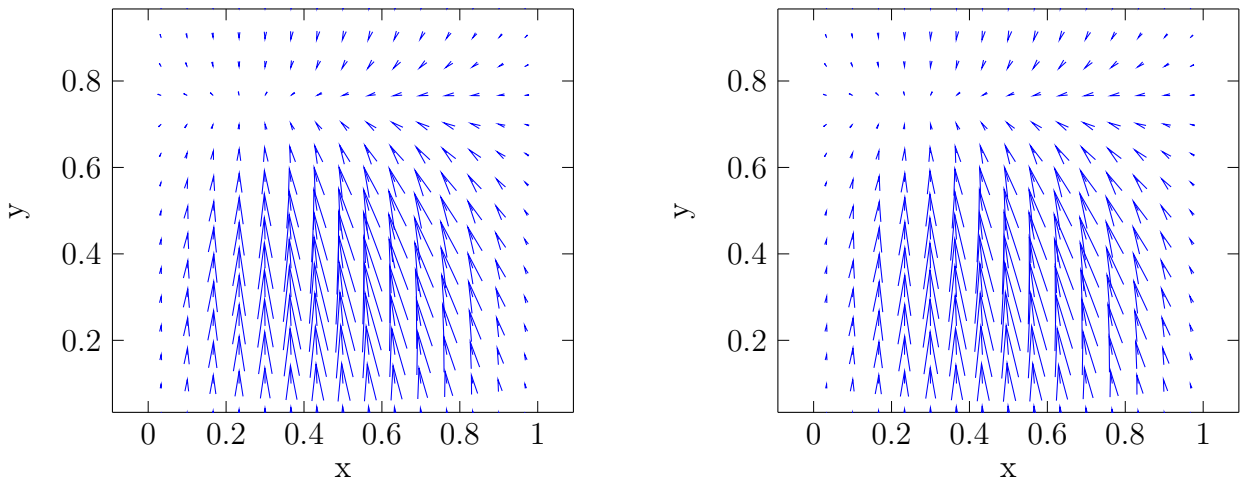

(a) Exact displacement field

(b) Approximate displacement field

Figure 2.4: Test 2: Displacement vector field : (a) Exact (b) Approximate at $T = 1/5$ for $M = 225$, $\delta t = 1/50$, $\mu = 7.6923E + 10$ and $\lambda = 6.5934E + 10$.

2.2 Incompressible Fluid Flow

2.2.1 Kinematics of Fluids

In fluid mechanics, the motion of a fluid is described using the *Eulerian description*, where the focus is on specific locations in space through which fluid flows over time. Let $\Omega_f \subset \mathbb{R}^d$ (with $d = 2$ or 3) denote the spatial domain occupied by the fluid.

The fundamental unknowns in incompressible fluid flow are:

- The **velocity field** $\boldsymbol{v} = \boldsymbol{v}(\boldsymbol{x}, t) \in \mathbb{R}^d$, which describes the velocity of the fluid particle at point $\boldsymbol{x} \in \Omega_f$ and time $t \in (0, T)$.
- The **pressure field** $p = p(\boldsymbol{x}, t) \in \mathbb{R}$, which corresponds to the scalar pressure exerted by the fluid at point $\boldsymbol{x}$ and time t.

In this framework, the behavior of the fluid is observed as it evolves through space and time. Unlike in solid mechanics, where the motion is typically described using material (Lagrangian) coordinates, fluid motion is best captured using spatial (Eulerian) coordinates due to its continuous deformation and transport properties.

We will assume that the fluid is:

- **Incompressible**, meaning its density remains constant and the volume of any fluid particle does not change with time.
- **Newtonian**, implying a linear relationship between the stress and the rate of strain.
- **Isothermal**, so that temperature effects are neglected.
- **Single-phase**, without mixtures or multiphase interactions.

These assumptions lead to a simplified and widely applicable model, suitable for describing many viscous fluid phenomena and forming the basis for fluid–structure interaction (FSI) problems considered in later chapters.

2.2.2 Governing Equations

The motion of an incompressible viscous fluid is governed by two fundamental physical principles:

1. **Conservation of mass**, which for incompressible fluids reduces to the condition of volume preservation:
$$\nabla \cdot \boldsymbol{v} = 0 \quad \text{in } (0, T) \times \Omega_f. \tag{2.21}$$

2. **Conservation of linear momentum**, which yields the *Navier–Stokes equations*:

$$\rho_f \left(\frac{\partial \boldsymbol{v}}{\partial t} + (\boldsymbol{v} \cdot \nabla)\boldsymbol{v} \right) - \nabla \cdot \boldsymbol{\sigma}_f(\boldsymbol{v}, p) = \boldsymbol{f}_f \quad \text{in } (0,T) \times \Omega_f, \tag{2.22}$$

where:

- $\rho_f > 0$ is the (constant) density of the fluid,
- $\boldsymbol{f}_f$ is the body force per unit volume (e.g., gravity),
- $\boldsymbol{\sigma}_f(\boldsymbol{v}, p)$ is the Cauchy stress tensor of the fluid.

Together, these equations describe the dynamics of an incompressible Newtonian fluid.

Nonlinear Advection Term and Reynolds Number

The term $(\boldsymbol{v} \cdot \nabla)\boldsymbol{v}$ in the momentum equation represents the *convective acceleration*, describing how the velocity of a fluid particle changes as it moves through a spatially varying velocity field. This term introduces nonlinearity into the Navier–Stokes equations and is responsible for a variety of complex behaviors such as turbulence and flow instabilities.

A key dimensionless parameter that governs the balance between inertial (convective) and viscous forces in a fluid is the **Reynolds number**, denoted Re. It is defined as:

$$\mathrm{Re} = \frac{\rho_f U L}{\mu_f}, \tag{2.23}$$

where:

- ρ_f is the fluid density,
- U is a characteristic velocity of the flow,
- L is a characteristic length scale (e.g., the diameter of a pipe or channel),
- μ_f is the dynamic viscosity of the fluid.

Interpretation:

- If $\mathrm{Re} \ll 1$, viscous forces dominate, and the flow is typically smooth and laminar; in this case, the convective term can often be neglected, leading to the linearized *Stokes equations*.
- If $\mathrm{Re} \gg 1$, inertial forces dominate, and the flow may become unstable or turbulent.

The Reynolds number plays a central role in determining the qualitative behavior of the flow and the choice of mathematical and numerical models. For a detailed derivation of the dimensionless form of the Navier–Stokes equations and the appearance of the Reynolds number (and other important numbers such as the Strouhal and Prandtl numbers...), see for example Chapter 3 of [71] or Chapter 7 of [59].

System Summary

We summarize the incompressible Navier–Stokes system as:

$$\begin{cases} \rho_f \left(\dfrac{\partial \boldsymbol{v}}{\partial t} + (\boldsymbol{v} \cdot \nabla)\boldsymbol{v} \right) - \nabla \cdot \boldsymbol{\sigma}_f(\boldsymbol{v}, p) = \boldsymbol{f}_f & \text{in } (0,T) \times \Omega_f, \\ \nabla \cdot \boldsymbol{v} = 0 & \text{in } (0,T) \times \Omega_f. \end{cases}$$

These equations are supplemented with initial and boundary conditions, which will be specified in the next subsections.

2.2.3 Newtonian Stress Tensor

In order to close the system of equations governing fluid motion, a constitutive law is needed to relate the stress tensor to the flow variables. For a Newtonian fluid, the Cauchy stress tensor $\boldsymbol{\sigma}_f$ is assumed to depend linearly on the rate of strain. Specifically, the constitutive relation is given by:

$$\boldsymbol{\sigma}_f(\boldsymbol{v}, p) = -p\boldsymbol{I} + 2\mu_f \, \boldsymbol{\varepsilon}(\boldsymbol{v}), \tag{2.24}$$

where:

- p is the scalar pressure field,
- $\mu_f > 0$ is the dynamic viscosity of the fluid,
- $\boldsymbol{I}$ is the identity tensor,
- $\boldsymbol{\varepsilon}(\boldsymbol{v})$ is the rate-of-strain tensor, defined by:

$$\boldsymbol{\varepsilon}(\boldsymbol{v}) = \frac{1}{2} \left(\nabla \boldsymbol{v} + (\nabla \boldsymbol{v})^\top \right).$$

Interpretation

The stress tensor consists of two parts:

- A **hydrostatic (isotropic)** part, $-p\boldsymbol{I}$, which accounts for the pressure acting equally in all directions,
- A **viscous (deviatoric)** part, $2\mu_f\boldsymbol{\varepsilon}(\boldsymbol{v})$, which represents the internal friction due to velocity gradients.

Remarks

- The fluid is assumed to be Newtonian and incompressible. More complex fluids (e.g., non-Newtonian, compressible) require different stress models.
- The rate-of-strain tensor $\boldsymbol{\varepsilon}(\boldsymbol{v})$ is symmetric and vanishes for rigid-body motions.
- The pressure p appears as a Lagrange multiplier associated with the incompressibility constraint $\nabla \cdot \boldsymbol{v} = 0$.

2.2.4 Boundary and Initial Conditions

To fully specify the fluid flow problem, the incompressible Navier–Stokes equations must be supplemented with appropriate boundary and initial conditions. These conditions depend on the physical configuration of the domain and the type of interaction with its surroundings.

Boundary Conditions

Let the boundary of the fluid domain Γ_f be partitioned into two disjoint parts:

$$\Gamma_f = \Gamma_D^f \cup \Gamma_N^f, \quad \Gamma_D^f \cap \Gamma_N^f = \emptyset,$$

where:

- Γ_D^f corresponds to portions of the boundary where the fluid velocity is prescribed (Dirichlet condition),
- Γ_N^f corresponds to portions where the traction (stress vector) is prescribed (Neumann condition).

The boundary conditions take the form:

$$\boldsymbol{v} = \boldsymbol{v}_D \quad \text{on } \Gamma_D^f, \tag{2.25}$$

$$\boldsymbol{\sigma}_f(\boldsymbol{v}, p) \cdot \boldsymbol{n} = \boldsymbol{t}_N \quad \text{on } \Gamma_N^f, \tag{2.26}$$

where:

- $\boldsymbol{n}$ is the outward unit normal to Γ_f,
- $\boldsymbol{v}_D$ is a prescribed velocity (e.g., zero for no-slip or specified inflow),
- $\boldsymbol{t}_N$ is the prescribed traction vector (e.g., pressure outflow or shear stress).

Initial Condition

The evolution problem is initialized by specifying the velocity field at time $t = 0$:

$$\boldsymbol{v}(x, 0) = \boldsymbol{v}_0(x) \quad \text{for a.e. } x \text{ in } \Omega_f, \tag{2.27}$$

where $\boldsymbol{v}_0$ is a given solenoidal (divergence-free) velocity field satisfying:

$$\nabla \cdot \boldsymbol{v}_0 = 0 \quad \text{in } \Omega_f. \tag{2.28}$$

Remarks

- The choice of boundary conditions should reflect the physical reality: no-slip on solid walls, inflow/outflow profiles on open boundaries, etc.
- The well-posedness of the Navier–Stokes problem depends critically on the compatibility of the boundary and initial conditions with the incompressibility constraint.
- In coupled problems (e.g., fluid–structure interaction), boundary conditions on the interface are replaced by transmission conditions, which will be discussed in chapter 3.5.2.

2.2.5 Special Case: Stokes Equations

In many situations involving slow, highly viscous, or small-scale flows, the inertial effects in the Navier–Stokes equations become negligible in comparison to viscous forces. Mathematically, this corresponds to taking the limit of vanishing Reynolds number $\mathrm{Re} \ll 1$, such as in microfluidics or lubrication theory.

Under this assumption, the nonlinear convective term $(\boldsymbol{v} \cdot \nabla)\boldsymbol{v}$ and the time derivative $\partial \boldsymbol{v}/\partial t$ may be neglected, leading to the **steady Stokes equations**:

$$\begin{cases} -\nabla \cdot \boldsymbol{\sigma}_f(\boldsymbol{v}, p) = \boldsymbol{f}_f & \text{in } \Omega_f, \\ \nabla \cdot \boldsymbol{v} = 0 & \text{in } \Omega_f, \end{cases} \tag{2.29}$$

or, equivalently (using the Newtonian constitutive law):

$$\begin{cases} -\mu_f \Delta \boldsymbol{v} + \nabla p = \boldsymbol{f}_f & \text{in } \Omega_f, \\ \nabla \cdot \boldsymbol{v} = 0 & \text{in } \Omega_f. \end{cases} \tag{2.30}$$

The more generalized Stokes problem is defined by

$$\eta \boldsymbol{v} - \nu \Delta \boldsymbol{v} + \nabla p = \boldsymbol{f} \text{ in } \Omega_f, \tag{2.31}$$

$$\nabla \cdot \boldsymbol{v} = 0 \text{ in } \Omega_f, \tag{2.32}$$

$$\boldsymbol{v} = \boldsymbol{g} \text{ on } \Gamma_f, \tag{2.33}$$

where $\nu > 0$ is the kinematic viscosity, $f \in H^{-1}(\Omega_f)$ and $\mathbf{g} \in H^{1/2}(\Gamma_f)$ are given vector functions such that $\boldsymbol{g}$ satisfies the compatibility condition

$$\int_{\Gamma_f} \boldsymbol{g} \cdot \boldsymbol{n} \, d\Gamma_f = 0. \tag{2.34}$$

The equation (2.31) is obtained after semi-descritization of the unsteady Stokes problem, equation (2.32) is the continuity (incompressibility) equation or the mass conservation equation. (2.33) is the Dirichlet condition on the boundary Γ_f of Ω_f.
Due to the fact that the pressure gradient ∇p, and not the pressure itself, appears in the Stokes equations, the pressure is specified up to an additive constant (i.e. p is a solution equivalent to $p + c$ is a solution for all constant c), which signifies the non-uniqueness of pressure. To ensure uniqueness, one often set the mean value of pressure to zero which eliminate the arbitrary constant.

$$\int_{\Omega_f} p \, d\Omega_f = 0. \tag{2.35}$$

The existence and uniqueness of solution for (2.31)-(2.33) is established as stated in the following theorem.

Theorem 2.1 (Existence and uniqueness of solution [43] p. 51)**.** *Let Ω be a connected open bounded domain of $\mathbb{R}^d$ with Lipschitz continuous boundary Γ. Then for any function $\boldsymbol{f} \in H^{-1}(\Omega)$ and any function $\boldsymbol{g} \in H^{1/2}(\Gamma)$ satisfying the compatibility condition (2.34), there exists a unique couple $(\boldsymbol{v}, p) \in H^1(\Omega) \times L^2_0(\Omega)$ satisfies the problem (2.31)–(2.33).*

With additional regularity assumptions, further results on the smoothness of the solution can be obtained.

Theorem 2.2 (Regularity of solution [43] p.54)**.**

1. *Let us suppose that hypotheses of Theorem 2.1. If* Γ *was* C^2*-regular,* $\boldsymbol{g} = 0$ *and* $\boldsymbol{f} \in L^r(\Omega)$ *for* $1 < r \leq 2$*. Then the Stokes problem (2.31)-(2.33) has a unique solution* $(\boldsymbol{v}, p)$ *in* $W^{2,r}(\Omega) \times (W^{1,r}(\Omega) \bigcap L^2_0(\Omega))$*.*
Furthermore, there exists a positive constant $C_r = C_r(\Omega)$ *such that:*

$$\|\boldsymbol{v}\|_{2,r,\Omega} + \|p\|_{1,r,\Omega} \leq C_r \|\boldsymbol{f}\|_{r,\Omega}. \tag{2.36}$$

2. *If* Γ *is only Lipschitz continuous, this result stay valid provided* Ω *being convex and* $d = 2$*.*

We emphasize that the Stokes problem can also be articulated as a saddle-point problem, We urge the interested readers to see [4,39,43] and references therein for more details.

Interpretation and Applications

- The Stokes equations describe **creeping flows**, in which viscous forces dominate completely.
- They are linear and easier to analyze both analytically and numerically than the full Navier–Stokes system.
- Stokes flows arise in various engineering and biomedical applications, such as:
  - Flow in porous media,
  - Motion of microorganisms in fluids,
  - Blood flow in small capillaries,
  - Viscous damping in micro-mechanical systems.

The Stokes model is also widely used as a linear approximation in fluid–structure interaction (FSI) studies, particularly when deriving theoretical results or performing preliminary numerical validation.

2.2.6 Remarks on Coupling and Well-Posedness

The incompressible Navier–Stokes and Stokes equations introduced above form the basis for modeling viscous fluid flow. In the context of this thesis, these models will later be coupled with elasticity equations to study fluid–structure interaction (FSI) problems.

Coupling with Elasticity

In fluid–structure interaction (FSI) problems, a portion of the fluid boundary coincides with that of an elastic solid. Across this interface, appropriate transmission conditions must be imposed to ensure the physical and mathematical consistency of the coupled problem.

Classical Interface Conditions. The most common coupling conditions are:

- **Kinematic condition (continuity of velocity):**

$$\boldsymbol{v} = \frac{\partial \boldsymbol{u}}{\partial t} \quad \text{on the interface,}$$

  ensuring that the fluid and solid share the same velocity at their common boundary, with no slip or separation.

- **Dynamic condition (balance of normal stress):**

$$\boldsymbol{\sigma}_f \cdot \boldsymbol{n}_f = \boldsymbol{\sigma}_s \cdot \boldsymbol{n}_s \quad \text{on the interface,}$$

  expressing Newton's third law: the fluid exerts a force on the solid, and the solid reacts with an equal and opposite force.

Generalized Interface Conditions. In this thesis, we adopt more general coupling conditions that account for interface effects such as damping, stiffness, and relaxation. These may involve:

- Weighted combinations of fluid and solid stresses on the interface,
- Discrete or distributed spring-like models with parameters such as mass and stiffness matrices,
- Averaged velocities and jump terms across the interface.

A typical generalized dynamic condition used in this work takes the form:

$$[\![\boldsymbol{\sigma} \cdot \boldsymbol{n}]\!] = S\,\overline{\boldsymbol{v}} - \boldsymbol{g}, \qquad \overline{\boldsymbol{\sigma} \cdot \boldsymbol{n}} = M\,[\![\boldsymbol{v}]\!] - \boldsymbol{h} \quad \text{on the interface,}$$

where:

- $[\![\cdot]\!]$ denotes the jump across the interface,

- $\overline{(\cdot)}$ denotes the average between the fluid and solid sides,
- M and S are positive definite matrix-valued functions defined on the interface,
- $\boldsymbol{g}$ and $\boldsymbol{h}$ are known source terms.

These generalized interface conditions are essential to accurately model certain physical effects, and to ensure stability or convergence in the numerical schemes proposed later in this work. A detailed derivation and motivation of these conditions will be presented in the corresponding chapters on the coupled problems.

Well-Posedness of the Fluid Problem

For the Navier–Stokes system, the existence and uniqueness of solutions depend on the spatial dimension, the regularity of the data, and the Reynolds number:

- In 2D, the problem admits a unique weak solution globally in time for reasonable data;
- In 3D, global existence of weak solutions is known (Leray), but uniqueness and regularity remain open problems;
- For the Stokes problem, the equations are linear and admit unique solutions under standard assumptions on data and boundary conditions.

In all cases, the incompressibility constraint $\nabla \cdot \boldsymbol{v} = 0$ introduces mathematical complexity, particularly in defining appropriate function spaces and ensuring the inf–sup (Ladyzhenskaya–Babuška–Brezzi) condition for well-posedness of the variational formulation.

Transition to Coupled Problems

The interface and transmission conditions described above will be treated rigorously in later chapters, where we develop the mathematical modeling, analysis, and numerical schemes for FSI problems involving incompressible viscous fluids and linearly elastic solids.

2.2.7 Discretization of Stokes Problem

Throught this section, we set $d = 2$ and $\boldsymbol{u} = (u^{(1)}, u^{(2)})$. We recall that the essential notions, spaces and discrete operators to establish the discrete collocated finite volume scheme of the generalized Stokes equations (2.29) or (2.30) are presented in section 1.2. Let $\mathscr{D} = (\mathscr{M}, \mathscr{E}, \mathscr{P})$ be an admissible mesh. For each control volume K of $\mathscr{M}$, the

discrete generalized Stokes problem (with homogeneous Dirichlet condition) is described as follows

$$\begin{cases} \eta \boldsymbol{v}_K - \nu \Delta_K \boldsymbol{v}_K + \nabla_K p_K = \boldsymbol{f}_K \\ \mathrm{div}_K(1, \boldsymbol{v}_K, \lambda, p_K) = 0 \end{cases} \tag{2.37}$$

where $\boldsymbol{f}_K = \frac{1}{\mathrm{m}_K} \int_K \boldsymbol{f}(\boldsymbol{x}) \mathrm{d}\boldsymbol{x}$ and supplemented by the descrete form of the pressure unicity condition (2.35)

$$\sum_{K \in \mathscr{M}} \mathrm{m}_K p_K = 0 \tag{2.38}$$

Although the discrete linear system stays the same, the solving method of the system can affect the error and convergence rate. Let us consider the block square matrix $\mathbf{P}$ and the column vectors $\mathbf{b}$ and $\mathbf{S}$

$$\mathbf{P} = \begin{pmatrix} \eta\mathbf{I} - \nu\mathbf{A} & 0 & \mathbf{B}_1^T \\ 0 & \eta\mathbf{I} - \nu\mathbf{A} & \mathbf{B}_2^T \\ \mathbf{B}_1 & \mathbf{B}_2 & \lambda\mathbf{D} \end{pmatrix} \quad \mathbf{b} = \begin{pmatrix} \mathbf{F}^{(1)} \\ \mathbf{F}^{(2)} \\ 0 \end{pmatrix} \quad \mathbf{S} = \begin{pmatrix} \mathbf{v}_{\mathscr{D}}^{(1)} \\ \mathbf{v}_{\mathscr{D}}^{(2)} \\ \mathbf{p}_{\mathscr{D}} \end{pmatrix}$$

where for $j = 1, 2$, $\mathbf{v}_{\mathscr{D}}^{(j)} = \left(v_{K_i}^{(j)}\right)_{i=1,M}$, $\mathbf{p}_{\mathscr{D}} = (p_{K_i})_{i=1,M}$, $\mathbf{F}^{(j)} = \left(F_i^{(j)}\right)_{i=1,M}$ with $F_i^{(j)} = \frac{1}{\mathrm{m}_{K_i}} \int_{K_i} f^{(j)}(\boldsymbol{x}) \mathrm{d}\boldsymbol{x}$, $\mathbf{I}$ is the identity matrix, $\boldsymbol{A}$ is the discrete Delta matrix, $\mathbf{B} = (\mathbf{B1}\ \mathbf{B2})$ is the divergence matrix, $\mathbf{B}^T$ is the gradient matrix and $\mathbf{D}$ is the matrix of stabilization terms. We note that $\mathbf{A}$, $\mathbf{B}_1$, $\mathbf{B}_2$, $\mathbf{D}$ and $\mathbf{I}$ are all square matrices of same size M, and $\mathbf{F}^{(1)}, \mathbf{F}^{(2)}, \mathbf{v}_{\mathscr{D}}^{(1)}, \mathbf{v}_{\mathscr{D}}^{(2)}$ and $\mathbf{p}_{\mathscr{D}}$ are all column vectors of same size M.

1. The direct approach is solving the system

$$\mathbf{PS} = \mathbf{b} \tag{2.39}$$

   using the either iterative solvers (or Krylov subspace methods) such as GMRES (Generalized Minimal Residual), BiCGSTAB (Biconjugate Gradient Stabilized),etc.... Or by direct methods specifically LU factorization, these methods have shown to be efficient in all numerical test cases.

2. Another procedure is to use a prediction-correction splitting method, such as the one described by Angot and al [4] which is based on the augmanted Lagrangian approach and Uzawa iterations. The continuity equation is considered as a optimization constraint and it is used only in the correction step. For $\mathbf{p}_{\mathscr{D}}^0 = 0$ and the parameters

λ_k and r_k the method reads

$$\begin{pmatrix} \mathbf{A} & 0 \\ 0 & \mathbf{A} \end{pmatrix} \begin{pmatrix} \tilde{\mathbf{v}}_{\mathscr{D}}^{(1)} \\ \tilde{\mathbf{v}}_{\mathscr{D}}^{(2)} \end{pmatrix} = \begin{pmatrix} \mathbf{F}^{(1)} \\ \mathbf{F}^{(2)} \end{pmatrix} \tag{2.40}$$

$$\left[\begin{pmatrix} \mathbf{A} & 0 \\ 0 & \mathbf{A} \end{pmatrix} + \frac{1}{\varepsilon} \begin{pmatrix} \mathbf{B}_1 & \mathbf{B}_2 \end{pmatrix} \begin{pmatrix} \mathbf{B}_1^T \\ \mathbf{B}_2^T \end{pmatrix} \right] \begin{pmatrix} \hat{\mathbf{v}}_{\varepsilon,\mathscr{D}}^{(1)} \\ \hat{\mathbf{v}}_{\varepsilon,\mathscr{D}}^{(2)} \end{pmatrix} = -\frac{1}{\varepsilon} \begin{pmatrix} \mathbf{B}_1^T \\ \mathbf{B}_2^T \end{pmatrix} \begin{pmatrix} \mathbf{B}_1 & \mathbf{B}_2 \end{pmatrix} \begin{pmatrix} \tilde{\mathbf{v}}_{\mathscr{D}}^{(1)} \\ \tilde{\mathbf{v}}_{\mathscr{D}}^{(2)} \end{pmatrix} \tag{2.41}$$

$$\mathbf{v}_{\varepsilon,\mathscr{D}}^{(j)} = \tilde{\mathbf{v}}_{\mathscr{D}}^{(j)} + \hat{\mathbf{u}}_{\varepsilon,\mathscr{D}}^{(j)} \quad \text{for } j = 1, 2 \quad \text{and} \quad \mathbf{p}_{\mathscr{D}}^{k+1} = \mathbf{p}_{\mathscr{D}}^{k} + \lambda_k \left(\mathbf{B}_1 \mathbf{v}_{\varepsilon,\mathscr{D}}^{(1)} + \mathbf{B}_2 \mathbf{v}_{\varepsilon,\mathscr{D}}^{(2)} \right) \tag{2.42}$$

2.2.8 Discretization of Navier-Stokes Problem

The discretization of the Navier–Stokes problem constitutes a crucial step in obtaining reliable and efficient numerical approximations of incompressible fluid flows. In this subsection, we describe the spatial and temporal discretization strategies adopted for the governing equations introduced earlier. The objective is to transform the continuous problem into a discrete system that preserves the main physical and mathematical properties of the original equations, such as mass and momentum conservation, while ensuring stability and accuracy. The finite volume framework is employed for the spatial discretization, providing a natural formulation based on local flux balances. Time integration is then performed using an appropriate scheme that allows for consistent coupling between the velocity and pressure fields.

2.2.8.1 Time-stepping schemes

For any time step size $\delta t > 0$, we approximate $\boldsymbol{v}(t^n, x)$ by $\boldsymbol{v}^n(x)$ ($\boldsymbol{v}$ for abbreviation) where $t^n = n\delta t$.

For the Navier-Stokes equations, many approaches can be chosen:

backward Euler method (BE): which is the most stable (but not the most accurate) scheme for ODE systems which reads, given $(\boldsymbol{v}^n, p^n)$ we seek $(\boldsymbol{v}^{n+1}, p^{n+1})$ solution to

$$\begin{aligned} \frac{\rho}{\delta t} \left(\boldsymbol{v}^{n+1} - \boldsymbol{v}^n \right) + \rho(\boldsymbol{v}^{n+1} \cdot \nabla)\boldsymbol{v}^{n+1} - \mu \Delta \boldsymbol{v}^{n+1} + \nabla p^{n+1} &= \boldsymbol{f}^{n+1} \quad in\ \Omega \\ \nabla \cdot \boldsymbol{v}^{n+1} &= 0 \quad in\ \Omega \end{aligned} \tag{2.43}$$

Linearized semi-implicit approach (LSE): A semi-implicit treatment consists in linearizing the convective term around the known velocity at time level n and applying

it to the unknown velocity at time level $n+1$. Given $(\boldsymbol{v}^n, p^n)$ we seek $(\boldsymbol{v}^{n+1}, p^{n+1})$ such that

$$\begin{aligned} \frac{\rho}{\delta t}\big(\boldsymbol{v}^{n+1} - \boldsymbol{v}^n\big) + \rho\big(\boldsymbol{v}^n \cdot \nabla\big)\boldsymbol{v}^{n+1} - \mu\Delta\boldsymbol{v}^{n+1} + \nabla p^{n+1} &= \boldsymbol{f}^{n+1} \quad \text{in } \Omega, \\ \nabla \cdot \boldsymbol{v}^{n+1} &= 0 \quad \text{in } \Omega. \end{aligned} \tag{2.44}$$

This choice yields a linear problem for $(\boldsymbol{v}^{n+1}, p^{n+1})$ at each time step, since the advective coefficient $\boldsymbol{v}^n$ is known. Rearranging (2.44) gives

$$\left(\rho\frac{1}{\delta t}\mathbf{I} + \rho(\boldsymbol{v}^n \cdot \nabla) - \mu\Delta\right)\boldsymbol{v}^{n+1} + \nabla p^{n+1} = \rho\frac{1}{\delta t}\boldsymbol{v}^n + \boldsymbol{f}^{n+1}. \tag{2.45}$$

The scheme is still first-order in time (same as backward Euler) unless paired with a higher-order time discretization. The linearization does not increase the temporal order.

Algorithm 1 Linearized Semi-Implicit Scheme (LSE)

Physical parameters ρ, μ; time step $\delta t > 0$; final time $T = N\,\delta t$; initial fields $(\boldsymbol{v}^0, p^0)$ satisfying $\nabla \cdot \boldsymbol{v}^0 = 0$. Velocity and pressure fields $(\boldsymbol{v}^{n+1}, p^{n+1})$ for $n = 0, \ldots, N-1$.
Initialization: Set $\boldsymbol{v}^0 = \boldsymbol{v}_0$, $p^0 = p_0$ on Ω.
$n = 0$ $N-1$ **1. Compute the right-hand side:**

$$\boldsymbol{RHS} = \rho\frac{1}{\delta t}\boldsymbol{v}^n + \boldsymbol{f}^{n+1}.$$

2. Form the linear operator:

$$\mathscr{A}^n(\boldsymbol{v}^{n+1}) = \rho\frac{1}{\delta t}\boldsymbol{v}^{n+1} + \rho(\boldsymbol{v}^n \cdot \nabla)\boldsymbol{v}^{n+1} - \mu\Delta\boldsymbol{v}^{n+1}.$$

3. Solve the linearized system:

$$\begin{cases} \mathscr{A}^n(\boldsymbol{v}^{n+1}) + \nabla p^{n+1} = \boldsymbol{RHS}, & \text{in } \Omega, \\ \nabla \cdot \boldsymbol{v}^{n+1} = 0, & \text{in } \Omega, \end{cases}$$

with suitable boundary conditions on $\partial\Omega$.
4. Update the solution: Set $\boldsymbol{v}^{n+1}$ and p^{n+1} as the current velocity and pressure fields.

Trapezoidal rule (TR): [58] also known as the *one-leg* trapezoidal rule , an A-stable scheme with second order accuracy in time which reads, given $(\boldsymbol{v}^n, p^n)$ we seek $(\boldsymbol{v}^{n+1}, p^{n+1})$

solution to

$$\begin{aligned}\frac{\rho}{\delta t}\left(\boldsymbol{v}^{n+1}-\boldsymbol{v}^{n}\right)+\rho\left[\left(\frac{\boldsymbol{v}^{n+1}+\boldsymbol{v}^{n}}{2}\right)\cdot\nabla\right]\left(\frac{\boldsymbol{v}^{n+1}+\boldsymbol{v}^{n}}{2}\right)-\mu\Delta\left(\frac{\boldsymbol{v}^{n+1}+\boldsymbol{v}^{n}}{2}\right)\\ +\nabla\left(\frac{p^{n+1}+p^{n}}{2}\right)=\boldsymbol{f}^{n+1/2}\quad in\ \Omega\\ \nabla\cdot\boldsymbol{v}^{n+1}=\underline{\mathbf{0}}\quad in\ \Omega\end{aligned}\tag{2.46}$$

For proof of stability for this method, see [58].

A variant to (2.46) is the *two-leg* trapezoidal scheme where the change is made replacing the nonlinear term as follows

$$\left[\left(\frac{\boldsymbol{v}^{n+1}+\boldsymbol{v}^{n}}{2}\right)\cdot\nabla\right]\left(\frac{\boldsymbol{v}^{n+1}+\boldsymbol{v}^{n}}{2}\right)\rightarrow\frac{(\boldsymbol{v}^{n+1}\cdot\nabla)\boldsymbol{v}^{n+1}}{2}+\frac{(\boldsymbol{v}^{n}\cdot\nabla)\boldsymbol{v}^{n}}{2}$$

of cours the *one-leg* and *two-leg* trapezoidal schemes obligate solving a nonlinear system each time-step. A way to reduce the calculation cost is to replace the nonlinear term in (2.46) with the linearized form $(\boldsymbol{v}^{n}\cdot\nabla)\boldsymbol{v}^{n+1}$, this lower the calculation cost by significant amount, however this generate a prominent drawback that is the loss of second order accuracy (only first order accuracy is reached).

A proven strategy to address this disadvantage is the use of linear extrapolation (LE), for example the linear extrapolation of $\boldsymbol{v}(t^{n+1/2})$

$$\boldsymbol{v}(t^{n+1/2})=\frac{3}{2}\boldsymbol{v}(t^{n})-\frac{1}{2}\boldsymbol{v}(t^{n-1})+O(\delta t^{2})$$

Noting

$$E[\boldsymbol{v}^{n},\boldsymbol{v}^{n-1}]:=\frac{3}{2}\boldsymbol{v}(t^{n})-\frac{1}{2}\boldsymbol{v}(t^{n-1})$$

the nonlinear term in trapezoidal scheme (2.46) can be replaced by

$$\left[\left(\frac{\boldsymbol{v}^{n+1}+\boldsymbol{v}^{n}}{2}\right)\cdot\nabla\right]\left(\frac{\boldsymbol{v}^{n+1}+\boldsymbol{v}^{n}}{2}\right)\rightarrow\left(E[\boldsymbol{v}^{n},\boldsymbol{v}^{n-1}]\cdot\nabla\right)\left(\frac{\boldsymbol{v}^{n+1}+\boldsymbol{v}^{n}}{2}\right)$$

Note that after this extrapolation technique, the nonlinearity is no longer a concern. The outcome method trapezoidal rule with linear extrapolation (TRLE) is unconditionally stable and second order accurate (in time), as you can verifie in [8, 11, 48, 85].

Projection method: due to their efficiency and simplicity in handling the incompressibility constraint of fluid flow, these methods are popular in CFD. They involve predicting an intermediate velocity field without considering the incompressibility constraint, and

then projecting this field onto a divergence-free space to enforce the incompressibility condition. A collection of recent papers from Angot and al [2,4,6,7] and many references therein described and analysed a new vector penalty-projection method (VPP) for different cases, here we present the one from [7] for incompressible flow with variable density and viscosity (constant case included), for a penalty parameter $0 < \varepsilon << 1$ and given $\rho^n, \boldsymbol{v}^n$ and p^n in Ω:

$$\frac{\rho^n}{\delta t}\left(\tilde{\boldsymbol{v}}^{n+1} - \boldsymbol{v}^n\right) + \rho^n\left(\boldsymbol{v}^n \cdot \nabla\right)\tilde{\boldsymbol{v}}^{n+1}\right) - 2\mu\nabla\cdot\left(\boldsymbol{d}(\tilde{\boldsymbol{v}}^{n+1})\right) + \nabla p^n = \boldsymbol{f}^n \qquad in\ \Omega \tag{2.47}$$

$$\tilde{\boldsymbol{v}}^{n+1}_{|\Gamma} = 0 \qquad on\ \Gamma \tag{2.48}$$

$$\varepsilon\hat{\boldsymbol{v}}^{n+1} - \nabla\left(\nabla\cdot\ \hat{\boldsymbol{v}}^{n+1}\right) = \nabla\left(\nabla\cdot\tilde{\boldsymbol{v}}^{n+1}\right) \qquad in\ \Omega \tag{2.49}$$

$$\hat{\boldsymbol{v}}^{n+1}_{|\Gamma} = 0 \qquad on\ \Gamma \tag{2.50}$$

$$\text{Correction of velocity } \tilde{\boldsymbol{v}}^{n+1} + \hat{\boldsymbol{v}}^{n+1} = \boldsymbol{v}^{n+1} \qquad in\ \Omega \tag{2.51}$$

$$\nabla\left(p^{n+1} - p^n\right) = -\frac{\rho^n}{\delta t}\hat{\boldsymbol{v}}^{n+1} \qquad in\ \Omega \tag{2.52}$$

$$\frac{1}{\delta t}\left(\rho^{n+1} - \rho^n\right) + \boldsymbol{v}^{n+1}\cdot\nabla\rho^n = 0 \qquad in\ \Omega \tag{2.53}$$

This method is proven to be second order accurate in time, the readers can reinspect within [2,4,6,7]. The algorithm of the VPP method is given by:

Algorithm 2 Procedure for the VPP solver

Input: $\boldsymbol{v}^n$, p^n, ρ^n, δt, μ, ε, $\boldsymbol{f}^n$
Output: $\boldsymbol{v}^{n+1}$, p^{n+1}, ρ^{n+1}
Initialization: Set the initial fields $\boldsymbol{v}^0$, p^0, ρ^0.
$n = 0$ to $N-1$
Step 1: Intermediate velocity Solve for $\tilde{\boldsymbol{v}}^{n+1}$:

$$\frac{\rho^n}{\delta t}\left(\tilde{\boldsymbol{v}}^{n+1} - \boldsymbol{v}^n\right) + \rho^n\left(\boldsymbol{v}^n \cdot \nabla\right)\tilde{\boldsymbol{v}}^{n+1} - 2\mu\nabla\cdot\left(\boldsymbol{d}(\tilde{\boldsymbol{v}}^{n+1})\right) + \nabla p^n = \boldsymbol{f}^n$$

Step 2: Divergence correction Solve for $\hat{\boldsymbol{v}}^{n+1}$:

$$\varepsilon\hat{\boldsymbol{v}}^{n+1} - \nabla\left(\nabla\cdot\hat{\boldsymbol{v}}^{n+1}\right) = \nabla\left(\nabla\cdot\tilde{\boldsymbol{v}}^{n+1}\right)$$

Step 3: Velocity correction

$$\boldsymbol{v}^{n+1} = \tilde{\boldsymbol{v}}^{n+1} + \hat{\boldsymbol{v}}^{n+1}$$

Step 4: Pressure update Solve for p^{n+1}:

$$\nabla\left(p^{n+1} - p^n\right) = -\frac{\rho^n}{\delta t}\hat{\boldsymbol{v}}^{n+1}$$

Step 5: Density update

$$\frac{1}{\delta t}\left(\rho^{n+1} - \rho^n\right) + \boldsymbol{v}^{n+1}\cdot\nabla\rho^n = 0$$

Output: Display or store $\boldsymbol{v}^{n+1}$, p^{n+1}, ρ^{n+1}.

2.2.8.2 Space discretization

We keep the same notation and mesh $\mathscr{D} = (\mathscr{M}, \mathscr{E}, \mathscr{P})$ introduced in Section 1.2 and in the previous subsection for the Stokes problem. Let $\delta t > 0$ be the time step and denote by $t^n = n\delta t$ the discrete times. For a cell $K \in \mathscr{M}$ the cell average (or cell unknown) at time t^n is denoted by $\boldsymbol{v}_K^n$ for the velocity and p_K^n for the pressure.

We use the first-order (LSE) linearized semi-implicit scheme (the same discrete operators are used for the projection method) that treats the convective term explicitly (from time level n) and the viscous and pressure terms implicitly (at time level $n+1$). The discrete momentum balance (4.3a) for cell K reads

$$\rho\,\frac{\boldsymbol{v}_K^{n+1} - \boldsymbol{v}_K^n}{\Delta t} + \mathrm{div}_K(\boldsymbol{v}^n, \boldsymbol{v}^{n+1}, \lambda, p^{n+1}) - \nu\,\Delta_K\boldsymbol{v}_K^{n+1} + \nabla_K p_K^{n+1} = \boldsymbol{f}_K^{n+1}, \tag{2.54}$$

where Δ_K, ∇_K and div_K are the discrete Laplace, gradient and divergence (or convection in this part) operators defined in Section 1.2, and $\boldsymbol{f}_K^{n+1}$ is the cell average of the forcing

at t^{n+1}.

The discrete incompressibility condition is enforced at t^{n+1} as in the Stokes discretization:

$$\operatorname{div}_K(1, \boldsymbol{v}_K^{n+1}, \lambda, p_K^{n+1}) = 0, \qquad \text{for all } K \in \mathscr{M}, \tag{2.55}$$

together with the discrete pressure uniqueness condition (same as for Stokes).

Coupling (2.55) and the momentum relation (2.44) yields a linear saddle-point system of the same block form as in the Stokes discretization (see equation (2.37)): at each time step we solve a linear system for $(\boldsymbol{v}_{\mathscr{D}}^{n+1}, \boldsymbol{p}_{\mathscr{D}}^{n+1})$.

2.2.9 Numerical Simulation

In order to evaluate the computational performance and efficiency of the numerical FV scheme described and analyzed previously, we pick several test problems using known analytical solutions allows to calculate the convergence rates.
All computations and figure production were carried out using a selfmade Matlab program on an Intel(R) Core(TM) i5 Laptop @ 1.70GHz and 8GB of RAM.

For $\left(\boldsymbol{v}^{(i)}, \mathbf{p}\right)$ being the vector of exact solution values on $\boldsymbol{x} \in \mathscr{P}$ with $i = 1, 2$, the relative errors of velocity and pressure are defined by:

$$e_h^{(i)} = \frac{\boldsymbol{v}^{(i)} - \boldsymbol{v}_{\mathscr{D}}^{(i)}}{\boldsymbol{v}^{(i)}} \ (i = 1, 2) \qquad\qquad \epsilon_K = \frac{p(\boldsymbol{x}_K) - p_K}{p(\boldsymbol{x}_K)}.$$

and the following associated norms are used to investigate the convergence rate

$$\|\boldsymbol{e}_{\mathscr{D}}\|_{\mathscr{D}} = \sqrt{\sum_{i=1}^{2} \left[e_{\mathscr{D}}^{(i)}, e_{\mathscr{D}}^{(i)}\right]_{\mathscr{D}}} \qquad\qquad \|\epsilon_{\mathscr{D}}\|_{0,\Omega} = \sqrt{\sum_{i=1}^{M} \epsilon_{K_i}^2}.$$

The first two test cases are for Stokes problem, while the last test if for Navier-Stokes equations.

Analytical Test 1: For the first test case, the computational domain is $\Omega = (0, 1) \times (0, 1)$, and the trigonometrical analytical solution of Stokes problem is

$$\begin{pmatrix} v_1 \\ v_2 \end{pmatrix} = \begin{pmatrix} \pi \sin^2(\pi x) \sin(2\pi y) \\ -\pi \sin(2\pi x) \sin^2(\pi y) \end{pmatrix}, \qquad p = \pi \sin(2\pi x) \sin(2\pi y).$$

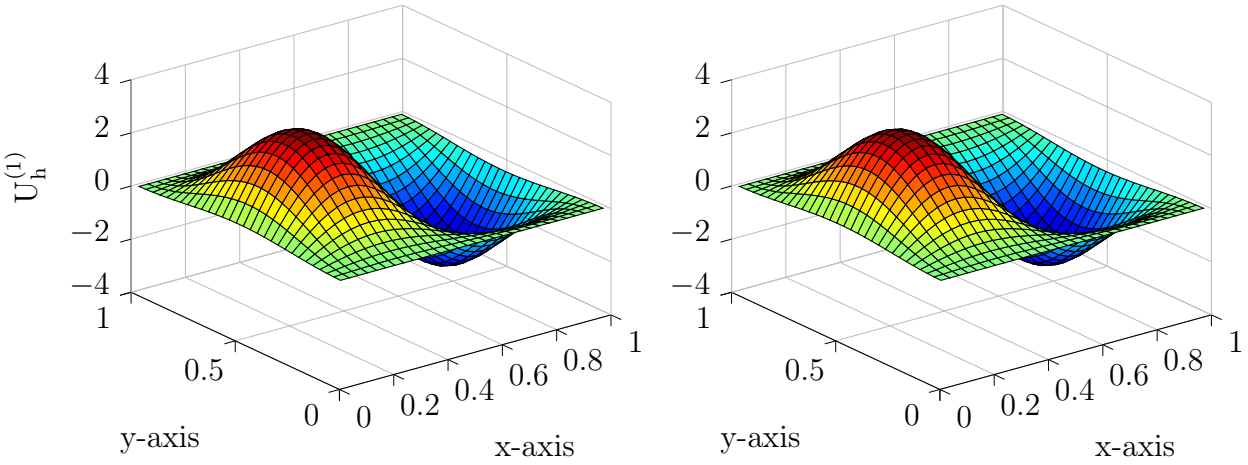

(a) LU factorization **(b)** Prediction-Correction

Figure 2.5: Test 1: Approximate velocity $\boldsymbol{v}_{\mathscr{D}}^{(1)}$ for $M = 900$ and $\varepsilon = \lambda = 0.1$

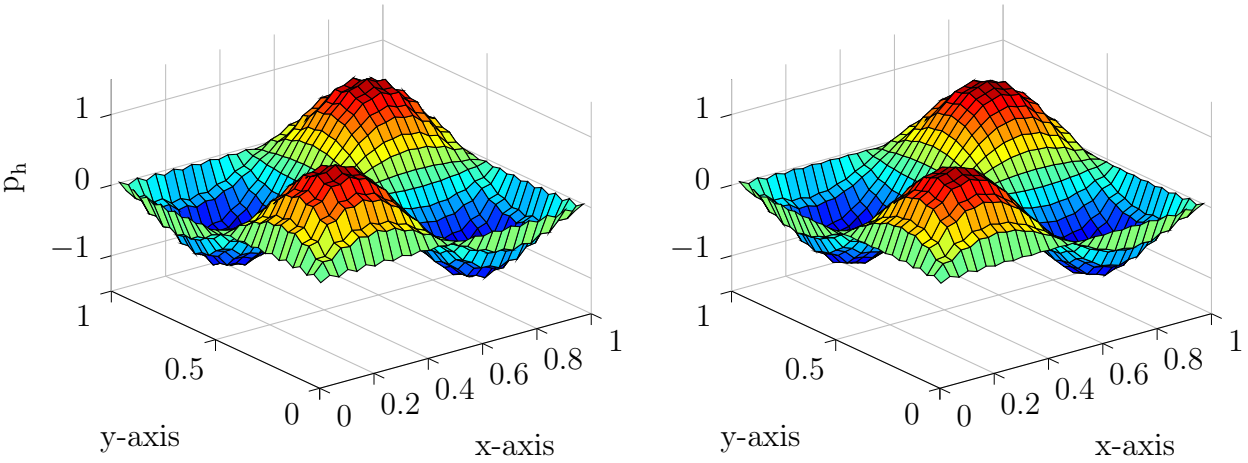

(a) LU factorization **(b)** Prediction-Correction

Figure 2.6: Test 1: Approximate pressure $p_{\mathscr{D}}$ for $M = 900$ and $\varepsilon = \lambda = 0.1$

Since the domain work is squared, we choose a rectangular grid which gives $M = Mx \times My$ rectangular (possibly squared) control volumes.

The following figures 2.5 and 2.6 shows the velocity first component and pressure 3D graphs, the graphs indicates the visual similarity between the LU and the prediction-correction solutions as far as the human eye can see.

The numerical results reported in Table 2.3 provide a direct comparison between the LU factorization and the prediction–correction approaches. For both methods, the displacement error $\|\boldsymbol{e}_{\mathscr{D}}\|$ clearly exhibits a second-order convergence rate as the mesh is refined, which represents the highest accuracy typically attainable with current finite volume discretizations (see [19, 28, 52] and many others). The pressure error $\|\boldsymbol{\epsilon}_{\mathscr{D}}\|$ converges with a rate ranging from approximately 1.0 to 1.4, depending on the solver used. While

the LU factorization approach yields slightly higher convergence rates for the strain variable, both methods demonstrate stable and consistent performance across all mesh sizes. These observations confirm the robustness, efficiency, and accuracy of the proposed finite volume formulation for the parameters $\nu = 0.1$ and $\lambda = 0.01$.

h	LU Factorization				Prediction–Correction			
	$\|\boldsymbol{e}_{\mathscr{D}}\|$	rate	$\|\boldsymbol{\epsilon}_{\mathscr{D}}\|$	rate	$\|\boldsymbol{e}_{\mathscr{D}}\|$	rate	$\|\boldsymbol{\epsilon}_{\mathscr{D}}\|$	rate
$\frac{1}{10}$	3.358E−2	–	2.844E−1	–	3.358E−2	–	2.844E−1	–
$\frac{1}{30}$	3.712E−3	2.0049	6.461E−2	1.3489	3.742E−3	2.0038	8.2898E−2	1.0496
$\frac{1}{50}$	1.335E−3	2.0023	3.208E−2	1.3709	1.3446E−3	2.0034	4.8671E−2	1.0425
$\frac{1}{70}$	6.807E−4	2.0008	2.011E−2	1.3878	6.8552E−4	2.0022	3.4503E−2	1.0224
$\frac{1}{90}$	4.118E−4	2.0003	1.409E−2	1.4124	4.1447E−4	2.0023	2.6731E−2	1.0155
$\frac{1}{110}$	2.756E−4	2.0000	1.057E−2	1.4337	2.7729E−4	2.0028	2.1816E−2	1.0126

Table 2.3: Test 1: Comparison of relative error norms and convergence rates for $\nu = 0.1$ and $\lambda = 0.01$ using LU factorization and prediction–correction approaches.

Analytical Test 2: For the second test case, one can choose a polynomial analytical solution for the same computational domain $\Omega = (0,1) \times (0,1)$.

$$\begin{pmatrix} v_1 \\ v_2 \end{pmatrix} = \begin{pmatrix} -2000(x-x^2)^2(y-y^2)(1-2y) \\ 2000(y-y^2)^2(x-x^2)(1-2x) \end{pmatrix}, \qquad p = 100\left(x^2+y^2-\frac{2}{3}\right).$$

The convergence rate is the same as in the first test case, so it will not be mentionned in this case.

In this test case, the results are illustrated through the velocity vector field (Figure 2.7) and the pressure contour plot (Figure 2.8), which allow for a clear visual comparison between the computed and exact solutions. The numerical approximations show a strong qualitative agreement with the analytical solution, indicating that the proposed scheme accurately reproduces the flow structure and pressure distribution.

Analytical Test 3: All computations and figure production of this test were carried out using a selfmade Matlab program on an AMD Ryzen™ 7 7735HS @ 5.0 GHz Processor and 16GB of RAM.

For the last test case, the computational domain is $\Omega = (0,1) \times (0,1)$, and the trigono-

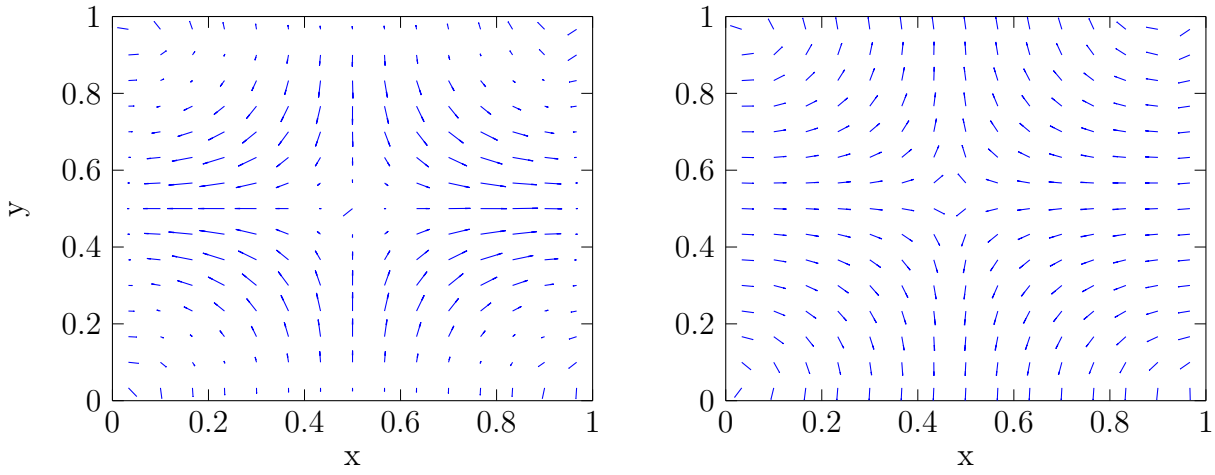

(a) LU factorization **(b)** Prediction-Correction

Figure 2.7: Test 2: Approximate velocity vector field $\boldsymbol{v}_{\mathscr{D}}$ for $M = 225$ and $\varepsilon = \lambda = 0.1$

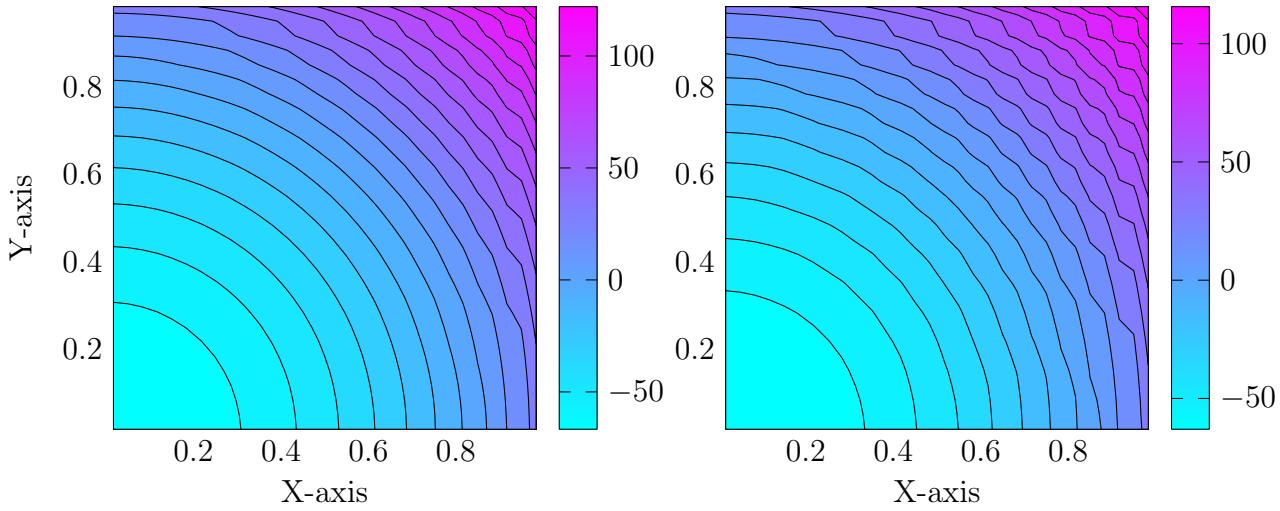

(a) LU factorization **(b)** Prediction-Correction

Figure 2.8: Test 2: Contour of approximate pressure $p_{\mathscr{D}}$ for $M = 900$ and $\varepsilon = \lambda = 0.1$

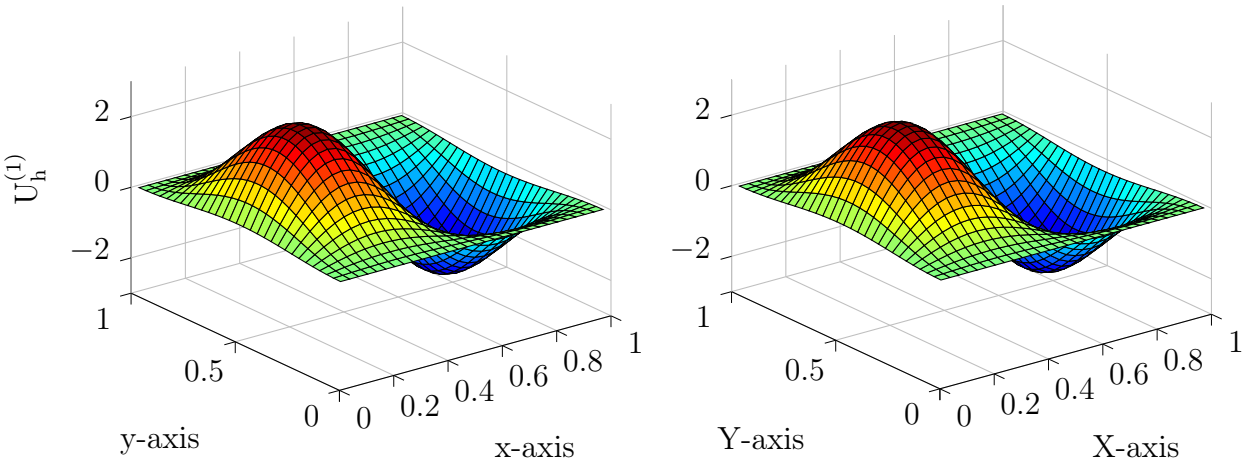

(a) Direct Solver **(b)** VPP Solver

Figure 2.9: Test 3: Approximate velocity $\boldsymbol{v}_{\mathscr{D}}^{(1)}$ at $t = 0.2$ for $M = 900$, $dt = 0.01$ and $\varepsilon = 10^{-3}$

metrical analytical solution of Navier-Stokes equations is

$$\begin{pmatrix} v_1 \\ v_2 \end{pmatrix} = \begin{pmatrix} \pi \sin^2(\pi x) \sin(2\pi y) e^{-t} \\ -\pi \sin(2\pi x) \sin^2(\pi y) e^{-t} \end{pmatrix}, \qquad p = \pi \sin(2\pi x) \sin(2\pi y) \left(1 - e^{-t}\right).$$

Since the domain work is squared, we choose a rectangular grid which gives $M = Mx \times My$ rectangular (possibly squared) control volumes.

Figure 2.9 presents the first component of the velocity field. The plot highlights the close visual agreement between the solutions obtained using the direct LU decomposition solver and the prediction-correction (VPP) method.

h	Direct LU solver			VPP solver with $\varepsilon = 10^{-3}$ and $r = 10^{-5}$		
	$\|\mathbf{e}_{\mathscr{D}}\|$	cv. rate	Exec. time (s)	$\|\mathbf{e}_{\mathscr{D}}\|$	cv. rate	Exec. time (s)
$\frac{1}{10}$	3.4205E−2	–	1.2136E−1	3.5057E−2	–	8.7285E−2
$\frac{1}{30}$	3.8457E−3	1.9892	3.968E+0	3.8855E−3	2.0023	3.5955E+0
$\frac{1}{50}$	1.4306E−3	1.9358	4.17E+1	1.4404E−3	1.9427	3.7979E+1
$\frac{1}{70}$	7.6733E−4	1.8514	2.5125E+2	7.8945E−4	1.7871	2.1107E+2
$\frac{1}{90}$	4.9521E−4	1.7426	1.274E+3	5.4346E−4	1.4857	9.8785E+2

Table 2.4: Test 3: Comparison of relative error norms, convergence rates, and execution times at $t = 0.2$ for $\nu = 1$ and $\delta t = 0.01$ using direct LU factorization and prediction–correction (VPP) approaches.

Table 2.4 presents a comparative analysis between the direct LU solver and the

prediction-correction (VPP) solver with time step size $\delta t = 10^{-2}$ and parameters $\varepsilon = 10^{-3}$ and $r = 10^{-5}$ for different space step sizes h. Both methods produce almost identical relative error norms, confirming the accuracy and consistency of the VPP scheme compared to the direct LU approach. The convergence rates start close to the second-order accuracy and then slightly decrease as the mesh is further refined. This behavior is commonly attributed to the accumulation of round-off errors and the increasing conditioning of the discrete system on finer grids. In terms of computational performance, the LU solver exhibits a rapid growth in execution time with mesh refinement, whereas the VPP solver achieves similar accuracy with noticeably reduced computational cost. This highlights the efficiency and scalability of the VPP approach for large-scale or high-resolution simulations where direct solvers become computationally demanding.

h	1/10	1/30	1/50	1/70	1/90
$\|\mathbf{e}_{\mathscr{D}}\|$	1.8275E−2	2.1302E−3	7.7645E−4	39804E−4	24118E−4
cv. rate	−	1.9564	1.9757	1.9859	1.9935

Table 2.5: Test 3: Relative error norms and convergence rates at $t = 0.0002$ for $\delta t = 10^{-5}$, and parameters $\varepsilon = 10^{-3}$, $r = 10^{-5}$ using the VPP solver.

When the time step size is reduced to $\delta t = 10^{-5}$ while keeping the same parameters $\varepsilon = 10^{-3}$ and $r = 10^{-5}$, the overall accuracy of the numerical solution improves noticeably. The relative error norms are significantly smaller compared to the case with $\delta t = 10^{-2}$, and the convergence rate remains consistently close to the theoretical second-order value across all mesh sizes, from $h = 1/10$ to $h = 1/90$. Unlike the previous configuration, no deterioration in the convergence rate is observed as the mesh is refined. This behavior indicates that temporal discretization errors were dominant in the previous test, and that reducing the time step allows the spatial accuracy of the scheme to reach its full second-order potential.

Chapter 3

Elastic–Elastic Interactions

Introduction

Elastic interactions between materials play a central role in many physical and engineering systems, including biomechanics, geomechanics, and composite structures. In many such systems, distinct elastic subdomains interact across interfaces where discontinuities in displacement or stress naturally arise. Accurately capturing these discontinuities poses substantial mathematical and numerical challenges.

The well-posedness of mathematical models for the Stokes / Brinkman problem with J.E.B.C. at fluid-porous interfaces has been rigorously analyzed in [3, 4], including the Whitaker–Ochoa-Tapia and Beavers–Joseph interface conditions. These works focus on fluid–porous interaction problems and provide a unified variational framework for various physically relevant interface conditions. In contrast, the treatment of linear elasticity problems involving an elastic medium coupled with an extended domain through J.E.B.C. has been addressed using fictitious domain approaches in [50, 80, 81], extending the methodology to elasticity interfaces.

In this chapter, we investigate the well-posedness of an elastic–elastic interaction problem governed by jump-embedded boundary conditions. We then study the asymptotic convergence of the model toward an elastic–elastic transmission problem with spring-type interface conditions. We begin by formulating the variational problem and establishing its well-posedness using classical tools from functional analysis. The analysis is then extended to special cases, such as the spring-law interface and its penalized approximation, for which we demonstrate strong convergence and derive *a priori* error estimates.

To address the computational aspects of our framework, we develop a finite volume method (FVM) specifically tailored to this class of problems, drawing on established techniques [19, 28, 36]. Our FVM implementation offers three key advantages: first, strict

enforcement of local conservation laws; second, robust handling of complex interface geometries; and third, a unified approach to various transmission conditions.

We validate our approach through extensive numerical experiments examining vertical, L-shaped, and rectangular interface configurations, which collectively demonstrate the method's accuracy and convergence properties under systematic grid refinement.

The novelty of this work is that, to the best of our knowledge, it is the first to rigorously establish the well-posedness and convergence analysis of elastic–elastic interaction models governed by J.E.B.C., combined with a finite volume discretization specifically designed to ensure local conservation and accurately handle complex interface geometries. This new framework generalizes existing fictitious domain approaches beyond fluid–porous systems to purely elastic coupled problems with discontinuous interface conditions.

3.1 A well-posed elastic–elastic problem with jump embedded boundary conditions

We work on the composite region

$$\Omega = \Omega_1 \cup \Sigma \cup \Omega_2,$$

where Ω_1 and Ω_2 are two subdomains joined along the interface Σ. For each $i \in \{1, 2\}$, let

$$\Gamma_i = \partial\overline{\Omega}_i \setminus \Sigma$$

be the portion of $\partial\Omega_i$ not lying on Σ. We denote by ν the normal outward unit vector on $\partial\Omega$, and by n the normal outward unit vector on the interface Σ, oriented from Ω_1 into Ω_2.

For $i = 1, 2$, let $\sigma_i(u_i) = \mathbb{C}_i : \varepsilon(u_i)$ denote the Cauchy stress tensor in the linear elasticity domain Ω_i, where u_i is the displacement field, $\varepsilon(u_i) = \frac{1}{2}(\nabla u_i + \nabla u_i^\top)$ is the infinitesimal strain tensor, and $\mathbb{C}_i$ is the fourth-order elasticity tensor, assumed to be symmetric and uniformly elliptic. The elastic–elastic transmission problem with jump-embedded boundary conditions, based on a fictitious domain approach, is posed on the

interface Σ and reads:

$$-\nabla \cdot \sigma_1(u) = f_1 \quad \text{in } \Omega_1, \tag{3.1}$$
$$-\nabla \cdot \sigma_2(u) = f_2 \quad \text{in } \Omega_2, \tag{3.2}$$
$$u = 0 \quad \text{on } \Gamma_1 \cup \Gamma_2, \tag{3.3}$$
$$[\![\sigma(u) \cdot n]\!]_\Sigma = M\overline{u}|_\Sigma - g \quad \text{on } \Sigma, \tag{3.4}$$
$$\overline{\sigma(u) \cdot n}|_\Sigma = S[\![u]\!]_\Sigma - h \quad \text{on } \Sigma, \tag{3.5}$$

with $f_i \in L^2(\Omega_i)^d$ and $u|_{\Omega_i} = u_i$ for $i = 1, 2$.

The jump and the arithmetic mean over Σ are defined as follows:

$$[\![u]\!]_\Sigma = u_2|_\Sigma - u_1|_\Sigma, \qquad [\![\sigma(u) \cdot n]\!]_\Sigma = \sigma_2(u_2) \cdot n - \sigma_1(u_1) \cdot n,$$
$$\overline{u}|_\Sigma = (u_2|_\Sigma + u_1|_\Sigma)/2, \quad \overline{\sigma(u) \cdot n}|_\Sigma = (\sigma_1(u_1) \cdot n + \sigma_2(u_2) \cdot n)/2.$$

The functions $g, h \in H^{1/2}(\Sigma)^d$ represent interface force terms and $M(x), S(x) \in \mathbb{R}^{d\times d}$ are L^∞ measurable functions with symmetric matrix values. These, together with $\mathbb{C}_1$ and $\mathbb{C}_2$, are assumed to satisfy the following ellipticity conditions: for $i = 1, 2$, let $\alpha_1, \alpha_2, M_0, S_0 > 0$ be constants such that

$$\mathbb{C}_i \in L^\infty(\Omega_i)^{d\times d} \text{ and } \mathbb{C}_i(x)\xi : \xi \geq \alpha_i|\xi|^2, \quad \text{a.e. in } \Omega_i, \quad \forall \xi \in \mathbb{R}^{d\times d}, \tag{A1}$$
$$M(x)\xi \cdot \xi \geq M_0|\xi|^2, \quad S(x)\xi \cdot \xi \geq S_0|\xi|^2, \quad \text{a.e. on } \Sigma, \quad \forall \xi \in \mathbb{R}^d, \tag{A2}$$

where $|\cdot|$ denotes the Frobenius norm.

Remark 3.1. *Throughout this chapter, we denote by u the global displacement field defined in the union domain $\Omega = \Omega_1 \cup \Omega_2$, such that*

$$u|_{\Omega_1} = u_1, \qquad u|_{\Omega_2} = u_2.$$

For notational convenience, we write u without subscripts and interpret it piecewise on each subdomain. Similarly, all expressions involving u, such as ∇u, $\varepsilon(u)$, and the bilinear form $a(u, w)$, are to be understood as acting separately on Ω_1 and Ω_2, with appropriate traces defined on the interface Σ.

Weak Formulation: The functional space required for the weak formulation is introduced below

$$W \equiv \{w \in L^2(\Omega)^d : w|_{\Omega_1} \in H^1_{0,\Gamma_1}(\Omega_1)^d,\ w|_{\Omega_2} \in H^1_{0,\Gamma_2}(\Omega_2)^d\},$$

with the norm:

$$\|w\|_W^2 = \|\nabla w\|_{0,\Omega_1}^2 + \|\nabla w\|_{0,\Omega_2}^2.$$

Hence, the variational formulation becomes: Find $u \in W$ such that for all $w \in W$,

$$a(u, w) = \ell(w), \tag{3.6}$$

with

$$\begin{aligned} a(u,w) = &\int_{\Omega_1} \mathbb{C}_1\varepsilon(u) : \varepsilon(w)\,dx + \int_{\Omega_2} \mathbb{C}_2\varepsilon(u) : \varepsilon(w)\,dx \\ &+ \int_\Sigma M\overline{u}|_\Sigma \cdot \overline{w}|_\Sigma\,ds + \int_\Sigma S[\![u]\!]_\Sigma \cdot [\![w]\!]_\Sigma\,ds, \end{aligned}$$

and

$$\ell(w) = \int_\Omega f \cdot w\,dx + \int_\Sigma g \cdot \overline{w}|_\Sigma\,ds + \int_\Sigma h \cdot [\![w]\!]_\Sigma\,ds,$$

where $\int_\Omega f \cdot w\,dx = \int_{\Omega_1} f_1 \cdot w\,dx + \int_{\Omega_2} f_2 \cdot w\,dx$.

Before we proceed with the solvability theorem, we state the following result, which will be used in its proof.

Proposition 3.1. *Let $u \in H^1(\Omega)^d$, and define*

$$\varepsilon(u) \;=\; \frac{1}{2}\big(\nabla u + (\nabla u)^\top\big)$$

as the symmetric gradient of u. Then the following estimate holds:

$$\|\varepsilon(u)\|_{L^2(\Omega)} \;\le\; \|\nabla u\|_{L^2(\Omega)}. \tag{3.7}$$

Proof. For each $x \in \Omega$, we write:

$$\nabla u = \varepsilon(u) + \omega(u), \quad \text{with } \omega(u) := (\nabla u - \nabla u^\top)/2,$$

so that $\varepsilon(u)$ is symmetric and $\omega(u)$ is skew-symmetric. The Frobenius inner product of these two matrices vanishes:

$$\langle \varepsilon(u), \omega(u) \rangle = 0,$$

and therefore, by the Pythagorean identity for matrices,

$$|\nabla u|^2 = |\varepsilon(u)|^2 + |\omega(u)|^2 \ge |\varepsilon(u)|^2.$$

Integrating over Ω taking square roots yields the desired inequality. □

Now, we present the following global solvability theorem.

Theorem 3.1 (Global Solvability of the Elastic/Elastic Model with J.E.B.C.)**.** *Let the volume forces $f_i \in L^2(\Omega_i)^d$ for $i = 1, 2$, and let the interface forces $g, h \in H^{1/2}(\Sigma)^d$. If $\mathbb{C}_1$, $\mathbb{C}_2$, M, and S satisfy the assumptions (A1)–(A2), then the problem (3.1)–(3.5) admits a* ***unique weak solution*** *$u \in W$ that satisfies the variational formulation (3.6).*

In addition, there exists a constant $C > 0$, depending only on the structural parameters (but not on the data), for which the following bound holds:

$$\|u\|_W \leq C \left(\|f\|_{0,\Omega} + \|h\|_{1/2,\Sigma} + \|g\|_{1/2,\Sigma} \right).$$

Proof. **Coercivity of $a(\cdot,\cdot)$:** Let $u \in W$. The bilinear form gives:

$$\begin{aligned} a(u,u) = &\int_{\Omega_1} \mathbb{C}_1\varepsilon(u) : \varepsilon(u)\, dx + \int_{\Omega_2} \mathbb{C}_2\varepsilon(u) : \varepsilon(u)\, dx \\ &+ \int_\Sigma M\overline{u}|_\Sigma \cdot \overline{u}|_\Sigma\, ds + \int_\Sigma S[\![u]\!]_\Sigma \cdot [\![u]\!]_\Sigma\, ds. \end{aligned}$$

From the uniform ellipticity assumption (A1) and by applying Korn's inequality on each subdomain Ω_i, we obtain, for $i = 1, 2$,

$$\begin{aligned} \int_{\Omega_i} \mathbb{C}_i\varepsilon(u) : \varepsilon(u)\, dx &\geq \alpha_i \|\varepsilon(u)\|^2_{0,\Omega_i} \\ &\geq \frac{\alpha_i}{C_i^2} \|\nabla u\|^2_{0,\Omega_i}, \end{aligned}$$

where $C_i > 0$ is the Korn constant in $H^1_{0,\Gamma_i}(\Omega_i)^d \subset H^1(\Omega_i)^d$, and $\alpha_i > 0$ is the ellipticity constant of $\mathbb{C}_i$.

For the interface terms, the coercivity assumption (A2) on M and S gives:

$$\int_\Sigma M\overline{u}|_\Sigma \cdot \overline{u}|_\Sigma\, ds \geq M_0 \|\overline{u}|_\Sigma\|^2_{0,\Sigma}, \quad \int_\Sigma S[\![u]\!]_\Sigma \cdot [\![u]\!]_\Sigma\, ds \geq S_0 \|[\![u]\!]_\Sigma\|^2_{0,\Sigma}.$$

Combining all contributions, we obtain:

$$\begin{aligned} a(u,u) &\geq \frac{\alpha_1}{C_1^2} \|\nabla u\|^2_{0,\Omega_1} + \frac{\alpha_2}{C_2^2} \|\nabla u\|^2_{0,\Omega_2} \\ &\quad + M_0 \|\overline{u}|_\Sigma\|^2_{0,\Sigma} + S_0 \|[\![u]\!]_\Sigma\|^2_{0,\Sigma} \\ &\geq c_0 \|u\|^2_W, \end{aligned}$$

where $c_0 := \min\left\{ \frac{\alpha_1}{C_1^2}, \frac{\alpha_2}{C_2^2} \right\} > 0$.

This establishes the coercivity of $a(\cdot,\cdot)$ on W.

Continuity of $a(\cdot,\cdot)$: To establish continuity of the bilinear form $a(u,w)$ on $W \times W$, we

demonstrate the existence of a constant $c_1 > 0$ such that

$$|a(u,w)| \le c_1 \|u\|_W \|w\|_W \quad \text{for all } u, w \in W.$$

The bilinear form consists of volume and interface terms. For the volume contributions, we use the boundedness of the elasticity tensors $\mathbb{C}_1$ and $\mathbb{C}_2$, together with inequality (3.7), to write:

$$\begin{aligned}\left| \int_{\Omega_i} \mathbb{C}_i \varepsilon(u) : \varepsilon(w)\, dx \right| &\le \|\mathbb{C}_i\|_{\infty,\Omega_i} \|\varepsilon(u)\|_{0,\Omega_i} \|\varepsilon(w)\|_{0,\Omega_i} \\ &\le \Lambda_i \|\nabla u\|_{0,\Omega_i} \|\nabla w\|_{0,\Omega_i},\end{aligned}$$

for some constants $\Lambda_i > 0$ with $i = 1, 2$.

The interface terms are handled using the trace inequality. Since the functions $u \in W$ satisfy $u|_{\Omega_i} \in H^1_{0,\Gamma_i}(\Omega_i)^d$, and since $\Sigma \subset \partial\Omega_i$ is Lipschitz for $i = 1, 2$, the trace inequality, combined with the Poincaré inequality, implies that

$$\begin{aligned}\|\overline{u}|_\Sigma\|_{0,\Sigma} &= \frac{1}{2}\|u_1|_\Sigma + u_2|_\Sigma\|_{0,\Sigma} \le c_1 \left(\|\nabla u_1\|_{0,\Omega_1} + \|\nabla u_2\|_{0,\Omega_2}\right) \le c_1' \|u\|_W, \\ \|[\![u]\!]_\Sigma\|_{0,\Sigma} &= \|u_2|_\Sigma - u_1|_\Sigma\|_{0,\Sigma} \le c_2 \left(\|\nabla u_1\|_{0,\Omega_1} + \|\nabla u_2\|_{0,\Omega_2}\right) \le c_2' \|u\|_W.\end{aligned} \tag{3.8}$$

As a result, the interface terms in the bilinear form satisfy

$$\left| \int_\Sigma M\overline{u}|_\Sigma \cdot \overline{w}|_\Sigma\, ds \right| \le \|M\|_{\infty,\Sigma} \|\overline{u}|_\Sigma\|_{0,\Sigma} \|\overline{w}|_\Sigma\|_{0,\Sigma} \le C_M \|u\|_W \|w\|_W,$$

and

$$\left| \int_\Sigma S[\![u]\!]_\Sigma \cdot [\![w]\!]_\Sigma\, ds \right| \le \|S\|_{\infty,\Sigma} \|[\![u]\!]_\Sigma\|_{0,\Sigma} \|[\![w]\!]_\Sigma\|_{0,\Sigma} \le C_S \|u\|_W \|w\|_W.$$

Combining the volume and interface estimates, we conclude that all contributions of the bilinear form are bounded by a constant times $\|u\|_W \|w\|_W$, and thus $a(\cdot,\cdot)$ is continuous on $W \times W$.

Continuity of $\ell(\cdot)$: We now prove that the linear form

$$\ell(w) := \int_\Omega f \cdot w\, dx + \int_\Sigma h \cdot [\![w]\!]_\Sigma\, ds + \int_\Sigma g \cdot w|_\Sigma\, ds,$$

is continuous on W.

Using the Cauchy–Schwarz inequality and the trace regularity of functions in W, we estimate:

$$|\ell(w)| \le \|f\|_{0,\Omega} \|w\|_{0,\Omega} + \|h\|_{1/2,\Sigma} \|[\![w]\!]_\Sigma\|_{1/2,\Sigma} + \|g\|_{1/2,\Sigma} \|w|_\Sigma\|_{1/2,\Sigma}.$$

Therefore, by applying the Poincaré inequality to the volume term and using inequality (3.8) for the interface terms, there exists a constant $c_2 > 0$ such that:

$$|\ell(w)| \leq c_2 \left(\|f\|_{0,\Omega} + \|h\|_{1/2,\Sigma} + \|g\|_{1/2,\Sigma} \right) \|w\|_W,$$

which proves the continuity of ℓ on W.

The existence and uniqueness of the solution are guaranteed by the Lax–Milgram theorem.

A priori estimate. Let $u \in W$ be the unique solution to the variational problem:

$$a(u, w) = \ell(w) \quad \text{for all } w \in W.$$

By coercivity of the bilinear form $a(\cdot, \cdot)$ and continuity of $\ell(\cdot)$, there exists $c_0 > 0$, $c_2 > 0$ such that

$$c_0 \|u\|_W^2 \leq c_2 \left(\|f\|_{0,\Omega} + \|h\|_{1/2,\Sigma} + \|g\|_{1/2,\Sigma} \right) \|u\|_W.$$

Assuming that $\|u\|_W \neq 0$, there exists a constant $C > 0$, independent of the data, such that

$$\|u\|_W \leq C \left(\|f\|_{0,\Omega} + \|h\|_{1/2,\Sigma} + \|g\|_{1/2,\Sigma} \right).$$

□

3.2 The elastic/elastic problem with interface jump conditions of Spring-Law type

We now consider the problem consisting of equations (3.1)–(3.3), along with interface jump conditions inspired by spring-law-type interface models:

$$[\![\sigma(u) \cdot n]\!]_\Sigma = Au|_\Sigma - g \quad \text{and} \quad [\![u]\!]_\Sigma = 0 \quad \text{on } \Sigma, \tag{3.9}$$

which gives the following problem denoted by (P_l):

$$\begin{cases} -\nabla \cdot \sigma_1(u) = f_1 & \text{in } \Omega_1, \\ -\nabla \cdot \sigma_2(u) = f_2 & \text{in } \Omega_2, \\ u = 0 & \text{on } \Gamma_1 \cup \Gamma_2, \\ [\![\sigma(u) \cdot n]\!]_\Sigma = Au|_\Sigma - g & \text{on } \Sigma, \\ [\![u]\!]_\Sigma = 0 & \text{on } \Sigma, \end{cases} \tag{P_l}$$

where A satisfies the same assumption as those on M above, and $g \in H^{1/2}(\Sigma)^d$ is a given interface force.

Remark 3.2. *In the case where $[\![u]\!]_\Sigma = q$ on Σ with $q \in H^{1/2}(\Sigma)^d$, we can apply a change of variable*

$$\tilde{u}_1 := u_1 \quad \text{in } \Omega_1, \qquad \tilde{u}_2 := u_2 - v \quad \text{in } \Omega_2,$$

where $v \in H^1(\Omega_2)^d$ is the lifting (inverse of the trace mapping) of q.

Hence, it follows that

$$[\![\tilde{u}]\!]_\Sigma = 0 \quad \text{and} \quad [\![\sigma(\tilde{u}) \cdot n]\!]_\Sigma = A\tilde{u}|_\Sigma - \tilde{g} \quad \text{on } \Sigma,$$

where $\tilde{g} := g + \sigma_2(v) \cdot n - (1/2)Aq$.

The proofs in the remainder of this chapter are made for the zero-jump condition across the interface.

The corresponding weak formulation of problem (P_l) reads:

Find u in the subspace V of W, such that:

$$\begin{aligned} \int_{\Omega_1} \mathbb{C}_1\varepsilon(u) : \varepsilon(w)\, dx + \int_{\Omega_2} \mathbb{C}_2\varepsilon(u) : \varepsilon(w)\, dx + \int_\Sigma Au|_\Sigma \cdot w|_\Sigma\, ds \\ = \int_\Omega f \cdot w\, dx + \int_\Sigma g \cdot w\, ds, \quad \forall w \in V, \end{aligned} \tag{3.10}$$

where $V \equiv \{w \in W : \quad [\![w]\!]_\Sigma = 0 \quad \text{on } \Sigma\}$.

Corollary 3 (Well-posedness for S-L.I.C. model)**.** *Let $f_i \in L^2(\Omega_i)^d$ for $i = 1, 2$, and let $g \in H^{1/2}(\Sigma)^d$. If $\mathbb{C}_1$ and $\mathbb{C}_2$ satisfy assumption (A1), and A satisfies assumption (A2), then there exists a unique solution $u \in V$ to the weak form (3.10).*

Furthermore, for some constant $C > 0$ the following estimate holds:

$$\|u\|_W \leq C \left(\|f\|_{0,\Omega} + \|g\|_{1/2,\Sigma} \right).$$

The proof of this corollary will not be presented here, as it is straightforward and follows directly from the Lax-Milgram theorem.

3.3 Penalized problem of elastic–elastic model with J.E.B.C.

Let us consider the penalized problem, denoted by (P_r), given by (3.1)-(3.5) with $h = 0$, $M = A$ and $S = \dfrac{1}{r}\boldsymbol{I}$. The weak form of the penalized problem (P_r) reads, for all $r > 0$:

Find $u_r \in W$ such that:

$$\begin{aligned}\int_{\Omega_1} \mathbb{C}_1\varepsilon(u_r) : \varepsilon(w)\,dx + \int_{\Omega_2} \mathbb{C}_2\varepsilon(u_r) : \varepsilon(w)\,dx + \int_\Sigma M\overline{u}_r|_\Sigma \cdot \overline{w}|_\Sigma\,ds \\ + \frac{1}{r}\int_\Sigma [\![u_r]\!]_\Sigma \cdot [\![w]\!]_\Sigma\,ds = \int_\Omega f\cdot w\,dx + \int_\Sigma g\cdot w\,ds, \quad \forall w \in W.\end{aligned} \tag{3.11}$$

Equivalently, the solution of (3.10) arises as the limit of the penalized problem (3.11) as the penalty parameter r tends to zero. The theorem below makes this convergence precise.

Theorem 3.2 (Convergence to the elastic/elastic model with S-L.I.C.)**.** *Let $f_i \in L^2(\Omega_i)^d$ for $i = 1, 2$, let $g \in H^{1/2}(\Sigma)^d$, and for each $r > 0$, let $u_r \in W$ be the unique weak solution of the penalized problem (P_r) (i.e., the solution of (3.11)).*

Then, as $r \to 0$, the sequence (u_r) converges strongly in W to the unique solution u of the weak form (3.10), with $[\![u]\!]_\Sigma = 0$ satisfied automatically.

Moreover, there exist two constants $C > 0$ and $C'(f_1, f_2, g) > 0$, independent of r, such that:

$$\|u_r - u\|_W \le C\sqrt{r}, \quad \text{and} \quad \|[\![u_r]\!]_\Sigma\|_{0,\Sigma} \le C'r.$$

Proof. We aim to show that the family $(u_r)_{r>0} \subset W$, consisting of solutions to the penalized problem (P_r), converges strongly in W to the unique solution $u \in V$ of the limit problem, with $[\![u]\!]_\Sigma = 0$. Before starting, let us assume that $\|u_r\|_W \neq 0$ and $\|[\![u_r - u]\!]_\Sigma\|_{0,\Sigma} \neq 0$; the cases where these quantities vanish are trivial and require no special handling.

Uniform estimate: Choosing $w = u_r$ in the weak form (3.11) and applying Korn's inequality and the coercivity of $\mathbb{C}_1$ and $\mathbb{C}_2$, we get for $i = 1, 2$

$$\int_{\Omega_i} \mathbb{C}_i\varepsilon(u) : \varepsilon(u)\,dx \ge \alpha_i \int_{\Omega_i} |\varepsilon(u)|^2\,dx \ge \frac{\alpha_i}{C_i}\int_{\Omega_i} |\nabla u|^2\,dx,$$

where $\alpha_i > 0$ and $C_i > 0$ are the coercivity constant of $\mathbb{C}_i$ and Korn's constant respectively, for $i = 1, 2$. That yields

$$\begin{aligned}c_0' \int_{\Omega_1\cup\Omega_2} |\nabla u|^2\,dx + \int_\Sigma M\overline{u}_r|_\Sigma \cdot \overline{u}_r|_\Sigma\,ds + \frac{1}{r}\int_\Sigma [\![u_r]\!]_\Sigma \cdot [\![u_r]\!]_\Sigma\,ds \\ \le C\left(\|f\|_{0,\Omega} + \|g\|_{1/2,\Sigma}\right)\|u_r\|_W,\end{aligned} \tag{3.12}$$

where $c_0' = \min\{\frac{\alpha_1}{C_1}, \frac{\alpha_2}{C_2}\}$ and $C > 0$.

Using the coercivity of $a(\cdot,\cdot)$, we obtain:

$$c\|u_r\|_W^2 + \frac{1}{r}\|[\![u_r]\!]_\Sigma\|_{0,\Sigma}^2 \le C\left(\|f\|_{0,\Omega} + \|g\|_{1/2,\Sigma}\right)\|u_r\|_W. \tag{3.13}$$

Dropping the interface term in the left-hand side and divide both sides by $c\|u_r\|_W$ to obtain, for a constant $c' > 0$:

$$\|u_r\|_W \leq c' \left(\|f\|_{0,\Omega} + \|g\|_{1/2,\Sigma} \right). \tag{3.14}$$

Again dropping a term in the left-hand side of (3.13), but this time we drop $c\|u_r\|_W$, then by using inequality (3.14) to the bound $\|u_r\|_W$ in the right-hand side of (3.13) we obtain:

$$\|[\![u_r]\!]_\Sigma\|_{0,\Sigma} \leq C'\sqrt{r}. \tag{3.15}$$

where $C' = C'(f_1, f_2, g) > 0$ is a constant depending of the data.

Convergence as $r \to 0$: From the uniform bound (3.14), the family $(u_r)_{r>0} \subset W$ is bounded in the Hilbert space W. Therefore, by the Banach–Alaoglu theorem, there exists a function $u \in W$ and a subsequence (still denoted u_r) such that

$$u_r \rightharpoonup u \quad \text{weakly in } W \quad \text{as } r \to 0.$$

Moreover, by the compact embedding $W \hookrightarrow L^2(\Omega)^d$, this convergence is strong in $L^2(\Omega)^d$.

In addition, from the uniform bound (3.15), the rescaled family $\left(\frac{1}{\sqrt{r}} [\![u_r]\!]_\Sigma \right)_{r>0}$ is bounded in the Hilbert space $L^2(\Sigma)^d$. Thus, by the Banach–Alaoglu theorem, there exists a function $\psi \in L^2(\Sigma)^d$ and a subsequence (still indexed by r) such that

$$\frac{1}{\sqrt{r}} [\![u_r]\!]_\Sigma \rightharpoonup \psi \quad \text{weakly in } L^2(\Sigma)^d \quad \text{as } r \to 0.$$

Moreover, we have $[\![u_r]\!]_\Sigma \to 0$ as $r \to 0$. Since the trace operator is continuous from W to $L^2(\Sigma)^d$, and $[\![u_r]\!]_\Sigma$ converges strongly to zero in $L^2(\Sigma)^d$, it follows that

$$[\![u]\!]_\Sigma = 0.$$

Therefore, u belongs to $V \subset W$.

Taking the limit $r \to 0$ in the weak formulation (3.11) with $w \in V$ and noting that $\overline{u}|_\Sigma = u|_\Sigma$, we recover the limit problem:

$$\int_{\Omega_1} \mathbb{C}_1 \varepsilon(u) : \varepsilon(w)\, dx + \int_{\Omega_2} \mathbb{C}_2 \varepsilon(u) : \varepsilon(w)\, dx + \int_\Sigma Mu \cdot w\, ds = \int_\Omega f \cdot w\, dx + \int_\Sigma g \cdot w\, ds,$$

which admits a unique solution in V as stated in corollary 3.

Error estimate: Let u_r and u be the solutions satisfying their respective variational

formulations, we subtract them to obtain:

$$\int_{\Omega_1} \mathbb{C}_1|\varepsilon(u_r-u)|^2\,dx + \int_{\Omega_2} \mathbb{C}_2|\varepsilon(u_r-u)|^2\,dx + \int_\Sigma M|\overline{u}_{r|\Sigma}-u|^2\,ds \\ +\frac{1}{r}\|[\![u_r-u]\!]_\Sigma\|^2_{0,\Sigma} = \int_\Sigma \psi\cdot[\![u_r-u]\!]_\Sigma\,ds.$$

Using the coercivity of $\mathbb{C}_1, \mathbb{C}_2$ and M and Cauchy-Scwharz inequality, we get

$$\begin{aligned}&\alpha_0\int_{\Omega_1\cup\Omega_2}|\varepsilon(u_r-u)|^2\,dx + M_0\|\overline{u}_{r|\Sigma}-u\|^2_\Sigma \\ &+\frac{1}{r}\|[\![u_r-u]\!]_\Sigma\|^2_{0,\Sigma} \le \|\psi\|_{0,\Sigma}\|[\![u_r-u]\!]_\Sigma\|_{0,\Sigma},\end{aligned} \tag{3.16}$$

where $\alpha_0 = \min\{\alpha_1,\alpha_2\}$.

Dropping some positive terms in the left-hand side and multiplying by $r/\|[\![u_r-u]\!]_\Sigma\|_{0,\Sigma}$ we get:

$$\|[\![u_r-u]\!]_\Sigma\|_{0,\Sigma} \le r\|\psi\|_{0,\Sigma}. \tag{3.17}$$

Since $[\![u]\!]_\Sigma = 0$, we have

$$\|[\![u_r-u]\!]_\Sigma\|_{0,\Sigma} = \|[\![u_r]\!]_\Sigma - [\![u]\!]_\Sigma\|_{0,\Sigma} = \|[\![u_r]\!]_\Sigma\|_{0,\Sigma},$$

and thus the error estimate becomes

$$\|[\![u_r]\!]_\Sigma\|_{0,\Sigma} \le r\|\psi\|_{0,\Sigma}.$$

Applying Young's inequality $ab \le a^2/2r + b^2r/2$ to the right-hand side of (3.16), we obtain

$$\alpha_0\|\varepsilon(u_r-u)\|^2_{0,\Omega} + M_0\|\overline{u}_{r|\Sigma}-u\|^2_{0,\Sigma} + \frac{1}{r}\|[\![u_r-u]\!]_\Sigma\|^2_{0,\Sigma} \\ \le \frac{1}{2r}\|[\![u_r-u]\!]_\Sigma\|^2_{0,\Sigma} + \frac{r}{2}\|\psi\|^2_{0,\Sigma}.$$

Now subtract $\frac{1}{2r}\|[\![u_r-u]\!]\|^2_{0,\Sigma}$ from both sides:

$$\alpha_0\|\varepsilon(u_r-u)\|^2_{0,\Omega} + M_0\|\overline{u_r}-u\|^2_{0,\Sigma} + \frac{1}{2r}\|[\![u_r-u]\!]\|^2_{0,\Sigma} \le \frac{r}{2}\|\psi\|^2_{0,\Sigma}.$$

Applying Korn's inequality to the first term and dropping the other terms on the left-hand

side, we obtain

$$\frac{\alpha_0}{C_0}\|(u_r - u)\|_W^2 \leq \frac{r}{2}\|\psi\|_{0,\Sigma}^2,$$

where $C_0 = \max\{C_1, C_2\} > 0$ with C_1 and C_2 are Korn's constants in Ω_1 and Ω_2 respectively. That leads to the final estimate

$$\|u_r - u\|_W \leq C\sqrt{r},$$

where $C(\psi) > 0$.

Thus, the proof is complete. □

3.4 Finite Volume discretization

We introduce a finite volume-based treatment of the linear elastic/elastic problem with J.E.B.C. over the domain $\Omega = \Omega_1 \cup \Sigma \cup \Omega_2$. Each subdomain is divided into a uniform Cartesian grid of non-overlapping rectangular control volumes K, with cell center denoted by x_K, and neighboring cells L with center x_L, enabling second-order accurate approximations using simple stencil-based schemes. This approach is widely applied in previous research in fluid dynamics [19,28,36] or in elasticity [49]. In Chapter 1, we introduced the general notion of an admissible mesh for finite volume discretizations (section 1.2). For the purposes of Chapter 3, we now restrict ourselves to a specific redefinition of admissible meshes adapted to the problem under consideration.

3.4.1 Admissible meshes

Let $\Omega = \Omega_1 \cup \Sigma \cup \Omega_2 \subset \mathbb{R}^d$ be a bounded open set (square for $d = 2$ or cube for $d = 3$). Let $\mathscr{D} = (\mathscr{M}, \mathscr{E}, \mathscr{P})$ denotes an admissible mesh (with $\mathscr{M} = \mathscr{M}_1 \cup \mathscr{M}_2$) as defined in [36], that is, for $i = 1, 2$:

Ω_i is partitioned into a finite sequance of convex subsets $\mathscr{M}_i$ of $\mathbb{R}^d$ (squares for $d = 2$ or cubes for $d = 3$). The elements $K \in \mathscr{M}_i$ are called control volumes of nonzero measure m_K.

Each control volume $K \in \mathscr{M}_i$ has the set $\mathscr{E}_K$ of edges (segments for $d = 2$ and squares for $d = 3$) e of size m_e and each edge e_K of K has a unit normal vector $\mathbf{n}_{e,K}$ outward to K. All edges in the mesh are collected in the set $\mathscr{E} = \bigcup_{K \in \mathscr{M}_1 \cup \mathscr{M}_2} \mathscr{E}_K = \mathscr{E}_{int} \cup \mathscr{E}_{ext} \cup \mathscr{E}_\Sigma$, where $\mathscr{E}_{int}$ include the interior edges (edges that does not coincide with Γ_1, Γ_2 and Σ), $\mathscr{E}_{ext}$ contains the exterior edges (edges that coincide with Γ_1 or Γ_2), and $\mathscr{E}_\Sigma$ is consists of

the edges of which overlap with Σ.

We refer with $\mathscr{P}$ to the set of points $(\mathbf{x}_K)_{K\in\mathscr{M}_i}$ satisfying the orthogonality condition.

The Euclidean distance $d(\mathbf{x}_K, e_K)$ is denoted $d_{K,e}$. For any $K \in \mathscr{M}_i$ and $L \in \mathscr{N}_K$ ($\mathscr{N}_K$ the neighboring control volumes of K), we denote by $e_{K|L} \in \mathscr{E}_K \cup \mathscr{E}_L$ the common edge between K and L we then abbreviate $\mathbf{n}_{KL} := \mathbf{n}_{K,K|L}$, we also set $d_{KL} = d_{K,K|L} + d_{L,K|L}$ the Euclidean distance $d(\mathbf{x}_K, \mathbf{x}_L)$.

3.4.2 Treatement of Internal cells

In our model, the stress tensor is given by the classical isotropic elasticity law $\sigma(u) = \lambda\,(\nabla\cdot u)\,\boldsymbol{I} + 2\mu\varepsilon(u)$, with $\varepsilon = \dfrac{1}{2}\left(\nabla u + (\nabla u)^\top\right)$. For a face $e \in \mathscr{E}_{int}$ shared by cells K and L both in $\mathscr{M}_1$ (or both in $\mathscr{M}_2$), with unit normal $n_{e,K}$ from K to L, we approximate the gradient of u in the direction of $n_{e,K}$ by

$$\nabla u|_e \approx \frac{u_L - u_K}{d_{KL}} \otimes n_{e,K},$$

where d_{KL} is the distance between the centers of K and L and we denote by u_K and u_L the cell-centered finite volume approximations of the displacement field u in the cells K and L, respectively. This gives a directional approximation of the displacement gradient.

From this, the symmetric strain tensor is approximated by

$$\varepsilon(u)|_e \approx \frac{1}{2d_{KL}}\left[(u_L - u_K)\otimes n_{e,K} + n_{e,K}\otimes(u_L - u_K)\right],$$

and the divergence of u is approximated by

$$(\nabla\cdot u)|_e \approx \frac{(u_L - u_K)\cdot n_{e,K}}{d_{KL}}.$$

Substituting into the stress tensor, we obtain the following discrete approximation of the normal stress on face e with respect to cell K:

$$\sigma_K\cdot n_{e,K} \approx \left(\lambda\frac{(u_L - u_K)\cdot n_{e,K}}{d_{KL}}\right) n_{e,K} + \frac{\mu}{d_{KL}}\left[(u_L - u_K) + \left((u_L - u_K)\cdot n_{e,K}\right) n_{e,K}\right].$$

An analogous formula holds for $\sigma_L\cdot n_{e,K}$ (i.e., stress evaluated from cell L, but still projected in the direction of $n_{e,K}$).

At the outer boundary of the domain, Dirichlet conditions are enforced by prescribing the value of the unknown u_K at boundary control volumes adjacent to the Dirichlet boundary. However, at the interface Σ, where jump and average transmission conditions

are imposed, we do not use the above flux expressions directly. Instead, we derive the interface fluxes by enforcing the transmission conditions (3.4)–(3.5), and combine them with the cell-centered unknowns u_K and u_L, as shown in the next subsection.

3.4.3 Treatment of the Interface Conditions on Σ

Let $e \in \mathscr{E}_\Sigma$ be the common face between the control volumes $K \in \mathscr{M}_1$ and $L \in \mathscr{M}_2$. We denote by $n_{e,K}$ the unit normal on e that points outward from K and by $n_{e,L} = -n_{e,K}$ the outward normal from L. Define the normal stresses with respect to the same geometric normal $n_{e,K}$ by

$$\tau_K := \sigma_K\, n_{e,K}, \qquad \tau_L := \sigma_L\, n_{e,K},$$

where $\sigma_K := \sigma_1(u_K)$ and $\sigma_L := \sigma_2(u_L)$.

The continuous interface conditions read

$$\begin{aligned} [\![\sigma(u)\cdot n]\!]_\Sigma &= M\,\overline{u}\big|_\Sigma - g, \\ \overline{\sigma(u)\cdot n}\big|_\Sigma &= S\,[\![u]\!]_\Sigma - h. \end{aligned}$$

Because the finite-volume method stores unknowns at cell centres, the natural first-order approximations on e are

$$[\![u]\!]_\Sigma \approx u_L - u_K, \qquad \overline{u}\big|_\Sigma \approx \frac{u_K + u_L}{2}.$$

Using the same normal $n_{e,K}$ for both sides, the jump and average of the normal stress become

$$[\![\sigma(u)\cdot n]\!]_\Sigma = \tau_L - \tau_K, \qquad \overline{\sigma(u)\cdot n}\big|_\Sigma = \frac{\tau_L + \tau_K}{2}.$$

Substituting these discrete counterparts of the jump and average into (3.4)–(3.5) yields the linear system

$$\begin{cases} \tau_L - \tau_K = \dfrac{M}{2}\,(u_K + u_L) - g, \\ \dfrac{\tau_L + \tau_K}{2} = S\,(u_L - u_K) - h. \end{cases} \tag{3.18}$$

Solving (3.18) for τ_K and τ_L, and recalling the definitions of τ_K and τ_L and the fact that both are expressed with respect to the single normal $n_{e,K}$, we arrive at the discrete interface flux condition

$$\begin{cases} \sigma_K \cdot n_{e,K} = (S - \dfrac{1}{4}M)u_L - (S + \dfrac{1}{4}M)u_K - g + \dfrac{1}{2}h, \\ \sigma_L \cdot n_{e,K} = (S + \dfrac{1}{4}M)u_L - (S - \dfrac{1}{4}M)u_K - g - \dfrac{1}{2}h. \end{cases} \tag{3.19}$$

Case N°	Interface conditions	Parameters on Σ
1	no-slip and stress continuity conditions	$h = g = 0, M = 0, S = \frac{1}{r}I$
2	slip and stress continuity conditions	$h = 0, g = \frac{1}{r}q, M = rI, S = \frac{1}{r}I$
3	no-slip and stress discontinuity conditions	$h \neq 0, g = 0, M = rI, S = \frac{1}{r}I$
4	slip and stress discontinuity conditions	$h \neq 0, g = \frac{1}{r}q, M = rI, S = \frac{1}{r}I$
5	Separate Fourier conditions	$S = \frac{1}{4}M = \frac{1}{r}I$

Table 3.1: Interface condition cases

Widely encountered cases in the literature related to classical elastic-elastic interaction problems can be derived from these conditions, and are special cases of the more comprehensive framework presented. By appropriately choosing the parameters in the interface conditions, we recover several well-known scenarios, which provide important insights and applications in various physical contexts. For that, let $r > 0$ be a real penalty parameter and let I be the identity matrix, different cases based on the choice of S, M, g and h are summerized in table 3.1.

3.4.4 Linear algebraic system

The final algebraic system is assembled for each displacement component resulting in:

$$\begin{pmatrix} A_1 & B \\ B & A_2 \end{pmatrix} \begin{pmatrix} U_x \\ U_y \end{pmatrix} = \begin{pmatrix} F_x \\ F_y \end{pmatrix} \tag{3.20}$$

where U_x and U_y are the descrete unknowns, and F_x, F_y are the descretization of source term using the mid-point rule, consistent with the FVM framework (we note that both vectors U_x and U_y both contain unknowns from Ω_1 and Ω_2 classified in a specific order based on our programming, and the vectors F_x and F_y also contain both source terms f_1 and f_2 and some lines also contain the interface contributions g and h). The linear system is solved iteratively using Preconditioned Conjugate Gradient, GMRES or Incomplete Cholesky preconditioned solvers.

3.5 Numerical Tests

In this section, we present numerical experiments to validate the accuracy and efficiency of the proposed model. The tests are performed on both homogeneous and heterogeneous

isotropic media, with comparisons to analytical solutions where available. The discrete relative error in the L^2-norm and the associated convergence rate are computed as:

$$E_h = \frac{\|U_{ex} - U_h\|_{L^2(\Omega_h)}}{\|U_{ex}\|_{L^2(\Omega_h)}}, \qquad \text{and} \qquad cv.rate = \frac{log\left(E_{h_{k+1}}\right) - log\left(E_{h_k}\right)}{log\left(h_{k+1}\right) - log\left(h_k\right)} \tag{3.21}$$

where U_{ex} is the vector of exact solution of the limit problem computed in the centers of CVs, and U_h is the vector of numerical solution.

In what follows, u_i is originally composed of two components $u_i = \left(u_i^{(1)}, u_i^{(2)}\right)^\top$, but for simplicity we suppose the components are equal (i.e. $u_i^{(1)} = u_i^{(2)}$ for $i = 1, 2$). We choose Young's modulus $E \approx 1.5429 \times 10^5 MPa$ and Poisson's ratio $\nu \approx 0.2857$, the Lame's coefficients corresponding to these values are $\lambda = 8 \times 10^5 MPa$ and $\mu = 6 \times 10^5 MPa$ or typical engineering materials such as titanium alloys, high-strength steels, or advanced ceramics. To better understand the geometric configurations addressed in the following test cases, we illustrate in Figure 3.1 three typical interface layouts between two subdomains.

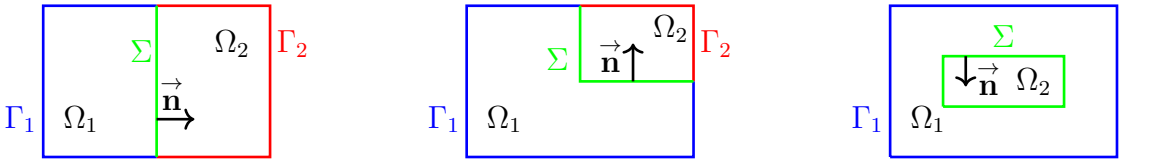

(a) Vertical Interface **(b)** L-shaped Interface **(c)** Rectangular Interface

Figure 3.1: Illustration of different interface configurations between two subdomains.

3.5.1 From Penalized Interface to Continuity Condition

In the first set of numerical experiments, we investigate the convergence of the proposed penalized interface formulation toward the classical *continuity condition*. This test is designed to validate the effectiveness of the penalization approach in approximating strong coupling conditions as the penalization parameter tends to zero. To this end, we consider two distinct interface geometries: the *L-shaped interface*, where the interface exhibits a corner structure connecting horizontal and vertical segments, and the *rectangular embedded interface*, where the interface surrounds a fully enclosed subdomain. These two configurations, illustrated in Figure 3.1, represent challenging geometries for interface problems and allow us to assess the method's accuracy in both standard and complex interface topologies. The convergence behavior is quantified by computing the difference between the solutions obtained with the penalized interface and those satisfying the exact continuity condition.

Test Case 1: L-Shaped Interface

We first validate the finite volume scheme on a unit square domain $\Omega = [0, 1.5]^2$ which is devided in two non-overlapping subregions $\Omega_1 = \Omega_x \cup \Omega_y$ and $\Omega_2 = [1, 1.5]^2$, with $\Omega_x = \{(x, y) \in \Omega \mid 0 < x < 1 \text{ and } 0 < y < 1.5\}$ and $\Omega_y = \{(x, y) \in \Omega \mid 0 < y < 1 \text{ and } 0 < x < 1.5\}$. Ω is meshed with uniform square cells of grid steps h ranging from 1/9 to 1/60. We consider the following interaction problem

$$\begin{cases} -\nabla \cdot \sigma_1(u) = f_1 & \text{in } \Omega_1, \\ -\nabla \cdot \sigma_2(u) = f_2 & \text{in } \Omega_2, \\ u = 0 & \text{on } \Gamma_1 \cup \Gamma_2, \\ [\![\sigma(u) \cdot n]\!]_\Sigma = g & \text{on } \Sigma \\ \overline{\sigma(u) \cdot n}|_\Sigma = \dfrac{1}{2r}[\![u]\!]_\Sigma & \text{on } \Sigma. \end{cases} \tag{P_L}$$

where $\sigma_1(u) = \sigma_2(u) = \lambda(\nabla \cdot u)\boldsymbol{I} + 2\mu\varepsilon(u)$. As stated in theorem 3.2, the solution of (P_L) tends to the solution of problem (P_l) with continuity condition ($[\![u]\!]_\Sigma = 0$). The analytical solution of the problem (P_l) is

$$\begin{aligned} u_1(x, y) &= 10xy(x - 1)(y - 1)(x - 1.5)(y - 1.5), \\ u_2(x, y) &= 10(x - 1)(y - 1)(x - 1.5)(y - 1.5), \end{aligned}$$

where u_i is the exact solution in Ω_i for $i = 1, 2$. The source terms f_1 and f_2 are constructed to satisfy the equations in Problem (P_L), and g is defined by

$$g(x, y) = \begin{cases} \begin{pmatrix} 5(2\mu + \lambda)(y - 1)^2 \left(y - \frac{3}{2}\right) \\ 5\mu(y - 1)^2 \left(y - \frac{3}{2}\right) \end{pmatrix}, & \text{if } x = 1,\ 1 \le y \le 1.5, \\ \begin{pmatrix} 5\mu x(x - 1) \left(x - \frac{3}{2}\right) \\ 5\lambda(x - 1)^2 \left(x - \frac{3}{2}\right) \end{pmatrix}, & \text{if } y = 1,\ 1 \le x \le 1.5. \end{cases}$$

The problem (P_L) is solved with different step-sizes h and a penalty parameter $r = h/(2\mu + \lambda)$. Table 3.2 summarizes the relative L^2-norm errors for varying grid steps h.

Table 3.2: Relative errors for solutions of test case 1.

h	1/9	1/18	1/30	1/60
$\frac{\|U_{ex} - U_h\|}{\|U_{ex}\|}$	5.5850×10^{-2}	1.8189×10^{-2}	9.9357×10^{-3}	4.8002×10^{-3}

In addition to the results presented in Table 3.2, Figure 3.2 shows a comparison be-

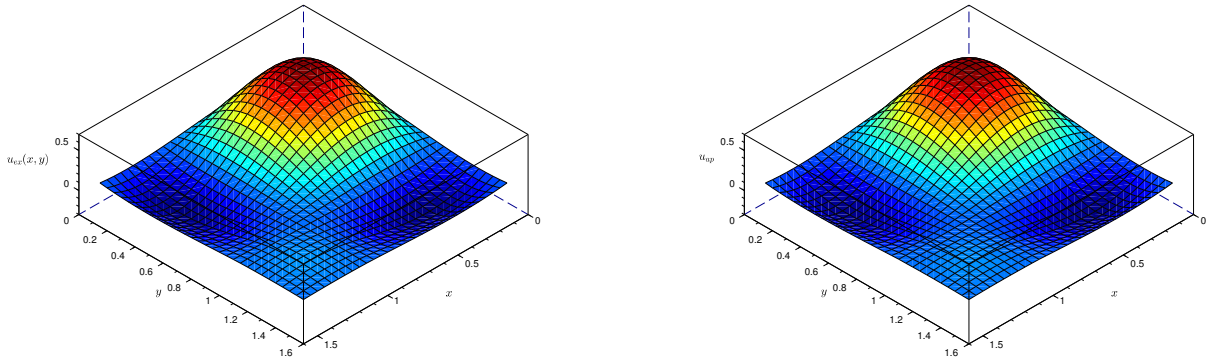

(a) Analytical solution **(b)** Numerical solution

Figure 3.2: Analytical and numerical solutions of test case 1.

tween the analytical solution of Problem (P_l) and the numerical solution of Problem (P_L). As can be seen, the two solutions are almost identical, demonstrating the high accuracy and robustness of the discretization method, as well as the effective convergence of the numerical solution of Problem (P_L) toward the analytical solution of the no-slip interaction problem (P_l). In Figure 3.3, the subfigure (a) depicts the projection of both analytical and numerical solutions on $y = x$, while subfigure (b) demonstrates a convergence rate between 1 and 2 (i.e. $1 \leq cv.\ rate \leq 2$) of the penalized problem (P_L), which validate the convergence results in Table 3.2 and Figure 3.2.

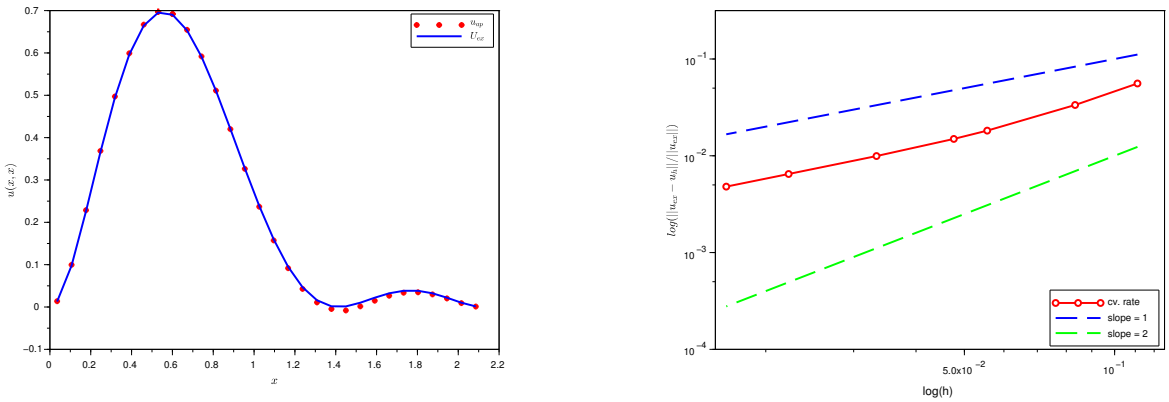

(a) Projection of solutions in the segment $y = x$ **(b)** Convergence rate

Figure 3.3: Projection of solutions on $y = x$ and convergence rate of test case 1.

Test Case 2: Rectangular Interface

For this case the interface Σ will take an rectangular shape. For that, let $\Omega = [0,1]^2$ be a rectangular domain subdevided in $\Omega_2 = [1/3, 2/3]^2$ and $\Omega_1 = \Omega \backslash \Omega_2$.

We reconsider the problem (P_L) is the new domain configuration, which will be denoted by (P_R). The analytical solution of the corresponding limit problem (P_l) is chosen as

$$u_1(x,y) = 10xy(x-1)(y-1)\left(x-\frac{1}{3}\right)\left(y-\frac{1}{3}\right)\left(x-\frac{2}{3}\right)\left(y-\frac{2}{3}\right),$$
$$u_2(x,y) = \left(x-\frac{1}{3}\right)\left(y-\frac{1}{3}\right)\left(x-\frac{2}{3}\right)\left(y-\frac{2}{3}\right),$$

where u_i is the exact solution in Ω_i for $i = 1, 2$. The source terms f_1, f_2 and the stress jump g are constructed to satisfy the equations in Problem (P_R), The problem (P_R) is solved with different step-sizes h and a penalty parameter $r = h^2/(2\mu + \lambda)$. Table 3.3 summarizes the relative L^2-norm errors for diverse grid steps h and r dependent of h.

Table 3.3: Relative errors for solutions of test case 2.

h	1/9	1/18	1/30	1/60
$\frac{\|U_{ex}-U_h\|}{\|U_{ex}\|}$	5.5850×10^{-2}	1.8188×10^{-2}	9.9356×10^{-3}	4.8002×10^{-3}

In Figure 3.4, the subfigure (a) illustrate the projection of both analytical and numerical solution on the segment $y = x$ for $h = 1/45$, which shows a good accuracy and robustness, while subfigure (b) demonstrates a convergence rate close to 1 of the penalized problem (P_R) for different step sizes $1/9 \leq h \leq 1/45$ and for a fixed $r = \min(h)^2/(2\mu+\lambda)$, which validate the results in Table 3.3.

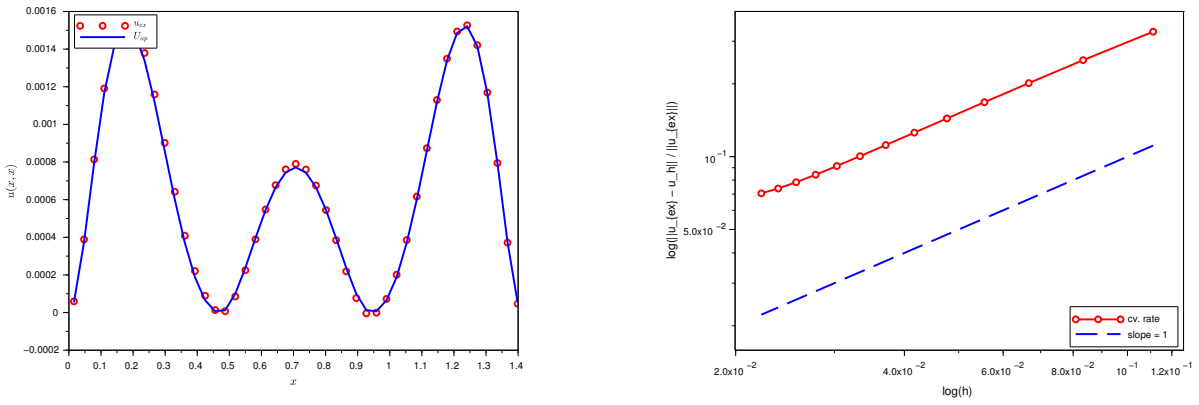

(a) Projection of solutions on $y = x$.

(b) Convergence rate for $r = \min(h)^2/(2\mu+\lambda)$.

Figure 3.4: Projection of solutions on $y = x$ and convergence rate of test case 2.

3.5.2 From Penalized Interface to Discontinuity Condition

In the second set of numerical experiments, we examine the convergence of the penalized interface formulation toward the classical *discontinuity interface condition* ($[\![u]\!]_\Sigma \neq 0$). To evaluate this behavior, we consider a simplified geometry involving a *vertical interface* between two subdomains. This configuration, shown in Figure 3.1, facilitates the assessment of the method's ability to recover the expected discontinuous behavior. This test shows the numerical penalized solution approximates the exact solution satisfying the discontinuity condition as the penalization parameter tends to zero.

Test Case 3: Vertical Interface

Let $\Omega = [0, 1.5] \times [0, 1]$ be a rectangular domain subdevided in $\Omega_1 = [0, 1] \times [0, 1]$ and $\Omega_2 = [1, 1.5] \times [0, 1]$, and let the interface $\Sigma = \{x = 1\} \times [0, 1]$.

The same previous problem, now denoted by (P_V), is reconsidered in the new configuration. The analytical solution of the respective limit problem (P_l) with $[\![u]\!]_\Sigma = \frac{1}{2}\sin(\pi y) - y(y-1)$ is given by

$$u_1(x, y) = x\left(x - \frac{3}{2}\right)\sin(\pi y),$$
$$u_2(x, y) = y(y-1)\cos(\pi x).$$

The source terms f_1 and f_2 are constructed to satisfy the equations in problem (P_V), and the stress jump g is defined, for every $y \in [0, 1]$, by

$$g(y) = \begin{pmatrix} \frac{2\mu+\lambda}{2}\sin(\pi y) + \lambda\left[-\frac{\pi}{2}\cos(\pi y) + (2y-1)\right] \\ \mu\left[-\frac{\pi}{2}\cos(\pi y) + (2y-1) + \frac{1}{2}\sin(\pi y)\right] \end{pmatrix}.$$

In Figure 3.5, We examine how the convergence rate varies as the penalization parameter is decreased, setting $r = \min(h)/(K(2\mu + \lambda))$ for different grid step sizes h ranging from 1.5/9 to 1.5/60 and for K values in $\{1, 10, 25, 50, 100\}$. The results in the figure indicate that the convergence rate generally lies between slopes of 1 and 2 for $K = \{5, 10, 50\}$, while for $K = 100$ and the finest mesh $h = 1.5/60$, the performance deteriorates, yielding lower convergence rates.

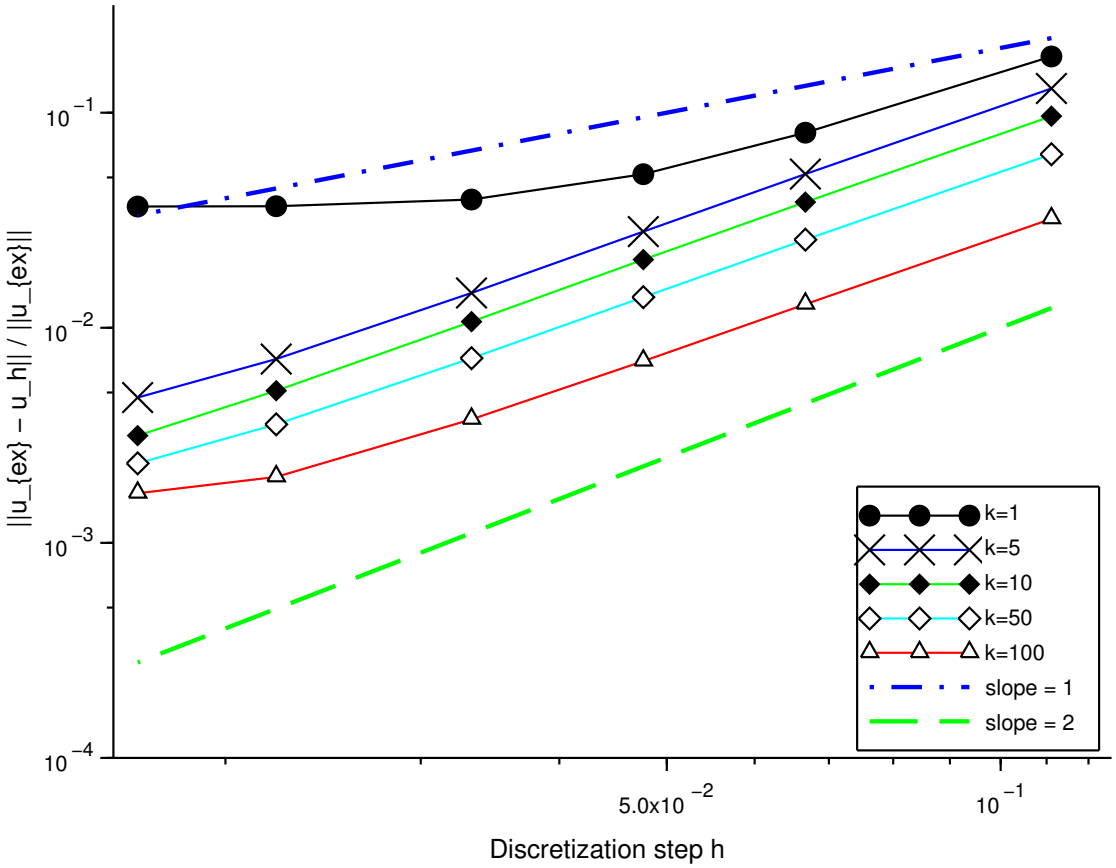

Figure 3.5: Effect of penalization to the cv.rate in test case 3.

Chapter 4

Fluid–Structure Interactions

Introduction

Fluid-Structure Interaction (FSI) problems describe the coupled behavior of a fluid and an elastic structure interacting through a shared interface, where forces and deformations are transmitted. Such interactions are critical in diverse engineering and physical systems, including blood flow in arteries [14, 60, 72, 76, 96], the aerodynamic response of aircraft wings [29, 92, 95], wind turbine dynamics [15], and the design of offshore structures [45]. Modeling and understanding FSI systems are fundamental for enhancing structural safety and fluid dynamic efficiency.

The mathematical and computational study of FSI addressing both theoretical foundations and numerical methods has been well developed in the literature. Classical FSI formulations impose standard interface conditions, such as no-slip velocity continuity and stress balance. Rigorous developments of these models incorporated advanced techniques, such as proving existence of local strong solution [69], or weak solution using semigroup theory [13], Galerkin approximation [18], or hybrid approximation schemes [93]. Studies of moving boundary FSI problems have also expanded, with notable contributions in [53, 70, 72, 73]. In addition, recent works have studied stochastic moving boundary problems in compressible fluid-structure interactions [53]. Efficient numerical techniques for simulating fluid-structure systems were also introduced in [17, 37, 41, 84, 91], with applications in aerospace and bioengineering fields. These contributions have widened the applicability of FSI models, offering more general formulations and techniques that go beyond classical assumptions of no-slip and stress continuity. However, these traditional approaches typically assume idealized coupling conditions, which limit their application in more complex scenarios.

This chapter develops a generalized framework for FSI that incorporates parame-

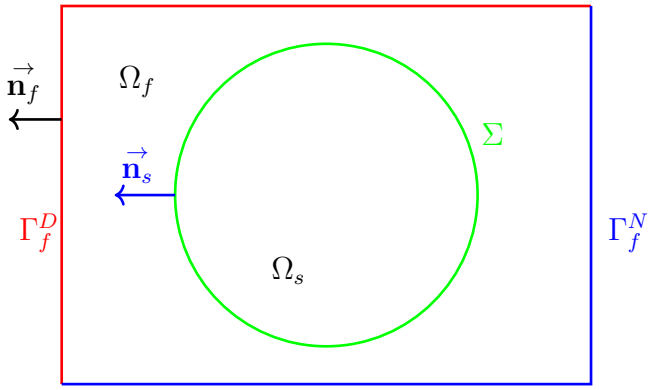

Figure 4.1: An example of an elastic domain Ω_s embedded in a fluid domain Ω_f

terized, fictitious domain-type interface conditions. By embedding the solid structure within an extended fluid domain, the coupling terms are reformulated to handle a wider spectrum of physical phenomena. This flexible approach captures partial slip and stress discontinuities, offering a unified model that extends beyond classical conditions. The weak formulation integrates these generalized conditions, and theoretical results on existence and uniqueness of solution are established using semigroup theory and functional analysis.

The chapter is organized as follows. Section 4.1 introduces the governing equations, initial and boundary conditions, and the functional framework. The weak formulation is developed in section 4.2. Proof of existence along with uniqueness for $d = 2$ are detailed in section 4.3.

4.1 Fluid-Structure Interaction Model

We consider a fluid-structure interaction (FSI) problem, where a deformable structure is immersed in a fluid domain. The fluid domain is denoted by $\Omega_f \subset \mathbb{R}^d$ (typically $d = 2$ or $d = 3$), and the structure domain is denoted by $\Omega_s \subset \mathbb{R}^d$. The interaction between the fluid and the structure occurs along the interface $\Sigma \subset \mathbb{R}^{d-1}$. The outer boundary of the fluid domain is denoted by $\Gamma_f = \Gamma_f^D \cup \Gamma_f^N$, where Γ_f^D represents the Dirichlet part and Γ_f^N represents the Neumann part of the boundary.

4.1.1 Governing equations, initial and boundary conditions

The fluid flow is described by the *incompressible Navier–Stokes equations*. Let $\boldsymbol{v}^f$ and p denote the velocity field and pressure of the fluid, respectively. The governing equations are:

- the momentum equation (Newton's second law):

$$\frac{\partial \boldsymbol{v}^f}{\partial t} + (\boldsymbol{v}^f \cdot \nabla)\boldsymbol{v}^f - \nabla \cdot \sigma_f(\boldsymbol{v}^f, p) = \boldsymbol{f}^f, \quad \text{in } (0,T) \times \Omega_f,$$

- the continuity equation (mass conservation):

$$\nabla \cdot \boldsymbol{v}^f = 0, \quad \text{in } (0,T) \times \Omega_f,$$

where the fluid stress tensor $\sigma_f(\boldsymbol{v}^f, p)$ is given by

$$\sigma_f(\boldsymbol{v}^f, p) = -p\boldsymbol{I} + 2\mu_f \varepsilon(\boldsymbol{v}^f), \quad \text{with} \qquad \varepsilon(\boldsymbol{v}^f) = \frac{1}{2}\left(\nabla \boldsymbol{v}^f + (\nabla \boldsymbol{v}^f)^\top\right)$$

being the rate-of-strain tensor (i.e., the symmetric part of the velocity gradient), μ_f the dynamic viscosity of the fluid, and $\boldsymbol{f}^f$ a volume force acting on the fluid.

The structure is governed by the *linear elastodynamics equation*. Let $\boldsymbol{u}^s$ denote the displacement field of the structure. Then,

$$\frac{\partial^2 \boldsymbol{u}^s}{\partial t^2} - \nabla \cdot \sigma_s(\boldsymbol{u}^s) = \boldsymbol{f}^s, \quad \text{in } (0,T) \times \Omega_s, \tag{4.1}$$

where the stress tensor is defined by

$$\sigma_s(\boldsymbol{u}^s) = 2\mu\, d(\boldsymbol{u}^s) + \lambda\ \mathrm{tr}(d(\boldsymbol{u}^s))I, \quad \text{with} \qquad d(\boldsymbol{u}^s) = \frac{1}{2}\left(\nabla \boldsymbol{u}^s + \nabla \boldsymbol{u}^{s\top}\right),$$

and μ_s and λ are the Lamé coefficients related to the Young's modulus E and Poisson's ratio ν, by

$$\mu_s = \frac{E}{2(1+\nu)}, \qquad \lambda_s = \frac{E\nu}{(1+\nu)(1-2\nu)}$$

Boundary conditions are specified for the fluid velocity and stress as follows:

$$\begin{aligned} \boldsymbol{v}^f &= \boldsymbol{0}, \quad \text{on } (0,T) \times \Gamma_f^D, \\ \sigma_f(\boldsymbol{v}^f, p) \cdot \boldsymbol{n}_N^f &= \boldsymbol{g}_N^f, \quad \text{on } (0,T) \times \Gamma_f^N, \end{aligned}$$

where $\boldsymbol{g}_N^f \in H^{1/2}(\Gamma_f^N)$ is a prescribed traction vector, and $\boldsymbol{n}_N^f$ is the unit outward normal to Γ_f^N with respect to the fluid domain Ω_f.

Initial conditions for both the fluid and the structure are given by:

$$\begin{aligned} \boldsymbol{v}^f|_{t=0} &= \boldsymbol{v}_0^f, \quad \text{in } \Omega_f, \\ \boldsymbol{u}^s|_{t=0} &= \boldsymbol{u}_0^s, \quad \left.\frac{\partial \boldsymbol{u}^s}{\partial t}\right|_{t=0} = \boldsymbol{v}_0^s, \quad \text{in } \Omega_s. \end{aligned}$$

In order to unify the fluid–structure interaction problem from a physical standpoint, we reformulate the structural equations using the velocity $\boldsymbol{v}^s = \dfrac{\partial \boldsymbol{u}^s}{\partial t}$ as the primary unknown in the solid domain. Applying this transformation to equation (4.1), we obtain the following velocity-based form of the structure's dynamics:

$$\frac{\partial \boldsymbol{v}^s}{\partial t} - \nabla \cdot \sigma_s\left(\boldsymbol{u}^s\right) = \boldsymbol{f}^s, \quad \text{in } (0,T) \times \Omega_s,$$

where the stress tensor $\sigma_s(\boldsymbol{u}^s)$ can equivalently be expressed in terms of the velocity as $\sigma_s\left(\int_0^t \boldsymbol{v}^s(\theta)\, d\theta\right)$.

To simplify the notation in the remainder of this chapter, we redefine the structural force term by incorporating the initial stress contribution $\nabla \cdot \sigma_s(\boldsymbol{u}_0^s)$ into the right-hand side. That is, we set

$$\boldsymbol{f}^s := \boldsymbol{f}^s + \nabla \cdot \sigma_s(\boldsymbol{u}_0^s).$$

This allows us to express the structural dynamics entirely in terms of the velocity $\boldsymbol{v}^s$, while still implicitly retaining the displacement through its integral over time.

4.1.2 Interface conditions

The interface conditions on $(0,T) \times \Sigma$ couple the fluid and the structure through the balance of stresses and velocities across the interface. They are given by:

$$\begin{aligned} [\![\sigma \cdot \boldsymbol{n}]\!]_\Sigma &\equiv \sigma_f \cdot \boldsymbol{n} - \sigma_s \cdot \boldsymbol{n} = \boldsymbol{M}\, \overline{\boldsymbol{v}}_{|\Sigma} - \boldsymbol{h}, \quad \text{on } (0,T) \times \Sigma, \\ \overline{\sigma \cdot \boldsymbol{n}}_{|\Sigma} &\equiv \frac{1}{2}\left(\sigma_f \cdot \boldsymbol{n} + \sigma_s \cdot \boldsymbol{n}\right) = \boldsymbol{S}\, [\![\boldsymbol{v}]\!]_\Sigma - \boldsymbol{g}, \quad \text{on } (0,T) \times \Sigma, \end{aligned}$$

where

$$\overline{\boldsymbol{v}}_{|\Sigma} \equiv \frac{1}{2}\left(\boldsymbol{v}_{|\Sigma}^f + \frac{\partial \boldsymbol{u}^s}{\partial t}_{|\Sigma}\right), \qquad [\![\boldsymbol{v}]\!]_\Sigma \equiv \boldsymbol{v}_{|\Sigma}^f - \frac{\partial \boldsymbol{u}^s}{\partial t}_{|\Sigma}.$$

$\boldsymbol{n} = \boldsymbol{n}_s$ denotes the unit outward normal to Σ with respect to the structure domain Ω_s. The functions $\boldsymbol{g}, \boldsymbol{h} \in L^2\left(0,T; H^{-1/2}(\Sigma)^d\right)$ represent interface force terms. The operators $\boldsymbol{S}, \boldsymbol{M} \in L^\infty(\Sigma)^{d \times d}$ are measurable, bounded matrix-valued functions that satisfy the

following ellipticity assumption:

$$\forall\, \xi \in \mathbb{R}^d, \quad \xi^\top \boldsymbol{M}(\boldsymbol{x})\, \xi > 0, \quad \xi^\top \boldsymbol{S}(\boldsymbol{x})\, \xi > 0, \quad \text{for a.e. } \boldsymbol{x} \in \Sigma. \tag{4.2}$$

Remark 4.1. *For brevity, we omit the subscript Σ in the notation for both the jump and the mean value across the interface. That is,*

$$[\![\boldsymbol{v}]\!] \equiv [\![\boldsymbol{v}]\!]_\Sigma, \quad \overline{\boldsymbol{v}} \equiv \overline{\boldsymbol{v}}_\Sigma, \quad [\![\sigma \cdot \boldsymbol{n}]\!] \equiv [\![\sigma \cdot \boldsymbol{n}]\!]_\Sigma, \quad \overline{\sigma \cdot \boldsymbol{n}} \equiv \overline{\sigma \cdot \boldsymbol{n}}_\Sigma.$$

We now summarize the full continuous model governing the fluid-structure interaction (FSI) problem which is given by (4.3) below:

$$\frac{\partial \boldsymbol{v}^f}{\partial t} + (\boldsymbol{v}^f \cdot \nabla)\boldsymbol{v}^f - \nabla \cdot \boldsymbol{\sigma}_f(\boldsymbol{v}^f, p^f) = \boldsymbol{f}^f \qquad \text{in } (0,T) \times \Omega_f, \tag{4.3a}$$

$$\nabla \cdot \boldsymbol{v}^f = 0 \qquad \text{in } (0,T) \times \Omega_f, \tag{4.3b}$$

$$\frac{\partial \boldsymbol{v}^s}{\partial t} - \nabla \cdot \boldsymbol{\sigma}_s(\boldsymbol{u}^s) = \boldsymbol{f}^s \qquad \text{in } (0,T) \times \Omega_s, \tag{4.3c}$$

$$\boldsymbol{v}^f = 0 \qquad \text{on } (0,T) \times \Gamma_f^D, \tag{4.3d}$$

$$\boldsymbol{\sigma}_f(\boldsymbol{v}^f, p^f) \cdot \boldsymbol{n} = \boldsymbol{g}_N^f \qquad \text{on } (0,T) \times \Gamma_f^N, \tag{4.3e}$$

$$[\![\sigma \cdot \boldsymbol{n}]\!] = \boldsymbol{M}\, \overline{\boldsymbol{v}} - \boldsymbol{h}, \qquad \text{on } (0,T) \times \Sigma, \tag{4.3f}$$

$$\overline{\sigma \cdot \boldsymbol{n}} = \boldsymbol{S}\, [\![\boldsymbol{v}]\!] - \boldsymbol{g}, \qquad \text{on } (0,T) \times \Sigma, \tag{4.3g}$$

$$\boldsymbol{v}^f(0, \boldsymbol{x}) = \boldsymbol{v}_0 \qquad \text{in } \Omega_f, \tag{4.3h}$$

$$\boldsymbol{u}^s(0, \boldsymbol{x}) = \boldsymbol{u}_0, \quad \boldsymbol{v}^s(0, \boldsymbol{x}) = \boldsymbol{u}_1 \qquad \text{in } \Omega_s. \tag{4.3i}$$

To gain more insight into the stress distribution at the fluid–structure interface, we express the normal stresses $\boldsymbol{\sigma}_f \cdot \boldsymbol{n}$ and $\boldsymbol{\sigma}_s \cdot \boldsymbol{n}$ in terms of the fluid and structure velocities $\boldsymbol{v}^f$ and $\boldsymbol{v}^s$. By rearranging the interface conditions (4.3f)–(4.3g), we decompose the stress contributions into terms depending on $\boldsymbol{v}^f$, $\boldsymbol{v}^s$, and the interface data $\boldsymbol{g}$ and $\boldsymbol{h}$. The resulting expressions for the normal stresses are given by:

$$\begin{cases} \boldsymbol{\sigma}_s \cdot \boldsymbol{n} = \left(\boldsymbol{S} - \dfrac{1}{4}\boldsymbol{M}\right) \boldsymbol{v}^f - \left(\boldsymbol{S} + \dfrac{1}{4}\boldsymbol{M}\right) \boldsymbol{v}^s - \boldsymbol{g} + \dfrac{1}{2}\boldsymbol{h}, & \text{on } (0,T) \times \Sigma, \\ \boldsymbol{\sigma}_f \cdot \boldsymbol{n} = \left(\boldsymbol{S} + \dfrac{1}{4}\boldsymbol{M}\right) \boldsymbol{v}^f - \left(\boldsymbol{S} - \dfrac{1}{4}\boldsymbol{M}\right) \boldsymbol{v}^s - \boldsymbol{g} - \dfrac{1}{2}\boldsymbol{h}, & \text{on } (0,T) \times \Sigma. \end{cases} \tag{4.4}$$

Having established the generalized interface conditions (4.3f)–(4.3g), we now turn our attention to specific, simplified cases that can be derived as limiting forms of this general framework. These classical models are widely encountered in the literature on fluid–

structure interaction and serve as special cases obtained through particular choices of the interface parameters. By appropriately selecting the coefficients $\boldsymbol{M}, \boldsymbol{S}, \boldsymbol{g}, \boldsymbol{h}$, we recover several well-known configurations that offer important insight into physical applications.

Let $\varepsilon > 0$ be a real penalty parameter, and let $\boldsymbol{I}$ denote the identity matrix.

- **Case 1 (No-slip with traction continuity):**
  Assume $\boldsymbol{h} = \boldsymbol{g} = \boldsymbol{0}$, $\boldsymbol{M} = \varepsilon \boldsymbol{I}$, and $\boldsymbol{S} = \dfrac{1}{\varepsilon}\boldsymbol{I}$. The interface conditions become

$$\begin{cases} [\![\boldsymbol{\sigma} \cdot \boldsymbol{n}]\!] = \varepsilon\, \overline{\boldsymbol{v}}, \\ \varepsilon\, \overline{\boldsymbol{\sigma} \cdot \boldsymbol{n}} = [\![\boldsymbol{v}]\!]. \end{cases}$$

  In the limit as $\varepsilon \to 0$, we obtain the classical interface conditions:

$$\begin{cases} [\![\boldsymbol{v}]\!] = \boldsymbol{0}, \\ [\![\boldsymbol{\sigma} \cdot \boldsymbol{n}]\!] = \boldsymbol{0}. \end{cases}$$

- **Case 2 (Velocity jump with traction continuity):**
  Assume $\boldsymbol{h} = \boldsymbol{0}$, $\boldsymbol{g} = \dfrac{1}{\varepsilon}\boldsymbol{q}$, $\boldsymbol{M} = \varepsilon \boldsymbol{I}$, and $\boldsymbol{S} = \dfrac{1}{\varepsilon}\boldsymbol{I}$. In the limit $\varepsilon \to 0$, the interface conditions reduce to:

$$\begin{cases} [\![\boldsymbol{v}]\!] = \boldsymbol{q}, \\ [\![\boldsymbol{\sigma} \cdot \boldsymbol{n}]\!] = \boldsymbol{0}. \end{cases}$$

- **Case 3 (No-slip with traction jump):**
  Assume $\boldsymbol{h} \neq \boldsymbol{0}$, $\boldsymbol{g} = \boldsymbol{0}$, $\boldsymbol{M} = \varepsilon \boldsymbol{I}$, and $\boldsymbol{S} = \dfrac{1}{\varepsilon}\boldsymbol{I}$. Then, as $\varepsilon \to 0$, the limiting interface conditions become:

$$\begin{cases} [\![\boldsymbol{v}]\!] = \boldsymbol{0}, \\ [\![\boldsymbol{\sigma} \cdot \boldsymbol{n}]\!] = \boldsymbol{h}. \end{cases}$$

- **Case 4 (Velocity and traction jump):**
  This case combines the previous two. Let $\boldsymbol{g} = \dfrac{1}{\varepsilon}\boldsymbol{q}$, $\boldsymbol{h} \neq \boldsymbol{0}$, $\boldsymbol{M} = \varepsilon \boldsymbol{I}$, and $\boldsymbol{S} = \dfrac{1}{\varepsilon}\boldsymbol{I}$. Then, as $\varepsilon \to 0$, we obtain:

$$\begin{cases} [\![\boldsymbol{v}]\!] = \boldsymbol{q}, \\ [\![\boldsymbol{\sigma} \cdot \boldsymbol{n}]\!] = \boldsymbol{h}. \end{cases}$$

All cases are summarized in Table 4.1.

Case #	Interface Conditions	Parameters on Σ
1	No-slip and stress continuity	$\boldsymbol{h} = \boldsymbol{g} = \boldsymbol{0}, \quad \boldsymbol{M} = \varepsilon \boldsymbol{I}, \quad \boldsymbol{S} = \frac{1}{\varepsilon}\boldsymbol{I}$
2	Slip and stress continuity	$\boldsymbol{h} = \boldsymbol{0}, \quad \boldsymbol{g} = \frac{1}{\varepsilon}\boldsymbol{q}, \quad \boldsymbol{M} = \varepsilon \boldsymbol{I}, \quad \boldsymbol{S} = \frac{1}{\varepsilon}\boldsymbol{I}$
3	No-slip and stress discontinuity	$\boldsymbol{h} \neq \boldsymbol{0}, \quad \boldsymbol{g} = \boldsymbol{0}, \quad \boldsymbol{M} = \varepsilon \boldsymbol{I}, \quad \boldsymbol{S} = \frac{1}{\varepsilon}\boldsymbol{I}$
4	Slip and stress discontinuity	$\boldsymbol{h} \neq \boldsymbol{0}, \quad \boldsymbol{g} = \frac{1}{\varepsilon}\boldsymbol{q}, \quad \boldsymbol{M} = \varepsilon \boldsymbol{I}, \quad \boldsymbol{S} = \frac{1}{\varepsilon}\boldsymbol{I}$

Table 4.1: Variants of interface conditions for fluid–structure interaction problems, based on the limiting behavior as $\varepsilon \to 0$.

4.1.3 Functional Spaces, Inner Products and Norms

We consider the following functional spaces for the fluid and structure problems. The fluid velocity $\boldsymbol{v}^f$ is sought in the Sobolev space

$$V_f \equiv \left\{ \boldsymbol{v}^f \in [H^1(\Omega_f)]^d : \nabla \cdot \boldsymbol{v}^f = 0 \text{ in } \Omega_f, \quad \boldsymbol{v}^f = \boldsymbol{0} \text{ on } \Gamma_f^D \right\},$$

while the fluid pressure p belongs to the space $L_0^2(\Omega_f)$.

The structure displacement $\boldsymbol{u}^s$ (or equivalently, its velocity $\boldsymbol{v}^s$) is sought in

$$V_s \equiv [H^1(\Omega_s)]^d.$$

For any $\boldsymbol{v}, \boldsymbol{w} \in V_f$, the space V_f is equipped with the inner product and associated norm:

$$(\boldsymbol{v}, \boldsymbol{w})_{1,\Omega_f} \equiv \int_{\Omega_f} \varepsilon(\boldsymbol{v}) : \varepsilon(\boldsymbol{w})\, d\boldsymbol{x}, \qquad \|\boldsymbol{v}\|_{1,\Omega_f}^2 = (\varepsilon(\boldsymbol{v}), \varepsilon(\boldsymbol{v}))_{1,\Omega_f},$$

where $\varepsilon(\boldsymbol{v}) = \dfrac{1}{2}(\nabla \boldsymbol{v} + \nabla \boldsymbol{v}^\top)$ is the symmetric part of the gradient.

For any $\boldsymbol{v}, \boldsymbol{w} \in [L^2(\Omega_\omega)]^d$ with $\omega \in \{f, s\}$, the standard L^2 inner product and norm are given by:

$$(\boldsymbol{v}, \boldsymbol{w})_{0,\omega} \equiv \int_{\Omega_\omega} \boldsymbol{v} \cdot \boldsymbol{w}\, d\boldsymbol{x}, \qquad \|\boldsymbol{v}\|_{0,\omega}^2 = (\boldsymbol{v}, \boldsymbol{v})_{0,\omega}.$$

For the structural space V_s, the inner product and associated norm are defined, for all $\boldsymbol{u}, \boldsymbol{v} \in V_s$, by:

$$(\boldsymbol{u}, \boldsymbol{v})_{1,s} \equiv \int_{\Omega_s} \boldsymbol{u} \cdot \boldsymbol{v}\, d\boldsymbol{x} + \int_{\Omega_s} \boldsymbol{\sigma}_s(\boldsymbol{u}) : \varepsilon(\boldsymbol{v})\, d\boldsymbol{x},$$

$$\|\boldsymbol{u}\|_{1,s}^2 = \|\boldsymbol{u}\|_{0,s}^2 + \int_{\Omega_s} \boldsymbol{\sigma}_s(\boldsymbol{u}) : \varepsilon(\boldsymbol{u})\, d\boldsymbol{x},$$

we also denote by $\langle \cdot, \cdot \rangle_\Sigma \equiv \langle \cdot, \cdot \rangle_{H^{-1/2}, H^{1/2}}$ the duality pairing between the Sobolev space

$H^{-1/2}(\Sigma)$ and $H^{1/2}(\Sigma)$.

We define the fluid and structure energy spaces by

$$H_s := [L^2(\Omega_s)]^d,$$

and

$$H_f := \left\{ v^f \in [L^2(\Omega_f)]^d \,;\, \nabla \cdot v^f = 0 \text{ in } \mathscr{D}'(\Omega_f), \quad v^f \cdot \boldsymbol{n} = 0 \text{ on } \Gamma_f^D \right\}.$$

Equivalently, H_f is the closure of V_f in $[L^2(\Omega_f)]^d$:

$$H_f = \overline{V_f}^{[L^2(\Omega_f)]^d}.$$

Equipped with the usual L^2-inner products, the spaces H_f and H_s are Hilbert spaces, and we have the continuous and dense embeddings

$$V_f \hookrightarrow H_f \hookrightarrow V_f', \qquad V_s \hookrightarrow H_s \hookrightarrow V_s'.$$

Finally, we define the product space:

$$V \equiv \left\{ \boldsymbol{v} = (\boldsymbol{v}^f, \boldsymbol{v}^s) \in V_f \times V_s : [\![\boldsymbol{\sigma} \cdot \boldsymbol{n}]\!] = \boldsymbol{M}\,\overline{\boldsymbol{v}} - \boldsymbol{h}, \quad \overline{\boldsymbol{\sigma} \cdot \boldsymbol{n}} = \boldsymbol{S}\,[\![\boldsymbol{v}]\!] - \boldsymbol{g} \right\}, \tag{4.5}$$

where the jump and average conditions are imposed on the interface Σ, and the vector field $\boldsymbol{v}$ consists of the fluid velocity $\boldsymbol{v}^f \in V_f$ and the structure velocity $\boldsymbol{v}^s \in V_s$.

For any $\boldsymbol{u}, \boldsymbol{v} \in L^2(\Omega_f) \times L^2(\Omega_s) \equiv \left\{ \boldsymbol{u} = (\boldsymbol{u}^f, \boldsymbol{u}^s) : \boldsymbol{u}^f \in L^2(\Omega_f),\ \boldsymbol{u}^s \in L^2(\Omega_s) \right\}$, we define the standard scalar product and norm:

$$(\boldsymbol{u}, \boldsymbol{v}) \equiv (\boldsymbol{u}^f, \boldsymbol{v}^f)_{0,f} + (\boldsymbol{u}^s, \boldsymbol{v}^s)_{0,s}, \qquad \|\boldsymbol{u}\|^2 \equiv \|\boldsymbol{u}^f\|_{0,f}^2 + \|\boldsymbol{u}^s\|_{0,s}^2. \tag{4.6}$$

For any $\boldsymbol{u}, \boldsymbol{v} \in V$, we define the corresponding H^1-based scalar product and norm by:

$$(\boldsymbol{u}, \boldsymbol{v})_1 \equiv (\boldsymbol{u}^f, \boldsymbol{v}^f)_{1,f} + (\boldsymbol{u}^s, \boldsymbol{v}^s)_{1,s}, \qquad \|\boldsymbol{u}\|_1^2 \equiv \|\boldsymbol{u}^f\|_{1,f}^2 + \|\boldsymbol{u}^s\|_{1,s}^2. \tag{4.7}$$

Remark 4.2 (Trace Regularity at the Interface)**.** *To ensure that the interface terms in the weak formulation are well-defined, we recall the trace regularity properties of Sobolev spaces. Since $v_f \in V_f \subset [H^1(\Omega_f)]^d$ and $v_s \in V_s \subset [H^1(\Omega_s)]^d$, their traces on the interface Σ are well-defined in $[H^{1/2}(\Sigma)]^d$. That is,*

$$v_f|_\Sigma, \quad v_s|_\Sigma \in [H^{1/2}(\Sigma)]^d.$$

Moreover, the normal components of the stress tensors $\sigma_f(v_f, p_f) \cdot n$ *and* $\sigma_s(u_s) \cdot n$ *belong to the dual space* $[H^{-1/2}(\Sigma)]^d$*. Thus, all interface terms such as*

$$\langle M\overline{v}, \overline{\varphi}\rangle_\Sigma, \quad \langle S[\![v]\!], [\![\varphi]\!]\rangle_\Sigma, \quad \langle h, \overline{\varphi}\rangle_\Sigma, \quad \langle g, [\![\varphi]\!]\rangle_\Sigma,$$

are rigorously defined through the duality pairing between $H^{-1/2}(\Sigma)^d$ *and* $H^{1/2}(\Sigma)^d$*.*

4.2 Weak Formulation

We now establish the weak formulation of the fluid-structure interaction problem.

Let $\boldsymbol{\varphi}^f \in V_f$, $q^f \in L^2(\Omega_f)$, and $\boldsymbol{\varphi}^s \in V_s$ be test functions corresponding to equations (4.3a), (4.3b), and (4.3c), respectively.

Multiplying the fluid momentum equation (4.3a) by $\boldsymbol{\varphi}^f$ and integrating over Ω_f, we obtain:

$$\int_{\Omega_f} \left(\frac{\partial \boldsymbol{v}^f}{\partial t} + (\boldsymbol{v}^f \cdot \nabla)\boldsymbol{v}^f \right) \cdot \boldsymbol{\varphi}^f \, d\boldsymbol{x} - \int_{\Omega_f} \nabla \cdot \boldsymbol{\sigma}_f(\boldsymbol{v}^f, p^f) \cdot \boldsymbol{\varphi}^f \, d\boldsymbol{x} = \int_{\Omega_f} \boldsymbol{f}^f \cdot \boldsymbol{\varphi}^f \, d\boldsymbol{x}.$$

Applying Green's formula to the second term on the left-hand side and incorporating the boundary contributions on Γ_f^N and the fluid–structure interface Σ, we obtain the weak form of the fluid momentum equation:

$$\begin{aligned} \left\langle \frac{\partial \boldsymbol{v}^f}{\partial t}, \boldsymbol{\varphi}^f \right\rangle_{V_f', V_f} + \left((\boldsymbol{v}^f \cdot \nabla)\boldsymbol{v}^f, \boldsymbol{\varphi}^f\right)_{0,f} + \left(\boldsymbol{\sigma}_f(\boldsymbol{v}^f, p^f), \nabla\boldsymbol{\varphi}^f\right)_{0,f} - \langle \boldsymbol{\sigma}_f(\boldsymbol{v}^f, p^f) \cdot \boldsymbol{n}_f, \boldsymbol{\varphi}^f\rangle_\Sigma \\ = \left(\boldsymbol{f}^f, \boldsymbol{\varphi}^f\right)_{0,f} + \langle \boldsymbol{g}_N^f, \boldsymbol{\varphi}^f\rangle_{\Gamma_f^N}, \quad \forall \boldsymbol{\varphi}^f \in V_f. \end{aligned} \tag{4.8}$$

The incompressibility constraint (4.3b) is enforced in weak form as:

$$\int_{\Omega_f} q^f \, \nabla \cdot \boldsymbol{v}^f \, d\boldsymbol{x} = 0, \quad \forall q^f \in L^2(\Omega_f). \tag{4.9}$$

For the structure, multiplying (4.3c) by $\boldsymbol{\varphi}^s \in V_s$ and integrating over Ω_s, we obtain:

$$\int_{\Omega_s} \frac{\partial \boldsymbol{v}^s}{\partial t} \cdot \boldsymbol{\varphi}^s \, d\boldsymbol{x} - \int_{\Omega_s} \nabla \cdot \boldsymbol{\sigma}_s(\boldsymbol{u}^s) \cdot \boldsymbol{\varphi}^s \, d\boldsymbol{x} = \int_{\Omega_s} \boldsymbol{f}^s \cdot \boldsymbol{\varphi}^s \, d\boldsymbol{x}.$$

Using Green's formula, the weak form becomes:

$$\left\langle \frac{\partial \boldsymbol{v}^s}{\partial t}, \boldsymbol{\varphi}^s \right\rangle_{V_s', V_s} + \left(\boldsymbol{\sigma}_s(\boldsymbol{u}^s), \nabla\boldsymbol{\varphi}^s\right)_{0,s} - \langle \boldsymbol{\sigma}_s \cdot \boldsymbol{n}_s, \boldsymbol{\varphi}^s\rangle_\Sigma = \left(\boldsymbol{f}^s, \boldsymbol{\varphi}^s\right)_{0,s}. \tag{4.10}$$

Adding equations (4.8) and (4.10), and substituting $\boldsymbol{\sigma}_f = -p^f \boldsymbol{I} + 2\mu_f \varepsilon(\boldsymbol{v}^f)$, we get the combined weak formulation:

$$\begin{aligned}\left\langle \frac{\partial \boldsymbol{v}^f}{\partial t}, \boldsymbol{\varphi}^f \right\rangle_{V_f', V_f} + \left\langle \frac{\partial \boldsymbol{v}^s}{\partial t}, \boldsymbol{\varphi}^s \right\rangle_{V_s', V_s} + \left((\boldsymbol{v}^f \cdot \nabla)\boldsymbol{v}^f, \boldsymbol{\varphi}^f\right)_{0,f} + \left(\varepsilon(\boldsymbol{v}^f), \varepsilon(\boldsymbol{\varphi}^f)\right)_{0,f} \\ + (\boldsymbol{\sigma}_s(\boldsymbol{u}^s), \varepsilon(\boldsymbol{\varphi}^s))_{0,s} - \langle \boldsymbol{\sigma}_f \cdot \boldsymbol{n}_f, \boldsymbol{\varphi}^f \rangle_\Sigma - \langle \boldsymbol{\sigma}_s \cdot \boldsymbol{n}_s, \boldsymbol{\varphi}^s \rangle_\Sigma \\ = \left(\boldsymbol{f}^f, \boldsymbol{\varphi}^f\right)_{0,f} + (\boldsymbol{f}^s, \boldsymbol{\varphi}^s)_{0,s} + \langle \boldsymbol{g}_N^f, \boldsymbol{\varphi}^f \rangle_{\Gamma_f^N}, \quad \forall \boldsymbol{\varphi}^f \in V_f, \forall \boldsymbol{\varphi}^s \in V_s.\end{aligned} \tag{4.11}$$

Now, applying the identity from [3, 50]

$$\langle u^+, v^+ \rangle_\Sigma - \langle u^-, v^- \rangle_\Sigma = \langle [\![u]\!], \overline{v} \rangle_\Sigma + \langle \overline{u}, [\![v]\!] \rangle_\Sigma, \tag{4.12}$$

and using the fact that $\boldsymbol{n}_s = -\boldsymbol{n}_f$, the interface terms in (4.11) become:

$$\begin{aligned}-\langle \boldsymbol{\sigma}_f \cdot \boldsymbol{n}_f, \boldsymbol{\varphi}^f \rangle_\Sigma - \langle \boldsymbol{\sigma}_s \cdot \boldsymbol{n}_s, \boldsymbol{\varphi}^s \rangle_\Sigma &= \langle [\![\boldsymbol{\sigma} \cdot \boldsymbol{n}_s]\!], \overline{\boldsymbol{\varphi}} \rangle_\Sigma + \langle \overline{\boldsymbol{\sigma} \cdot \boldsymbol{n}_s}, [\![\boldsymbol{\varphi}]\!] \rangle_\Sigma \\ &= \langle \boldsymbol{M}\, \overline{\boldsymbol{v}}, \overline{\boldsymbol{\varphi}} \rangle_\Sigma - \langle \boldsymbol{h}, \overline{\boldsymbol{\varphi}} \rangle_\Sigma + \langle \boldsymbol{S}[\![\boldsymbol{v}]\!], [\![\boldsymbol{\varphi}]\!] \rangle_\Sigma - \langle \boldsymbol{g}, [\![\boldsymbol{\varphi}]\!] \rangle_\Sigma.\end{aligned}$$

Definition 4.1 (Weak Solution of the FSI Problem)**.** *Let* $\left(\boldsymbol{v}_0^f, \boldsymbol{v}_0^s, \boldsymbol{u}_0^s\right) \in V_f \times V_s \times V_s$, *and let* $T > 0$. *A pair* $(\boldsymbol{v}^f, \boldsymbol{v}^s) \in L^\infty(0, T; V_f \times V_s)$, *with* $\dfrac{\partial \boldsymbol{v}^f}{\partial t} \in L^2(0, T; V_f')$ *and* $\dfrac{\partial \boldsymbol{v}^s}{\partial t} \in L^2(0, T; V_s')$ *is called a* weak solution *of problem* (4.3) *if:*

- *Initial conditions are satisfied:*

$$\boldsymbol{v}^f(0) = \boldsymbol{v}_0^f, \quad \boldsymbol{v}^s(0) = \boldsymbol{v}_0^s, \quad \boldsymbol{u}^s(0) = \boldsymbol{u}_0^s.$$

- *For almost every* $t \in (0, T)$ *and for all test functions* $(\boldsymbol{\varphi}^f, \boldsymbol{\varphi}^s) \in V_f \times V_s$,

$$\begin{aligned}\left\langle \frac{\partial \boldsymbol{v}^f}{\partial t}, \boldsymbol{\varphi}^f \right\rangle_{V_f', V_f} + \left\langle \frac{\partial \boldsymbol{v}^s}{\partial t}, \boldsymbol{\varphi}^s \right\rangle_{V_s', V_s} + \left((\boldsymbol{v}^f \cdot \nabla)\boldsymbol{v}^f, \boldsymbol{\varphi}^f\right)_{0,f} \\ + \left(\varepsilon(\boldsymbol{v}^f), \varepsilon(\boldsymbol{\varphi}^f)\right)_{0,f} + \left(\sigma_s(\boldsymbol{u}^s), \varepsilon(\boldsymbol{\varphi}^s)\right)_{0,s} \\ + \langle \boldsymbol{M}\overline{\boldsymbol{v}}, \overline{\boldsymbol{\varphi}} \rangle_\Sigma + \langle \boldsymbol{S}[\![\boldsymbol{v}]\!], [\![\boldsymbol{\varphi}]\!] \rangle_\Sigma \\ = \left(\boldsymbol{f}^f, \boldsymbol{\varphi}^f\right)_{0,f} + \left(\boldsymbol{f}^s, \boldsymbol{\varphi}^s\right)_{0,s} + \langle \boldsymbol{g}_N^f, \boldsymbol{\varphi}^f \rangle_{\Gamma_f^N} + \langle \boldsymbol{h}, \overline{\boldsymbol{\varphi}} \rangle_\Sigma + \langle \boldsymbol{g}, [\![\boldsymbol{\varphi}]\!] \rangle_\Sigma,\end{aligned} \tag{4.13}$$

  where $\langle \cdot, \cdot \rangle_{V', V}$ *denotes the duality pairing between* V' *and* V.

4.3 Existence of Solution

4.3.1 Auxiliary Problem and Abstract Nonlinear Evolution

To establish the existence of a solution to the fluid–structure interaction problem, we follow the same approach as in [13] where nonlinear semigroup theory is used. To that end, we define the operators

$$\begin{aligned}(B\boldsymbol{u},\boldsymbol{v}) &\equiv \big((\boldsymbol{u}^f\cdot\nabla)\boldsymbol{u}^f,\boldsymbol{v}^f\big)_{0,f},\\ (A_B\boldsymbol{u},\boldsymbol{v}) &\equiv \big(\varepsilon(\boldsymbol{u}^f),\varepsilon(\boldsymbol{v}^f)\big)_{0,f}+\big(\sigma_s(\boldsymbol{u}^s),\varepsilon(\boldsymbol{v}^s)\big)_{0,s}+\langle\boldsymbol{M}\overline{\boldsymbol{u}},\overline{\boldsymbol{v}}\rangle_\Sigma+\langle\boldsymbol{S}[\![\boldsymbol{u}]\!],[\![\boldsymbol{v}]\!]\rangle_\Sigma+(B\boldsymbol{u},\boldsymbol{v}),\\ (\boldsymbol{F},\boldsymbol{v}) &\equiv (\boldsymbol{f},\boldsymbol{v})_0+\langle\boldsymbol{g}_N,\boldsymbol{v}^f\rangle_{\Gamma_f^N}+\langle\boldsymbol{h},\overline{\boldsymbol{v}}\rangle_\Sigma+\langle\boldsymbol{g},[\![\boldsymbol{v}]\!]\rangle_\Sigma,\end{aligned}$$

and we analyzing the abstract nonlinear evolution equation derived from (4.13):

$$\frac{d\boldsymbol{v}}{dt}+A_B(\boldsymbol{v})=\boldsymbol{F},\quad \boldsymbol{v}(0)=(\boldsymbol{v}_0^f,\boldsymbol{v}_0^s)\in V_f\times V_s, \tag{4.14}$$

where the domain of A_B is

$$\mathscr{D}(A_B)=\Big\{\boldsymbol{v}\in V\;\Big|\;\sigma_s(\boldsymbol{u}^s)\in[L^2(\Omega_s)]^{d\times d},\;[\![\sigma\cdot\boldsymbol{n}]\!]_\Sigma=\boldsymbol{M}\overline{\boldsymbol{v}}-\boldsymbol{h},\;\overline{\sigma\cdot\boldsymbol{n}}_\Sigma=\boldsymbol{S}[\![\boldsymbol{v}]\!]-\boldsymbol{g}\Big\}. \tag{4.15}$$

Let $L:V\to V'$ be a nonlinear operator assumed to satisfy the same conditions as in [13]: it is locally Lipschitz, with $L(0)=0$, and for every $\eta>0$, there exists a constant $C_\eta>0$ such that for all $\boldsymbol{u},\boldsymbol{v}\in V_f$,

$$|(L\boldsymbol{u}-L\boldsymbol{v},\boldsymbol{u}-\boldsymbol{v})_{0,f}|\le\eta\|\boldsymbol{u}-\boldsymbol{v}\|_{1,f}^2+C_\eta\|\boldsymbol{u}-\boldsymbol{v}\|_{0,f}^2. \tag{4.16}$$

To facilitate the analysis, we consider an auxiliary problem in which the nonlinear convective operator B is replaced by the operator L (accordingly A_B is replaced by A_L), that leads to the auxilary problem for almost every $t\in(0,T)$ and for all test functions $(\boldsymbol{\varphi}^f,\boldsymbol{\varphi}^s)\in V_f\times V_s$,

$$\begin{aligned}&\left\langle\frac{\partial\boldsymbol{v}^f}{\partial t},\boldsymbol{\varphi}^f\right\rangle_{V_f',V_f}+\left\langle\frac{\partial\boldsymbol{v}^s}{\partial t},\boldsymbol{\varphi}^s\right\rangle_{V_s',V_s}+\big(L\boldsymbol{v},\boldsymbol{\varphi}\big)+\big(\varepsilon(\boldsymbol{v}^f),\varepsilon(\boldsymbol{\varphi}^f)\big)_{0,f}\\ &\qquad+\big(\sigma_s(\boldsymbol{u}^s),\varepsilon(\boldsymbol{\varphi}^s)\big)_{0,s}+\langle\boldsymbol{M}\overline{\boldsymbol{v}},\overline{\boldsymbol{\varphi}}\rangle_\Sigma+\langle\boldsymbol{S}[\![\boldsymbol{v}]\!],[\![\boldsymbol{\varphi}]\!]\rangle_\Sigma\\ &=\big(\boldsymbol{f}^f,\boldsymbol{\varphi}^f\big)_{0,f}+\big(\boldsymbol{f}^s,\boldsymbol{\varphi}^s\big)_{0,s}+\langle\boldsymbol{g}_N^f,\boldsymbol{\varphi}^f\rangle_{\Gamma_f^N}+\langle\boldsymbol{h},\overline{\boldsymbol{\varphi}}\rangle_\Sigma+\langle\boldsymbol{g},[\![\boldsymbol{\varphi}]\!]\rangle_\Sigma,\end{aligned} \tag{4.17}$$

The first step is to prove that the operator A_L generates a C_0-semigroup on V. This is the aim of the following lemma.

Lemma 4.1. *Let L be a nonlinear operator satisfying property (4.16). Then, the operator A_L, with domain $\mathscr{D}(A_L)$ as defined in (4.15), generates a strongly continuous (nonlinear) semigroup on V.*

Proof. The proof is established once we show that A_L is ω-m-accretive (from Crandall–Liggett theorem 1.9).

ω-accretivity: Assume $\boldsymbol{u} = \boldsymbol{u}_1 - \boldsymbol{u}_2 \in \mathscr{D}(A_L)$, then:

$$\begin{aligned}(A_L\boldsymbol{u}, \boldsymbol{u}) &= (A_L\boldsymbol{u}_1 - A_L\boldsymbol{u}_2, \boldsymbol{u}) \\ &= \big(\varepsilon(\boldsymbol{u}^f), \varepsilon(\boldsymbol{u}^f)\big)_{0,f} + (\sigma_s(\boldsymbol{u}^s), \varepsilon(\boldsymbol{u}^s))_{0,s} + \langle \boldsymbol{M}\overline{\boldsymbol{u}}, \overline{\boldsymbol{u}}\rangle_\Sigma + \langle \boldsymbol{S}[\![\boldsymbol{u}]\!], [\![\boldsymbol{u}]\!]\rangle_\Sigma \\ &\quad + \Big(L\boldsymbol{u}_1^f - L\boldsymbol{u}_2^f, \boldsymbol{u}_1^f - \boldsymbol{u}_2^f\Big)_{0,f} \\ &\geq \|\boldsymbol{u}^f\|_{1,f}^2 - \eta\|\boldsymbol{u}^f\|_{1,f}^2 - C_\eta\|\boldsymbol{u}^f\|_{0,f}^2.\end{aligned}$$

We now consider the operator $\omega\boldsymbol{I} + A_L$ instead of A_L. Then we have:

$$\begin{aligned}((\omega\boldsymbol{I} + A_L)\boldsymbol{u}, \boldsymbol{u}) &\geq \omega\|\boldsymbol{u}^f\|_{0,f}^2 + \|\boldsymbol{u}^f\|_{1,f}^2 - \eta\|\boldsymbol{u}^f\|_{1,f}^2 - C_\eta\|\boldsymbol{u}^f\|_{0,f}^2 \\ &= (1-\eta)\|\boldsymbol{u}^f\|_{1,f}^2 + (\omega - C_\eta)\|\boldsymbol{u}^f\|_{0,f}^2.\end{aligned}$$

By choosing $\eta > 0$ and $\omega > 0$ such that $1 - \eta > 0$ and $\omega - C_\eta > 0$, it follows that:

$$(A_L\boldsymbol{u}, \boldsymbol{u}) + \omega\|\boldsymbol{u}\|_0^2 \geq 0, \tag{4.18}$$

which shows that A_L is ω-accretive.

Maximality: From the accretivity estimate proved previously, there exists $\omega \geq 0$ such that A_L is ω-accretive. Let $\alpha > \omega$.

We consider the operator $\alpha I + A_L$. For any $u, v \in V$, we have

$$\langle(\alpha I + A_L)u - (\alpha I + A_L)v, u - v\rangle \geq (\alpha - \omega)\|u - v\|_V^2,$$

which shows that $\alpha I + A_L$ is strongly monotone.

Moreover, all linear terms in A_L are continuous, and the nonlinear operator L is locally Lipschitz; hence $\alpha I + A_L$ is hemicontinuous. Finally, the coercivity follows from the presence of the term $\alpha\|u\|_V^2$.

Therefore, all assumptions of the Browder–Minty theorem 1.11 are satisfied, and $\alpha I + A_L$ is surjective from V onto V'. This proves that A_L is ω-m-accretive.

Since A_L is ω-m-accretive, it generates a strongly continuous nonlinear semigroup on V. □

Corollary 4. *For every data $(\boldsymbol{v}_0^f, \boldsymbol{v}_0^s) \in \mathscr{D}(A_L)$, and for $\boldsymbol{u}_0^s \in V_s$, the semigroup solution $(\boldsymbol{v}^f, \boldsymbol{v}^s)$ satisfies, for all $t \in (0,T)$, the variational formulation (4.17) with L instead of B.*

The proof is straightforward; the reader may refer to Corollary 3.1 of [13] for a detailed argument.

Theorem 4.1. *Let $(\boldsymbol{v}_0^f, \boldsymbol{v}_0^s) \in V_f \times V_s$, $\boldsymbol{u}_0^s \in V_s$, and let $(\boldsymbol{v}^f, \boldsymbol{v}^s)$ be the corresponding semigroup solutions given by Lemma 4.1. Then the solutions $(\boldsymbol{v}^f, \boldsymbol{v}^s)$ satisfy the variational formulation (4.17).*

The key point of this theorem is to show that even when the initial data lie in the larger space $V_s \times V_f$ (instead of $\mathscr{D}(A_L)$), the semigroup solution still satisfies the variational formulation.

Proof. The proof relies on the density of $\mathscr{D}(A_L)$ in $V = V_f \times V_s$.

Since A_L is ω-m-accretive on V, its resolvent $(I+\lambda A_L)^{-1}$ is well defined, single-valued, and nonexpansive on V. Moreover, it satisfies the strong convergence property

$$\lim_{\lambda \to 0^+} (I + \lambda A_L)^{-1} \boldsymbol{y} = \boldsymbol{y} \quad \text{in } V,$$

for all $\boldsymbol{y} \in V$ (see [22, Chapter II,]).

Let $(\boldsymbol{v}_0^f, \boldsymbol{v}_0^s) \in V_f \times V_s$ be arbitrary. For $\alpha > 0$, define

$$(\boldsymbol{v}_0^{f,\alpha}, \boldsymbol{v}_0^{s,\alpha}) := \left(I + \frac{1}{\alpha} A_L \right)^{-1} (\boldsymbol{v}_0^f, \boldsymbol{v}_0^s).$$

Then $(\boldsymbol{v}_0^{f,\alpha}, \boldsymbol{v}_0^{s,\alpha}) \in \mathscr{D}(A_L)$ and

$$(\boldsymbol{v}_0^{f,\alpha}, \boldsymbol{v}_0^{s,\alpha}) + \frac{1}{\alpha} A_L (\boldsymbol{v}_0^{f,\alpha}, \boldsymbol{v}_0^{s,\alpha}) = (\boldsymbol{v}_0^f, \boldsymbol{v}_0^s).$$

Letting $\alpha \to \infty$ yields

$$(\boldsymbol{v}_0^{f,\alpha}, \boldsymbol{v}_0^{s,\alpha}) \longrightarrow (\boldsymbol{v}_0^f, \boldsymbol{v}_0^s) \quad \text{strongly in } V,$$

which proves that $\mathscr{D}(A_L)$ is dense in V.

For each $\alpha > 0$, let $(\boldsymbol{v}^{f,\alpha}, \boldsymbol{v}^{s,\alpha})$ be the semigroup solution with initial data $(\boldsymbol{v}_0^{f,\alpha}, \boldsymbol{v}_0^{s,\alpha})$. By the previous corollary, each of these solutions satisfies the variational formulation (4.17). Using the contraction property of the semigroup and passing to the limit $\alpha \to \infty$, we conclude that the semigroup solution corresponding to $(\boldsymbol{v}_0^f, \boldsymbol{v}_0^s)$ also satisfies (4.17). □

Now, we return to the original operator B but with a more general form:

$$\begin{aligned} B(u,v) &\equiv (u\cdot\nabla)v, \\ B(u) &\equiv B(u,u), \\ b(u,v,w) &\equiv ((u\cdot\nabla)v,w)\,. \end{aligned} \tag{4.19}$$

Let us also consider a truncation of the nonlinear operator B, and let it be $B_n : V_f \to V_f'$ defined by

$$B_n(v) \equiv \begin{cases} B(v), & \|v\|_1 \le n, \\ n^2\dfrac{B(v)}{\|v\|_1^2}, & \|v\|_1 \ge n. \end{cases} \tag{4.20}$$

The nonlinear operator B_n verifies property (4.16) and the same properties as L (see Lemma 3.5 of [13] for a detailed proof), meaning that the existence of a semigroup solution corresponding to the operator $A_n \equiv A_{B_n}$ is guaranteed. It satisfies the following weak formulation:

$$\begin{aligned} \left(\frac{\partial \boldsymbol{v}^{f,n}}{\partial t},\boldsymbol{\varphi}^f\right)_{0,f} + \left(\frac{\partial \boldsymbol{v}^{s,n}}{\partial t},\boldsymbol{\varphi}^s\right)_{0,s} + \left(\varepsilon(\boldsymbol{v}^{f,n}),\varepsilon(\boldsymbol{\varphi}^f)\right)_{0,f} + (\sigma_s(\boldsymbol{u}^{s,n}),\varepsilon(\boldsymbol{\varphi}^s))_{0,s} \\ + \left(B_n(\boldsymbol{v}^{f,n}),\boldsymbol{\varphi}^f\right)_{0,f} + \langle \boldsymbol{M}\,\overline{\boldsymbol{v}^n},\overline{\boldsymbol{\varphi}}\rangle_\Sigma + \langle \boldsymbol{S}[\![\boldsymbol{v}^n]\!],[\![\boldsymbol{\varphi}]\!]\rangle_\Sigma \\ = \left(\boldsymbol{f}^f,\boldsymbol{\varphi}^f\right)_{0,f} + (\boldsymbol{f}^s,\boldsymbol{\varphi}^s)_{0,s} + \langle \boldsymbol{g}_N^f,\boldsymbol{\varphi}^f\rangle_{\Gamma_f^N} + \langle \boldsymbol{h},\overline{\boldsymbol{\varphi}}\rangle_\Sigma + \langle \boldsymbol{g},[\![\boldsymbol{\varphi}]\!]\rangle_\Sigma. \end{aligned} \tag{4.21}$$

What remains is to prove that, by passing to the limit as $n\to\infty$, the result remains valid. This is the goal of the next theorem.

Before that, we state the following lemma from [13] regarding the properties of the trilinear form $b(\cdot,\cdot,\cdot)$.

Lemma 4.2 ([13, 33, 88]). *The trilinear form $b(\cdot,\cdot,\cdot)$, given in (4.19), satisfies the following properties for all $u\in V_f$, $v,w\in[H^1(\Omega_f)]^d$, where $d=\dim(\Omega_f)$:*

1. *For $p_1,p_2,p_3\ge 0$ such that*

$$\begin{cases} p_1+p_2+p_3 \ge \dfrac{d}{2}, & \text{if } p_i \ne \dfrac{d}{2} \text{ for all } i\in\{1,2,3\}, \\ p_1+p_2+p_3 > \dfrac{d}{2}, & \text{if } p_i = \dfrac{d}{2} \text{ for some } i\in\{1,2,3\}, \end{cases}$$

then there exists a constant $C>0$ such that

$$|((u\cdot\nabla)v,w)| \le C\,\|u\|_{p_1,f}\,\|v\|_{p_2+1,f}\,\|w\|_{p_3,f}.$$

2. *If $d = 2$, then there exist constants $C_1, C_2 > 0$ such that*

$$|b(u, v, w)| \leq C_1 \|u\|_{1/2,f} \|v\|_{1,f} \|w\|_{1/2,f} + C_2 \|u\|_{1/2,f} \|v\|_{3/4,f} \|w\|_{3/4,f}.$$

3. *If $d = 3$, then there exist constants $C_3, C_4 > 0$ such that*

$$|b(u, v, w)| \leq C_3 \|u\|_{1/2,f} \|v\|_{1,f} \|w\|_{1,f},$$
$$|b(u, v, w)| \leq C_4 \|u\|_{3/4,f} \|v\|_{1,f} \|w\|_{3/4,f}.$$

4. *The trilinear form satisfies the skew-symmetry property:*

$$b(u, v, w) = -b(u, w, v), \quad \text{in particular, } b(u, u, u) = 0.$$

Before stating the theorem and its proof, we present the following result, which will be needed in the energy estimates.

Proposition 4.1. *Let $u^s \in H^1(0, T; H^1(\Omega_s))$ and set $v^s = \partial_t u^s$. Let $\sigma_s(u) = \mathbb{C} : \varepsilon(u)$ be the linear elasticity stress tensor, where $\mathbb{C}$ is symmetric and positive definite. Then the following properties hold:*

1. *For all $u^s, v^s \in H^1(\Omega_s)$,*

$$(\sigma_s(u^s), \varepsilon(v^s))_{0,s} = (\varepsilon(v^s), \sigma_s(u^s))_{0,s} = (\varepsilon(u^s), \sigma_s(v^s))_{0,s}.$$

2. *For a.e. $t \in (0, T)$, the following identity holds:*

$$\frac{1}{2} \frac{d}{dt} (\sigma_s(u^s(t)), \varepsilon(u^s(t)))_{0,s} = (\sigma_s(u^s(t)), \varepsilon(v^s(t)))_{0,s}.$$

Proof. **(i)** Since $\mathbb{C}$ is symmetric and $\varepsilon(u)$ and $\varepsilon(v)$ are symmetric tensors. The symmetry of the scalar product is trivial

$$(\sigma_s(u), \varepsilon(v))_{0,s} = (\varepsilon(v), \sigma_s(u))_{0,s}.$$

(ii) Let $u^s \in H^1(0, T; H^1(\Omega_s))$ and set $v^s = \partial_t u^s$. The mapping

$$t \mapsto (\sigma_s(u^s(t)), \varepsilon(u^s(t)))_{0,s}$$

is absolutely continuous. Using the chain rule in Hilbert spaces, we obtain

$$\frac{d}{dt}(\sigma_s(u^s),\varepsilon(u^s)) = (\sigma_s(\partial_t u^s),\varepsilon(u^s)) + (\sigma_s(u^s),\varepsilon(\partial_t u^s)).$$

By part (i),

$$(\sigma_s(\partial_t u^s),\varepsilon(u^s)) = (\sigma_s(u^s),\varepsilon(\partial_t u^s)).$$

Hence,

$$\frac{d}{dt}(\sigma_s(u^s),\varepsilon(u^s)) = 2(\sigma_s(u^s),\varepsilon(\partial_t u^s)).$$

Therefore,

$$\frac{1}{2}\frac{d}{dt}(\sigma_s(u^s(t)),\varepsilon(u^s(t)))_{0,s} = (\sigma_s(u^s(t)),\varepsilon(v^s(t)))_{0,s},$$

for almost every $t \in (0,T)$.

□

Theorem 4.2. *For every initial condition $(\boldsymbol{v}_0^f, \boldsymbol{v}_0^s, \boldsymbol{u}_0^s) \in V_f \times V_s \times V_s$, there exists a solution*

$$(\boldsymbol{v}^f, \boldsymbol{v}^s) \in C([0,T]; H_f \times H_s) \cap L^2(0,T; V_f \times V_s),$$

with

$$\partial_t \boldsymbol{v}^s \in L^1(0,T;V_s'), \quad \partial_t \boldsymbol{v}^f \in L^1(0,T;V_f'), \quad B(\boldsymbol{v}^f) \in L^1(0,T;V_f'),$$

and

$$\boldsymbol{u}^s \in H^1(0,T;V_s), \qquad \partial_t \boldsymbol{u}^s = \boldsymbol{v}^s,$$

such that for all $(\boldsymbol{\varphi}^f, \boldsymbol{\varphi}^s) \in V_f \times V_s$ and for a.e. $t \in (0,T)$,

$$\begin{aligned} \left\langle \frac{\partial \boldsymbol{v}^f}{\partial t}, \boldsymbol{\varphi}^f \right\rangle_{V_f', V_f} + \left\langle \frac{\partial \boldsymbol{v}^s}{\partial t}, \boldsymbol{\varphi}^s \right\rangle_{V_s', V_s} + \big(\varepsilon(\boldsymbol{v}^f), \varepsilon(\boldsymbol{\varphi}^f)\big)_{0,f} \\ + (\sigma_s(\boldsymbol{u}^s), \varepsilon(\boldsymbol{\varphi}^s))_{0,s} + \langle B(\boldsymbol{v}^f), \boldsymbol{\varphi}^f \rangle_{V_f', V_f} \\ + \langle \boldsymbol{M}\overline{\boldsymbol{v}}, \overline{\boldsymbol{\varphi}} \rangle_\Sigma + \langle \boldsymbol{S}[\![\boldsymbol{v}]\!], [\![\boldsymbol{\varphi}]\!] \rangle_\Sigma \\ = \big(\boldsymbol{f}^f, \boldsymbol{\varphi}^f\big)_{0,f} + (\boldsymbol{f}^s, \boldsymbol{\varphi}^s)_{0,s} + \langle \boldsymbol{g}_N^f, \boldsymbol{\varphi}^f \rangle_{\Gamma_f^N} + \langle \boldsymbol{h}, \overline{\boldsymbol{\varphi}} \rangle_\Sigma + \langle \boldsymbol{g}, [\![\boldsymbol{\varphi}]\!] \rangle_\Sigma. \end{aligned} \tag{4.22}$$

Proof. From Theorem 4.1, one can conclude the existence of semigroup solutions $(\boldsymbol{v}^{s,n}, \boldsymbol{v}^{f,n}) \in V_s \times V_f$. The desired result should be achieved once we take $n \to \infty$ in the weak formulation (4.21). For that, some a priori bounds are needed.

Step 1: A priori bounds Let us consider the weak form (4.21) with the test functions $\boldsymbol{\varphi}^f = \boldsymbol{v}^{f,n}$, $\boldsymbol{\varphi}^s = \boldsymbol{v}^{s,n}$. Using the property $b(\boldsymbol{v}^{f,n}, \boldsymbol{v}^{f,n}, \boldsymbol{v}^{f,n}) = 0$, we obtain:

$$\begin{aligned}\frac{1}{2}\frac{d}{dt}\left(\left\|\boldsymbol{v}^{f,n}(t)\right\|_{0,f}^2 + \|\boldsymbol{v}^{s,n}(t)\|_{0,s}^2\right) + (\sigma_s(\boldsymbol{u}^{s,n}(t)), \varepsilon(\boldsymbol{v}^{s,n}(t)))_{0,s} + \left\|\varepsilon(\boldsymbol{v}^{f,n}(t))\right\|_{0,f}^2 \\ + \langle \boldsymbol{M}\,\overline{\boldsymbol{v}^n(t)}, \overline{\boldsymbol{v}^n(t)}\rangle_\Sigma + \langle \boldsymbol{S}[\![\boldsymbol{v}^n(t)]\!], [\![\boldsymbol{v}^n(t)]\!]\rangle_\Sigma \\ = \left(\boldsymbol{f}^f(t), \boldsymbol{v}^{f,n}(t)\right)_{0,f} + (\boldsymbol{f}^s(t), \boldsymbol{v}^{s,n}(t))_{0,s} + \langle \boldsymbol{g}_N^f(t), \boldsymbol{v}^{f,n}(t)\rangle_{\Gamma_f^N} \\ + \langle \boldsymbol{h}(t), \overline{\boldsymbol{v}^n(t)}\rangle_\Sigma + \langle \boldsymbol{g}(t), [\![\boldsymbol{v}^n(t)]\!]\rangle_\Sigma.\end{aligned} \tag{4.23}$$

Applying the ellipticity assumption (4.2) on M ans S, and integrating over the time interval $(0,t)$, for almost every $t \in (0,T)$, yields:

$$\begin{aligned}\frac{1}{2}\left(\left\|\boldsymbol{v}^{f,n}(t)\right\|_{0,f}^2 + \|\boldsymbol{v}^{s,n}(t)\|_{0,s}^2\right) + \int_0^t \left\|\varepsilon(\boldsymbol{v}^{f,n}(s))\right\|_{0,f}^2 ds + \int_0^t (\sigma_s(\boldsymbol{u}^{s,n}(s)), \varepsilon(\boldsymbol{v}^{s,n}(s)))_{0,s}\, ds \\ + \boldsymbol{M}_0 \int_0^t \|\overline{\boldsymbol{v}^n(s)}\|_{1/2,\Sigma}^2 ds + \boldsymbol{S}_0 \int_0^t \|[\![\boldsymbol{v}^n(s)]\!]\|_{1/2,\Sigma}^2 ds \\ \leq \int_0^t \left(\boldsymbol{f}^f(s), \boldsymbol{v}^{f,n}(s)\right)_{0,f} ds + \int_0^t (\boldsymbol{f}^s(s), \boldsymbol{v}^{s,n}(s))_{0,s}\, ds + \int_0^t \langle \boldsymbol{g}_N^f(s), \boldsymbol{v}^{f,n}(s)\rangle_{\Gamma_f^N} ds \\ + \int_0^t \langle \boldsymbol{h}(s), \overline{\boldsymbol{v}^n(s)}\rangle_\Sigma\, ds + \int_0^t \langle \boldsymbol{g}(s), [\![\boldsymbol{v}^n(s)]\!]\rangle_\Sigma\, ds + \frac{1}{2}\left(\left\|\boldsymbol{v}_0^f\right\|_{0,f}^2 + \|\boldsymbol{v}_0^s\|_{0,s}^2\right).\end{aligned} \tag{4.24}$$

Using *ii.* from proposition 4.1 in inequality (4.24) we get

$$\begin{aligned}\frac{1}{2}\left(\left\|\boldsymbol{v}^{f,n}(t)\right\|_{0,f}^2 + \|\boldsymbol{v}^{s,n}(t)\|_{0,s}^2\right) + \int_0^t \left\|\varepsilon(\boldsymbol{v}^{f,n}(s))\right\|_{0,f}^2 ds + \frac{1}{2}(\sigma_s(\boldsymbol{u}^{s,n}(t)), \varepsilon(\boldsymbol{u}^{s,n}(t)))_{0,s} \\ + \boldsymbol{M}_0 \int_0^t \|\overline{\boldsymbol{v}^n(s)}\|_{1/2,\Sigma}^2 ds + \boldsymbol{S}_0 \int_0^t \|[\![\boldsymbol{v}^n(s)]\!]\|_{1/2,\Sigma}^2 ds \\ \leq \int_0^t \left(\boldsymbol{f}^f(s), \boldsymbol{v}^{f,n}(s)\right)_{0,f} ds + \int_0^t (\boldsymbol{f}^s(s), \boldsymbol{v}^{s,n}(s))_{0,s}\, ds + \int_0^t \langle \boldsymbol{g}_N^f(s), \boldsymbol{v}^{f,n}(s)\rangle_{\Gamma_f^N} ds \\ + \int_0^t \langle \boldsymbol{h}(s), \overline{\boldsymbol{v}^n(s)}\rangle_\Sigma\, ds + \int_0^t \langle \boldsymbol{g}(s), [\![\boldsymbol{v}^n(s)]\!]\rangle_\Sigma\, ds \\ + \frac{1}{2}\left(\left\|\boldsymbol{v}_0^f\right\|_{0,f}^2 + \|\boldsymbol{v}_0^s\|_{0,s}^2 + (\sigma_s(\boldsymbol{u}_0^s), \varepsilon(\boldsymbol{u}_0^s))_{0,s}\right).\end{aligned} \tag{4.25}$$

Applying Cauchy-Schwarz inequality to the right-hand side terms in (4.25) gives:

$$\begin{aligned}\frac{1}{2}\left(\left\|\boldsymbol{v}^{f,n}(t)\right\|_{0,f}^2+\|\boldsymbol{v}^{s,n}(t)\|_{0,s}^2\right)+\int_0^t\left\|\varepsilon(\boldsymbol{v}^{f,n}(s))\right\|_{0,f}^2\,ds+\frac{1}{2}\left(\sigma_s(\boldsymbol{u}^{s,n}(t)),\varepsilon(\boldsymbol{u}^{s,n}(t))\right)_{0,s}\\ +\boldsymbol{M}_0\int_0^t\|\overline{\boldsymbol{v}^n(s)}\|_{1/2,\Sigma}^2\,ds+\boldsymbol{S}_0\int_0^t\|[\![\boldsymbol{v}^n(s)]\!]\|_{1/2,\Sigma}^2\,ds\\ \leq\int_0^t\left\|\boldsymbol{f}^f(s)\right\|_{0,f}\left\|\boldsymbol{v}^{f,n}(s)\right\|_{0,f}\,ds+\int_0^t\|\boldsymbol{f}^s(s)\|_{0,s}\|\boldsymbol{v}^{s,n}(s)\|_{0,s}\,ds\\ +\int_0^t\|\boldsymbol{h}(s)\|_{1/2,\Sigma}\left\|\overline{\boldsymbol{v}^n(s)}\right\|_{1/2,\Sigma}\,ds+\int_0^t\|\boldsymbol{g}(s)\|_{1/2,\Sigma}\|[\![\boldsymbol{v}^n(s)]\!]\|_{1/2,\Sigma}\,ds\\ +\int_0^t\left\|\boldsymbol{g}_N^f(s)\right\|_{1/2,\Gamma_f^N}\left\|\boldsymbol{v}^{f,n}(s)\right\|_{1/2,\Gamma_f^N}\,ds+\frac{1}{2}\left(\left\|\boldsymbol{v}_0^f\right\|_{0,f}^2+\|\boldsymbol{v}_0^s\|_{0,s}^2+\left(\sigma_s(\boldsymbol{u}_0^s),\varepsilon(\boldsymbol{u}_0^s)\right)_{0,s}\right)\end{aligned}\tag{4.26}$$

From the coercivity of the elasticity tensor together with Korn's inequality (see [30]), we know that

$$\left(\sigma_s(\boldsymbol{u}^{s,n}(t)),\varepsilon(\boldsymbol{u}^{s,n}(t))\right)_{0,s}\geq c_s\,\|\boldsymbol{u}^{s,n}(t)\|_{1,s}^2\quad\text{and}\quad\|\varepsilon(v^{f,n}(t))\|_{0,f}^2\geq c_6\|v^{f,n}(t)\|_{1,f}^2.\tag{4.27}$$

Applying (4.27) to inequality (4.26) yields

$$\begin{aligned}\frac{1}{2}\left(\left\|\boldsymbol{v}^{f,n}(t)\right\|_{0,f}^2+\|\boldsymbol{v}^{s,n}(t)\|_{0,s}^2\right)+c_6\int_0^t\left\|\boldsymbol{v}^{f,n}(s)\right\|_{1,f}^2\,ds+\frac{1}{4}\left(\sigma_s(\boldsymbol{u}^{s,n}(t)),\varepsilon(\boldsymbol{u}^{s,n}(t))\right)_{0,s}\\ +\frac{c_5}{4}\|\boldsymbol{u}^{s,n}(t)\|_{1,s}^2+\boldsymbol{M}_0\int_0^t\|\overline{\boldsymbol{v}^n(s)}\|_{1/2,\Sigma}^2\,ds+\boldsymbol{S}_0\int_0^t\|[\![\boldsymbol{v}^n(s)]\!]\|_{1/2,\Sigma}^2\,ds\\ \leq\int_0^t\left\|\boldsymbol{f}^f(s)\right\|_{0,f}\left\|\boldsymbol{v}^{f,n}(s)\right\|_{0,f}\,ds+\int_0^t\|\boldsymbol{f}^s(s)\|_{0,s}\|\boldsymbol{v}^{s,n}(s)\|_{0,s}\,ds\\ +\int_0^t\|\boldsymbol{h}(s)\|_{1/2,\Sigma}\left\|\overline{\boldsymbol{v}^n(s)}\right\|_{1/2,\Sigma}\,ds+\int_0^t\|\boldsymbol{g}(s)\|_{1/2,\Sigma}\|[\![\boldsymbol{v}^n(s)]\!]\|_{1/2,\Sigma}\,ds\\ +\int_0^t\left\|\boldsymbol{g}_N^f(s)\right\|_{1/2,\Gamma_f^N}\left\|\boldsymbol{v}^{f,n}(s)\right\|_{1/2,\Gamma_f^N}\,ds+\frac{1}{2}\left(\left\|\boldsymbol{v}_0^f\right\|_{0,f}^2+\|\boldsymbol{v}_0^s\|_{0,s}^2+\left(\sigma_s(\boldsymbol{u}_0^s),\varepsilon(\boldsymbol{u}_0^s)\right)_{0,s}\right)\end{aligned}\tag{4.28}$$

By applying Young's inequality $ab \leq \frac{1}{2c}a^2 + \frac{c}{2}b^2$, we obtain:

$$\begin{aligned}
&\frac{1}{2}\left(\left\|\boldsymbol{v}^{f,n}(t)\right\|_{0,f}^2 + \|\boldsymbol{v}^{s,n}(t)\|_{0,s}^2\right) + c_6\int_0^t \left\|\boldsymbol{v}^{f,n}(s)\right\|_{1,f}^2\, ds \\
&\quad + \frac{1}{4}\left(\sigma_s(\boldsymbol{u}^{s,n}(t)), \varepsilon(\boldsymbol{u}^{s,n}(t))\right)_{0,s} + \frac{c_5}{4}\|\boldsymbol{u}^{s,n}(t)\|_{1,s}^2 \\
&\quad + \boldsymbol{M}_0\int_0^t \|\overline{\boldsymbol{v}^n(s)}\|_{1/2,\Sigma}^2\, ds + \boldsymbol{S}_0\int_0^t \|[\![\boldsymbol{v}^n(s)]\!]\|_{1/2,\Sigma}^2\, ds \\
&\quad \leq \frac{1}{2c_7}\int_0^t \left\|\boldsymbol{f}^f(s)\right\|_{0,f}^2\, ds + \frac{c_7}{2}\int_0^t \left\|\boldsymbol{v}^{f,n}(s)\right\|_{0,f}^2\, ds \\
&\quad + \frac{1}{2c_8}\int_0^t \|\boldsymbol{f}^s(s)\|_{0,s}^2\, ds + \frac{c_8}{2}\int_0^t \|\boldsymbol{v}^{s,n}(s)\|_{0,s}^2\, ds \\
&\quad + \frac{1}{2c_9}\int_0^t \|\boldsymbol{h}(s)\|_{1/2,\Sigma}^2\, ds + \frac{c_9}{2}\int_0^t \left\|\overline{\boldsymbol{v}^n(s)}\right\|_{1/2,\Sigma}^2\, ds \\
&\quad + \frac{1}{2c_{10}}\int_0^t \|\boldsymbol{g}(s)\|_{1/2,\Sigma}^2\, ds + \frac{c_{10}}{2}\int_0^t \|[\![\boldsymbol{v}^n(s)]\!]\|_{1/2,\Sigma}^2\, ds \\
&\quad + \frac{1}{2c_{11}}\int_0^t \left\|\boldsymbol{g}_N^f(s)\right\|_{1/2,\Gamma_f^N}^2\, ds + \frac{c_{11}}{2}\int_0^t \left\|\boldsymbol{v}^{f,n}(s)\right\|_{1/2,\Gamma_f^N}^2\, ds \\
&\quad + \frac{1}{2}\left(\left\|\boldsymbol{v}_0^f\right\|_{0,f}^2 + \|\boldsymbol{v}_0^s\|_{0,s}^2 + \left(\sigma_s(\boldsymbol{u}_0^s), \varepsilon(\boldsymbol{u}_0^s)\right)_{0,s}\right)
\end{aligned} \tag{4.29}$$

Using the following trace and a Poincaré-type inequalities:

$$\|\boldsymbol{v}^{\boldsymbol{f},\boldsymbol{n}}\|_{1/2,\Gamma_f^N} \leq c_{12}\|\boldsymbol{v}^{\boldsymbol{f},\boldsymbol{n}}\|_{1,f} \text{ and } \|\boldsymbol{v}^{\boldsymbol{f},\boldsymbol{n}}\|_{0,f} \leq c_{13}\|\boldsymbol{v}^{\boldsymbol{f},\boldsymbol{n}}\|_{1,f}, \tag{4.30}$$

we get after summing the known terms in one term denoted by $F = F(f^f, f^s, g_N^f, h, g)$ and for a constant $C = C(c_7, c_8, c_9, c_{10}, c_{11}) > 0$

$$\begin{aligned}
&\frac{1}{2}\left(\left\|\boldsymbol{v}^{f,n}(t)\right\|_{0,f}^2 + \|\boldsymbol{v}^{s,n}(t)\|_{0,s}^2\right) + c_6\int_0^t \left\|\boldsymbol{v}^{f,n}(s)\right\|_{1,f}^2\, ds + \frac{1}{4}\left(\sigma_s(\boldsymbol{u}^{s,n}(t)), \varepsilon(\boldsymbol{u}^{s,n}(t))\right)_{0,s} \\
&+ \frac{c_5}{4}\|\boldsymbol{u}^{s,n}(t)\|_{1,s}^2 + \boldsymbol{M}_0\int_0^t \|\overline{\boldsymbol{v}^n(s)}\|_{1/2,\Sigma}^2\, ds + \boldsymbol{S}_0\int_0^t \|[\![\boldsymbol{v}^n(s)]\!]\|_{1/2,\Sigma}^2\, ds \\
&\leq \left(\frac{c_7c_{13} + c_{11}c_{12}}{2}\right)\int_0^t \left\|\boldsymbol{v}^{f,n}(s)\right\|_{1,f}^2\, ds + \frac{c_8}{2}\int_0^t \|\boldsymbol{v}^{s,n}(s)\|_{0,s}^2\, ds \\
&+ \frac{c_9}{2}\int_0^t \left\|\overline{\boldsymbol{v}^n(s)}\right\|_{1/2,\Sigma}^2\, ds + \frac{c_{10}}{2}\int_0^t \|[\![\boldsymbol{v}^n(s)]\!]\|_{1/2,\Sigma}^2\, ds \\
&+ \frac{1}{2}\left(\left\|\boldsymbol{v}_0^f\right\|_{0,f}^2 + \|\boldsymbol{v}_0^s\|_{0,s}^2 + \left(\sigma_s(\boldsymbol{u}_0^s), \varepsilon(\boldsymbol{u}_0^s)\right)_{0,s}\right) + C\int_0^t \boldsymbol{F}(\boldsymbol{f}^f, \boldsymbol{f}^s, \boldsymbol{g}_N^f, \boldsymbol{h}, \boldsymbol{g})(s)\, ds
\end{aligned} \tag{4.31}$$

We now absorb terms from the right-hand side into the left-hand side by comparing the

coefficients of the common integrals.

1. Absorbing the fluid dissipation term. We absorb the term

$$\left(\frac{c_7c_{13}+c_{11}c_{12}}{2}\right)\int_0^t \|\boldsymbol{v}^{f,n}(s)\|_{1,f}^2\,ds$$

into the left-hand side term

$$c_6\int_0^t \|\boldsymbol{v}^{f,n}(s)\|_{1,f}^2\,ds$$

which is possible if we choose the constants c_7 and c_{11} from Young's inequality to satisfy the inequality

$$\boxed{c_6 > \frac{c_7c_{13}+c_{11}c_{12}}{2}.}$$

2. Absorbing the interface mean and jump terms. We absorb

$$\frac{c_9}{2}\int_0^t \|\overline{\boldsymbol{v}^n(s)}\|_{1/2,\Sigma}^2\,ds \quad\text{and}\quad \frac{c_{10}}{2}\int_0^t \|[\![\boldsymbol{v}^n(s)]\!]\|_{1/2,\Sigma}^2\,ds,$$

repectively into

$$\boldsymbol{M}_0\int_0^t \|\overline{\boldsymbol{v}^n(s)}\|_{1/2,\Sigma}^2\,ds \quad\text{and}\quad \boldsymbol{S}_0\int_0^t \|[\![\boldsymbol{v}^n(s)]\!]\|_{1/2,\Sigma}^2\,ds,$$

provided that c_9 and c_{10} are chosen to verify

$$\boxed{\boldsymbol{M}_0 > \frac{c_9}{2}} \quad\text{and}\quad \boxed{\boldsymbol{S}_0 > \frac{c_{10}}{2}.}$$

3. Remaining terms. The remaining term

$$\frac{c_8}{2}\int_0^t \|\boldsymbol{v}^{s,n}(s)\|_{0,s}^2\,ds$$

cannot be absorbed and will be handled later using Grönwall's inequality.

We obtain the following absorbed inequality:

$$\begin{aligned}
&\frac{1}{2}\left(\|\boldsymbol{v}^{f,n}(t)\|_{0,f}^2+\|\boldsymbol{v}^{s,n}(t)\|_{0,s}^2\right)+\frac{c_5}{4}\|\boldsymbol{u}^{s,n}(t)\|_{1,s}^2+\frac{1}{4}\left(\sigma_s(\boldsymbol{u}^{s,n}(t)),\varepsilon(\boldsymbol{u}^{s,n}(t))\right)_{0,s}\\
&\quad+\int_0^t\|\boldsymbol{v}^{s,n}(s)\|_{1,s}^2\,ds+\theta_1\int_0^t\|\boldsymbol{v}^{f,n}(s)\|_{1,f}^2\,ds+\theta_2\int_0^t\|\overline{\boldsymbol{v}^n(s)}\|_{1/2,\Sigma}^2\,ds+\theta_3\int_0^t\|[\![\boldsymbol{v}^n(s)]\!]\|_{1/2,\Sigma}^2\,ds\\
&\leq\frac{1}{2}\left(\|\boldsymbol{v}_0^f\|_{0,f}^2+\|\boldsymbol{v}_0^s\|_{0,s}^2+(\sigma_s(\boldsymbol{u}_0^s),\varepsilon(\boldsymbol{u}_0^s))_{0,s}\right)+\frac{c_8}{2}\int_0^t\|\boldsymbol{v}^{s,n}(s)\|_{0,s}^2\,ds\\
&\quad+C\int_0^t\boldsymbol{F}(\boldsymbol{f}^f,\boldsymbol{f}^s,\boldsymbol{g}_N^f,\boldsymbol{h},\boldsymbol{g})(s)\,ds,
\end{aligned}\tag{4.32}$$

where:

$$\theta_1:=c_6-\frac{c_7c_{13}+c_{11}c_{12}}{2},\qquad\theta_2:=\boldsymbol{M}_0-\frac{c_9}{2},\qquad\theta_3:=\boldsymbol{S}_0-\frac{c_{10}}{2}.$$

We define the energy functional for every $n>0$:

$$\begin{aligned}
E^n(t):=&\|\boldsymbol{v}^{f,n}(t)\|_{0,f}^2+\|\boldsymbol{v}^{s,n}(t)\|_{0,s}^2+\|\boldsymbol{u}^{s,n}(t)\|_{1,s}^2+(\sigma_s(\boldsymbol{u}^{s,n}(t)),\varepsilon(\boldsymbol{u}^{s,n}(t)))_{0,s}\\
&+\int_0^t\left[\|\boldsymbol{v}^{f,n}(s)\|_{1,f}^2+\|\overline{\boldsymbol{v}^n(s)}\|_{1/2,\Sigma}^2+\|[\![\boldsymbol{v}^n(s)]\!]\|_{1/2,\Sigma}^2\right]ds.
\end{aligned}\tag{4.33}$$

This directly yields the inequality

$$\|\boldsymbol{v}^{s,n}(t)\|_{0,s}^2\leq E^n(t).\tag{4.34}$$

which gives

$$\int_0^t\|\boldsymbol{v}^{s,n}(t)\|_{0,s}^2\,ds\leq\int_0^t E^n(t)\,ds.\tag{4.35}$$

Using inequality (4.32) and (4.34), and noting that all terms on the left-hand side are non-negative, we obtain:

$$E^n(t)\leq C_0+\frac{c_8}{2}\int_0^t E^n(s)\,ds+\int_0^t F(s)\,ds,$$

where:

$$\begin{aligned}
C_0&:=\|\boldsymbol{v}_0^f\|_{0,f}^2+\|\boldsymbol{v}_0^s\|_{0,s}^2+(\sigma_s(\boldsymbol{u}_0^s),\varepsilon(\boldsymbol{u}_0^s))_{0,s},\\
F(s)&:=C\cdot\boldsymbol{F}(\boldsymbol{f}^f,\boldsymbol{f}^s,\boldsymbol{g}_N^f,\boldsymbol{h},\boldsymbol{g})(s).
\end{aligned}$$

We now apply Grönwall's inequality (theorem 1.10 Chap 1) to get:

$$\boxed{E^n(t)\leq\left(C_0+\int_0^t F(s)\,ds\right)\exp\left(\frac{c_8}{2}t\right).}$$

Therefore, the velocities and displacement satisfy the a priori bound:

$$\boxed{\begin{aligned}&\|\boldsymbol{v}^{f,n}(t)\|_{0,f}^2+\|\boldsymbol{v}^{s,n}(t)\|_{0,s}^2+\|\boldsymbol{u}^{s,n}(t)\|_{1,s}^2+(\sigma_s(\boldsymbol{u}^{s,n}(t)),\varepsilon(\boldsymbol{u}^{s,n}(t)))_{0,s}\\&+\int_0^t\left[\|\boldsymbol{v}^{f,n}(s)\|_{1,f}^2+\|\overline{\boldsymbol{v}^n(s)}\|_{1/2,\Sigma}^2+\|[\![\boldsymbol{v}^n(s)]\!]\|_{1/2,\Sigma}^2\right]ds.\\&\leq\left(\|\boldsymbol{v}_0^f\|_{0,f}^2+\|\boldsymbol{v}_0^s\|_{0,s}^2+(\sigma_s(\boldsymbol{u}_0^s),\varepsilon(\boldsymbol{u}_0^s))_{0,s}+\int_0^t F(s)\,ds\right)e^{\frac{c_8}{2}T}.\end{aligned}} \tag{4.36}$$

Let us now use the notation

$$M(t):=\int_0^t\boldsymbol{F}(s)\,ds,\quad\text{and}\quad C_0:=\|\boldsymbol{v}_0^f\|_{0,f}^2+\|\boldsymbol{v}_0^s\|_{0,s}^2+(\sigma_s(\boldsymbol{u}_0^s),\varepsilon(\boldsymbol{u}_0^s))_{0,s}+M(T).$$

We can deduce from inequality (4.36) some a priori bounds:

A priori bounds for $\boldsymbol{v}^{f,n}$:

$$\|\boldsymbol{v}^{f,n}(t)\|_{0,f}^2\leq C_0e^{\frac{c_8}{2}T}, \tag{4.37}$$

$$\int_0^T\|\boldsymbol{v}^{f,n}(t)\|_{0,f}^2\,ds\leq C_0Te^{\frac{c_8}{2}T}. \tag{4.38}$$

$$\int_0^t\|\boldsymbol{v}^{f,n}(t)\|_{1,f}^2\,ds\leq C_0e^{\frac{c_8}{2}T}. \tag{4.39}$$

A priori bounds for $u^{s,n}$ and $\boldsymbol{v}^{s,n}$:

$$\|\boldsymbol{u}^{s,n}(t)\|_{1,s}^2\leq C_0e^{\frac{c_8}{2}T}. \tag{4.40}$$

$$\|\boldsymbol{v}^{s,n}(t)\|_{0,s}^2\leq C_0e^{\frac{c_8}{2}T}. \tag{4.41}$$

$$\int_0^T\|\boldsymbol{v}^{s,n}(t)\|_{0,s}^2\,ds\leq C_0Te^{\frac{c_8}{2}T}. \tag{4.42}$$

A priori bound on the elastic potential energy:

$$(\sigma_s(\boldsymbol{u}^{s,n}(t)),\varepsilon(\boldsymbol{u}^{s,n}(t)))_{0,s}\leq C_0Te^{\frac{c_8}{2}T}. \tag{4.43}$$

The a priori estimates derived above yield the following regularity properties:

$$\begin{aligned}\boldsymbol{v}^{f,n}&\in L^\infty(0,T;L^2(\Omega_f))\cap L^2(0,T;V^f),\\\boldsymbol{v}^{s,n}&\in L^\infty(0,T;L^2(\Omega_s)),\\\boldsymbol{u}^{s,n}&\in L^\infty(0,T;V^s),\\\overline{\boldsymbol{v}^n},[\![\boldsymbol{v}^n]\!]&\in L^2(0,T;H^{1/2}(\Sigma)),\end{aligned} \tag{4.44}$$

Step 2: Passing to the limit in the linear terms From (4.41–4.42), $\boldsymbol{v}^{s,n}$ is uniformly bounded in $L^2(0,T;V_s)$. Hence, we can extract a subsequence (still denoted $\boldsymbol{v}^{s,n}$) such that

$$\boldsymbol{v}^{s,n} \rightharpoonup \boldsymbol{v}^s \quad \text{in } L^2(0,T;V_s).$$

To justify strong convergence results that are needed later, we invoke classical compactness results. First, the Rellich–Kondrachov theorem ensures that the embedding

$$H^1(\Omega) \hookrightarrow L^2(\Omega)$$

is compact for bounded Lipschitz domains. This implies that sequences bounded in $L^2(0,T;H^1(\Omega))$ may have subsequences that converge strongly in $L^2(0,T;L^2(\Omega))$.

In addition, the Aubin–Lions lemma states that if a sequence u_n is bounded in $L^2(0,T;H^1(\Omega))$ and $\partial_t u_n$ is bounded in $L^2(0,T;H^{-1}(\Omega))$, then (up to a subsequence) $u_n \to u$ strongly in $L^2(0,T;L^2(\Omega))$. These compactness results justify the strong convergence of $v_{s,n} \to v_s$ and $v_{f,n} \to v_f$ in $L^2(0,T;L^2)$, which is crucial for handling the nonlinear and interface terms in the limit.

This convergence implies the weak convergence of the time derivative:

$$\frac{d}{dt}(\boldsymbol{v}^{s,n}, \boldsymbol{\varphi}^s)_{0,s} \to \frac{d}{dt}(\boldsymbol{v}^s, \boldsymbol{\varphi}^s)_{0,s} \quad \text{in } H^{-1}(0,T),$$

for all $\boldsymbol{\varphi}^s \in V_s$ independent of time.

Moreover, we have

$$(\sigma_s(\boldsymbol{u}^{s,n}), \varepsilon(\boldsymbol{\varphi}))_{0,s} \to (\sigma_s(\boldsymbol{u}^s), \varepsilon(\boldsymbol{\varphi}))_{0,s} \quad \text{a.e. in } t,$$

for all $\boldsymbol{\varphi} \in V_s$.

On the other hand, from the uniform bound of $\boldsymbol{v}^{f,n}$ in $L^2(0,T;V_f)$, we can extract a subsequence $\boldsymbol{v}^{f,n} \rightharpoonup \boldsymbol{v}^f$ weakly in $L^2(0,T;V_f)$, which gives

$$(\varepsilon(\boldsymbol{v}^{f,n}), \varepsilon(\boldsymbol{\varphi}^f))_{0,f} \to (\varepsilon(\boldsymbol{v}^f), \varepsilon(\boldsymbol{\varphi}^f))_{0,f} \quad \text{a.e. in } t,$$

for all $\boldsymbol{\varphi}^f \in V_f$.

Step 3: Passing to the limit in the nonlinear term. As in [13], it remains to show that for all time-independent $\boldsymbol{\varphi}^f \in V_f$, we have

$$\int_{t_0}^{t} \left(B_n(\boldsymbol{v}^{f,n}) - B(\boldsymbol{v}^f), \boldsymbol{\varphi}^f\right)_{0,f} dt \to 0. \tag{4.45}$$

Let $D_n \equiv \{t \in (0,T);\ \|\boldsymbol{v}^{f,n}(t)\|_{1,f} \geq n\}$, and denote by $m(D_n)$ its Lebesgue measure.

We recall that there exists a constant $C \equiv C(\boldsymbol{v}_0^f, \boldsymbol{v}_0^s, \boldsymbol{f}^f, \boldsymbol{f}^s, \boldsymbol{g}_N^f, \boldsymbol{h}, \boldsymbol{g}, T) > 0$ such that

$$\int_{D_n} \|\boldsymbol{v}^{f,n}(s)\|_{1,f}^2 \, ds \leq C, \tag{4.46}$$

which implies

$$C \geq \int_{D_n} \|\boldsymbol{v}^{f,n}(s)\|_{1,f}^2 \, ds \geq m(D_n) \cdot n^2, \tag{4.47}$$

hence,

$$m(D_n) \leq \frac{C}{n^2}. \tag{4.48}$$

Step 4: Passing to the limit in the interface terms. We now verify the convergence of the interface terms. Since $v_{f,n} \to v_f$ weakly in $L^2(0,T;V_f)$ and $v_{s,n} \to v_s$ weakly in $L^2(0,T;V_s)$, and the trace operator $H^1(\Omega) \to H^{1/2}(\Sigma)$ is continuous, it follows that

$$v_{f,n}|_\Sigma \rightharpoonup v_f|_\Sigma, \quad v_{s,n}|_\Sigma \rightharpoonup v_s|_\Sigma \quad \text{in } L^2(0,T;H^{1/2}(\Sigma)^d).$$

Hence, the jumps and averages also converge weakly in $L^2(0,T;H^{1/2}(\Sigma)^d)$. Since the matrices $M(x)$, $S(x)$ are bounded and measurable with uniformly positive eigenvalues (see ellipticity condition (1.2)), the bilinear forms

$$\langle M\overline{v_n}, \overline{\varphi}\rangle_\Sigma, \quad \langle S[\![v_n]\!], [\![\varphi]\!]\rangle_\Sigma$$

are continuous in the weak topology of $L^2(0,T;H^{1/2}(\Sigma)^d)$. Therefore, for any test function $\varphi \in V$, we have

$$\langle Mv_n, \varphi\rangle_\Sigma \to \langle Mv, \varphi\rangle_\Sigma, \quad \langle S[\![v_n]\!], [\![\varphi]\!]\rangle_\Sigma \to \langle S[\![v]\!], [\![\varphi]\!]\rangle_\Sigma.$$

The source interface terms $\langle h, \varphi\rangle_\Sigma$ and $\langle g, [\![\varphi]\!]\rangle_\Sigma$ do not depend on n, and hence converge trivially. Thus, all interface contributions pass to the limit in the variational formulation.

With that established, the remainder of the proof follows exactly as in [13]. This completes the proof of the global existence of weak solutions. □

Theorem 4.3 (Uniqueness of solution for n=2)**.** *Let $\Omega_f, \Omega_s \subset \mathbb{R}^2$. The weak solution to the interaction problem (4.3a)–(4.3i) is unique.*

Proof. Given $(\boldsymbol{u}_0^s, \boldsymbol{v}_0^s, \boldsymbol{v}_0^f) \in V_s \times V_s \times V_f$.

Let (v_1^f, v_1^s) and (v_2^f, v_2^s) be two weak solutions of (P) with the same initial data.

We assume the existence of two solutions $(\boldsymbol{v}_1^s, \boldsymbol{v}_1^f), (\boldsymbol{v}_2^s, \boldsymbol{v}_2^f) \in V_s \times V_f$ of the weak form (4.22). Then $(\boldsymbol{v}^s, \boldsymbol{v}^f) = (\boldsymbol{v}_2^s - \boldsymbol{v}_1^s, \boldsymbol{v}_2^f - \boldsymbol{v}_1^f)$ satisfy, for all $\boldsymbol{\varphi}^f \in V_f, \boldsymbol{\varphi}^s \in V_s$, the following

$$\begin{aligned}&\left(\frac{\partial \boldsymbol{v}^f}{\partial t}, \boldsymbol{\varphi}^f\right)_{0,f} + \left(\frac{\partial \boldsymbol{v}^s}{\partial t}, \boldsymbol{\varphi}^s\right)_{0,s} + \left(\varepsilon(\boldsymbol{v}^f), \varepsilon(\boldsymbol{\varphi}^f)\right)_{0,f} + \left(\sigma_s\left(\boldsymbol{u}^s\right), \varepsilon(\boldsymbol{\varphi}^s)\right)_{0,s} \\ &+b\left(\boldsymbol{v}_2^f, \boldsymbol{v}_2^f, \boldsymbol{\varphi}^f\right) - b\left(\boldsymbol{v}_1^f, \boldsymbol{v}_1^f, \boldsymbol{\varphi}^f\right) + <\boldsymbol{M}\overline{\boldsymbol{v}}, \overline{\boldsymbol{\phi}}>_\Sigma + <\boldsymbol{S}[\![\boldsymbol{v}]\!], [\![\boldsymbol{\phi}]\!]>_\Sigma = 0\end{aligned} \tag{4.49}$$

By using the identity $\boldsymbol{v}_2^f = \boldsymbol{v}_1^f + \boldsymbol{v}^f$ and the bilinearity of b in its first two arguments, we manipulate the term $b(\boldsymbol{v}_2^f, \boldsymbol{v}_2^f, \boldsymbol{\varphi}^f)$ to get

$$\begin{aligned}b(\boldsymbol{v}_2^f, \boldsymbol{v}_2^f, \boldsymbol{\varphi}^f) &= b(\boldsymbol{v}_1^f + \boldsymbol{v}^f, \boldsymbol{v}_1^f + \boldsymbol{v}^f, \boldsymbol{\varphi}^f) \\ &= b(\boldsymbol{v}_1^f, \boldsymbol{v}_1^f + \boldsymbol{v}^f, \boldsymbol{\varphi}^f) + b(\boldsymbol{v}^f, \boldsymbol{v}_1^f + \boldsymbol{v}^f, \boldsymbol{\varphi}^f) \\ &= b(\boldsymbol{v}_1^f, \boldsymbol{v}_1^f, \boldsymbol{\varphi}^f) + b(\boldsymbol{v}_1^f, \boldsymbol{v}^f, \boldsymbol{\varphi}^f) + b(\boldsymbol{v}^f, \boldsymbol{v}_2^f, \boldsymbol{\varphi}^f).\end{aligned}$$

Subtracting the new expression of $b(\boldsymbol{v}_2^f, \boldsymbol{v}_2^f, \boldsymbol{\varphi}^f)$ into (4.49), we obtain:

$$\begin{aligned}&\left(\frac{\partial \boldsymbol{v}^f}{\partial t}, \boldsymbol{\varphi}^f\right)_{0,f} + \left(\frac{\partial \boldsymbol{v}^s}{\partial t}, \boldsymbol{\varphi}^s\right)_{0,s} + \left(\varepsilon(\boldsymbol{v}^f), \varepsilon(\boldsymbol{\varphi}^f)\right)_{0,f} + b\left(\boldsymbol{v}_1^f, \boldsymbol{v}^f, \boldsymbol{\varphi}^f\right) + b\left(\boldsymbol{v}^f, \boldsymbol{v}_2^f, \boldsymbol{\varphi}^f\right) \\ &\qquad + \left(\sigma_s\left(\boldsymbol{u}^s\right), \varepsilon(\boldsymbol{\varphi}^s)\right)_{0,s} + <\boldsymbol{M}\overline{\boldsymbol{v}}, \overline{\boldsymbol{\phi}}>_\Sigma + <\boldsymbol{S}[\![\boldsymbol{v}]\!], [\![\boldsymbol{\phi}]\!]>_\Sigma = 0\end{aligned} \tag{4.50}$$

Taking $\boldsymbol{\varphi}^f = \boldsymbol{v}^f$ and $\boldsymbol{\varphi}^s = \boldsymbol{v}^s$ and noting that $b(\boldsymbol{v}_1^f, \boldsymbol{v}^f, \boldsymbol{v}^f) = 0$ (because $\nabla \cdot \boldsymbol{v}_1^f = 0$) and dropping some positive terms due to the coercivity of M and S yields

$$\frac{1}{2}\frac{d}{dt}\|\boldsymbol{v}^f\|_{0,f}^2 + \frac{1}{2}\frac{d}{dt}\|\boldsymbol{v}^s\|_{0,s}^2 + \left(\varepsilon(\boldsymbol{v}^f), \varepsilon(\boldsymbol{v}^f)\right)_{0,f} + \left(\sigma_s\left(\boldsymbol{u}^s\right), \varepsilon(\boldsymbol{v}^s)\right)_{0,s} \leq -b\left(\boldsymbol{v}^f, \boldsymbol{v}_2^f, \boldsymbol{v}^f\right) \tag{4.51}$$

Now using properties of the trilinear form b in dimension $d = 2$ (see lemma 4.2), we bound the term $b\left(\boldsymbol{v}^f, \boldsymbol{v}_2^f, \boldsymbol{v}^f\right)$ as

$$\begin{aligned}\left|b\left(\boldsymbol{v}^f, \boldsymbol{v}_2^f, \boldsymbol{v}^f\right)\right| &\leq c_1\|\boldsymbol{v}^f\|_{1/2,f}\|\boldsymbol{v}_2^f\|_{1,f}\|\boldsymbol{v}^f\|_{1/2,f} + c_2\|\boldsymbol{v}^f\|_{1/2,f}\|\boldsymbol{v}_2^f\|_{3/4,f}\|\boldsymbol{v}^f\|_{3/4,f} \\ &\leq c_1\|\boldsymbol{v}^f\|_{0,f}\|\boldsymbol{v}^f\|_{1,f}\|\boldsymbol{v}_2^f\|_{1,f} + c_2\|\boldsymbol{v}^f\|_{0,f}^{3/4}\|\boldsymbol{v}^f\|_{1,f}^{5/4}\|\boldsymbol{v}_2^f\|_{1,f}^{3/4}\|\boldsymbol{v}_2^f\|_{0,f}^{1/4}\end{aligned} \tag{4.52}$$

Applying Young's inequality gives

$$\left|b\left(\boldsymbol{v}^f, \boldsymbol{v}_2^f, \boldsymbol{v}^f\right)\right| \leq 4c_1^2\|\boldsymbol{v}^f\|_{0,f}^2\|\boldsymbol{v}_2^f\|_{1,f}^2 + \frac{1}{2}\|\boldsymbol{v}^f\|_{1,f}^2 + 4^{3/5}c_2^{8/3}\|\boldsymbol{v}^f\|_{0,f}^2\|\boldsymbol{v}_2^f\|_{1,f}^2\|\boldsymbol{v}_2^f\|_{0,f}^{2/3} \tag{4.53}$$

Setting $y(t) = \|\boldsymbol{v}^f(t)\|_{0,f}^2 + \|\boldsymbol{v}^s(t)\|_{0,s}^2$, $K_1 = 4c_1^2$ and $K_2 = 4^{3/5}c_2^{8/3}$ and using the estimates

above, the inequality (4.51) becomes

$$\frac{1}{2}\|\boldsymbol{v}^f(t)\|^2_{0,f} + \frac{1}{2}\frac{d}{dt}y(t) \leq \|\boldsymbol{v}^f(t)\|^2_{0,f}\|\boldsymbol{v}^f_2(t)\|^2_{1,f}\left(K_1 + K_2\|\boldsymbol{v}^f_2(t)\|^{2/3}_{0,f}\right) \tag{4.54}$$

We drop the term $\|\boldsymbol{v}^f(t)\|^2_{0,f}$ and integrate in time

$$\begin{aligned} y(t) &\leq y(0) + \int_0^t \|\boldsymbol{v}^f(s)\|^2_{0,f}\|\boldsymbol{v}^f_2(s)\|^2_{1,f}\left(K_1 + K_2\|\boldsymbol{v}^f_2(s)\|^{2/3}_{0,f}\right) ds \\ &\leq y(0) + \int_0^t y(s)\|\boldsymbol{v}^f_2(s)\|^2_{1,f}\left(K_1 + K_2\|\boldsymbol{v}^f_2(s)\|^{2/3}_{0,f}\right) ds \end{aligned} \tag{4.55}$$

Finally, we apply Gronwall's inequality and use the boundedness of any weak solution $\boldsymbol{v}^f_2 \in L^2(0,T;V^f) \cup L^\infty(0,T;H)$:

$$y(t) \leq y(0)\ exp\left[\left(K_1 + K_2\|\boldsymbol{v}^f_2(s)\|^{2/3}_{L^\infty(0,T;H)}\right)\int_0^t \|\boldsymbol{v}^f_2(s)\|^2_{1,s}ds\right] \tag{4.56}$$

However, the initial condition $y(0) = \|\boldsymbol{v}^f(0,\cdot)\|^2_{0,f} + \|\boldsymbol{v}^s(0,\cdot)\|^2_{0,s}$ is identically null, and the right hand side of inequality (4.56) is finite. Hence, $y(t) = 0$ a.e. t, thus $(v^f, v^s) = 0$ meaning that $v^f_1 = v^f_2$ and $v^s_1 = v^s_2$, and uniqueness is acquired. □

Conclusion

This doctoral research has focused on the analysis, modeling, and numerical simulation of coupled elastic–fluid systems under *generalized interface conditions*, with an emphasis on finite–volume discretization. Starting from a rigorous functional framework, we established existence and stability results for elastic–elastic and fluid–structure interaction problems where the classical continuity of velocity and stress is replaced or complemented by matrix–valued impedance (Robin-type) interface laws. These results clarify the mathematical conditions that ensure well-posedness and energy balance when additional stiffness or damping effects are present at the interface.

On the computational side, we developed *finite volume schemes* that preserve local conservation, handle interface jump conditions, and reproduce the continuous energy estimates at the discrete level. Penalized formulations were introduced to simplify implementation and to prove convergence toward the exact coupled model. A series of *numerical experiments* confirmed the theoretical predictions, demonstrated the stability and accuracy of the proposed schemes, and illustrated how the choice of interface parameters influences the dynamic response of the coupled system.

Beyond their immediate mathematical interest, these contributions provide practical tools for simulating complex fluid–structure interactions where thin interfacial layers, imperfect contact, or stabilization requirements must be represented. The framework is versatile enough to accommodate a wide range of applications, from biomedical flows to engineering structures.

Several *perspectives for future work* naturally emerge:

- Extension to *nonlinear structural models* and *three-dimensional large-scale simulations*;
- Incorporation of *turbulent or high-Reynolds flows* and adaptive mesh refinement;
- Optimization of *Robin parameters* and development of efficient preconditioners for large coupled systems;
- Application of the methodology to *patient-specific hemodynamic problems* or to in-

dustrial FSI scenarios.

In conclusion, the thesis achieves its dual objective of advancing the *theoretical understanding* of generalized fluid–structure coupling and providing *robust numerical tools* for their simulation. It lays a foundation for further interdisciplinary research at the interface of applied mathematics, computational mechanics, and engineering practice.

Bibliography

[1] Allaire, G. (2005). *Analyse numérique et optimisation: Une introduction à la modélisation mathématique et à la simulation numérique* (2nd ed.). Éditions École Polytechnique.

[2] Angot, P., & Latché, J. C. (2009). Vector penalty-projection methods for the solution of unsteady incompressible flows. *International Journal on Finite Volumes*.

[3] Angot, P. (2010). A fictitious domain model for the Stokes/Brinkman problem with jump embedded boundary conditions. *Comptes Rendus de l'Académie des Sciences – Série I, Mathématiques*, 348(11–12), 697–702.

[4] Angot, P. (2011). On the well-posed coupling between free fluid and porous viscous flows. *Applied Mathematics Letters*, 24(6), 803–810.

[5] Angot, P., Caltagirone, J. P., & Fabrie, P. (2012). A new fast method to compute saddle-points in constrained optimization and applications. *Journal of Applied Mathematics*, 25, 245–351.

[6] Angot, P., Caltagirone, J. P., & Fabrie, P. (2012). A fast vector penalty-projection method for incompressible non-homogeneous or multiphase Navier–Stokes problems. *Applied Mathematics Letters*, 25, 1681–1688.

[7] Angot, P., Caltagirone, J. P., & Fabrie, P. (2016). A kinematic vector penalty-projection method for incompressible flow with variable density. *Comptes Rendus de l'Académie des Sciences – Série I, Mathématiques*, 354(11), 1124–1131.

[8] Armero, F., & Simo, J. C. (1996). Long-term dissipativity of time-stepping algorithms for an abstract evolution equation. *Computer Methods in Applied Mechanics and Engineering*, 131, 41–90.

[9] Badia, S., Nobile, F., & Vergara, C. (2009). Robin–Robin preconditioned Krylov methods for fluid–structure interaction problems. *Computer Methods in Applied Mechanics and Engineering*, 198(33–36), 2768–2784.

[10] Badia, S., Quaini, A., & Quarteroni, A. (2014). Splitting methods based on algebraic factorization for fluid–structure interaction. *SIAM Journal on Scientific Computing*, 36(2), A491–A515.

[11] Baker, G. A. (1976). Galerkin approximations for the Navier–Stokes equations. Technical Report, Harvard University.

[12] Bali, R., & Awasthi, U. (2011). Mathematical model of blood flow in small blood vessel in the presence of magnetic field. *Applied Mathematics*, 2, 264–269.

[13] Barbu, V., Grujić, Z., Lasiecka, I., & Tuffaha, A. (2007). Existence of the energy-level weak solutions for a nonlinear fluid-structure interaction model. In F. Botelho, T. Hagen, & J. Jamison (Eds.), *Contemporary Mathematics* (Vol. 440, pp. 55–82). American Mathematical Society.

[14] Bazilevs, Y., Calo, V. M., Zhang, Y., & Hughes, T. J. R. (2006). Isogeometric fluid–structure interaction analysis with applications to arterial blood flow. *Computational Mechanics*, 38, 310–322.

[15] Bazilevs, Y., Hsu, M., Kiendl, J., Wüchner, R., & Bletzinger, K. (2011). 3D simulation of wind turbine rotors at full scale. Part II: Fluid–structure interaction modeling with composite blades. *International Journal for Numerical Methods in Fluids*, 65, 236–253.

[16] Bergmann, M., Martin, L., & Serre, E. (2009). A finite-volume method for the simulation of fluid–structure interaction problems. *Journal of Computational Physics*, 228(16), 6316–6332.

[17] Bergmann, M., Fondanèche, A., & Iollo, A. (2022). An Eulerian finite-volume approach of fluid-structure interaction problems on quadtree meshes. *Journal of Computational Physics*, 471, 111647.

[18] Boffi, D., & Gastaldi, L. (2021). On the existence and uniqueness of the solution to a fluid–structure interaction problem. *Journal of Differential Equations*, 279, 136–161.

[19] Boukabache, A., & Kechkar, N. (2019). A unified stabilized finite volume method for Stokes and Darcy equations. *Journal of the Korean Mathematical Society*, 56(4), 1083–1112.

[20] Boukabache, A. (2022). A locally stabilized collocated finite volume method for the stationary Stokes problem. *Mathematical Methods in the Applied Sciences*, 45(17), 11714–11735. https://doi.org/10.1002/mma.8476

[21] Boyer, F., & Fabrie, P. (2012). *Mathematical tools for the study of the incompressible Navier–Stokes equations and related models*. Springer.

[22] Brézis, H. (1973). *Opérateurs maximaux monotones et semi-groupes de contractions dans les espaces de Hilbert*, North-Holland, Amsterdam.

[23] Brézis, H. (1983). *Analyse fonctionnelle: Théorie et applications*. Paris: Dunod.

[24] Brézis, H. (2011). *Functional Analysis, Sobolev Spaces and Partial Differential Equations*, Universitext, Springer, New York.

[25] Causin, P., Gerbeau, J. F., & Nobile, F. (2005). Added-mass effect in the design of partitioned algorithms for fluid–structure problems. *Computer Methods in Applied Mechanics and Engineering*, 194(42–44), 4506–4527.

[26] Cembranos, P., & Mendoza, J. (1997). *Banach spaces of vector-valued functions*. Lecture Notes in Mathematics (Vol. 1676). Springer.

[27] Chaskalovic, J. (2014). *Mathematical and numerical methods for partial differential equations: Applications for engineering sciences*. Springer.

[28] Chénier, E., Eymard, R., Herbin, R., & Touazi, O. (2008). Collocated finite volume schemes for the simulation of natural convective flows on unstructured meshes. *International Journal for Numerical Methods in Fluids*, 56(11), 2045–2068.

[29] Chouly, F., Van Hirtum, A., Lagrée, P. Y., Paoli, J. R., Pelorson, X., & Payan, Y. (2006). Simulation of the retroglossal fluid-structure interaction during obstructive sleep apnea. In M. Harders & G. Székely (Eds.), *Biomedical Simulation* (Vol. 4072, pp. 48–57). Springer.

[30] Ciarlet, P. G. (1988). *Mathematical elasticity, Vol. 1: Three-dimensional elasticity*. North-Holland.

[31] Ciarlet, P. G. (1997). *Mathematical elasticity, Vol. 2: Theory of plates*. Elsevier.

[32] Ciarlet, P. G. (2000). *Mathematical elasticity, Vol. 3: Theory of shells*. Elsevier.

[33] Constantin, P., & Foiaş, C. (1989). *Navier–Stokes equations*. University of Chicago Press.

[34] Crandall, M. G., & Liggett, T. M. (1971). Generation of Semi-Groups of Nonlinear Transformations on General Banach Spaces. American Journal of Mathematics, 93(2), 265–298.

[35] Evans, L. C. (2010). *Partial differential equations* (2nd ed.). American Mathematical Society.

[36] Ciarlet, P. G., & Lions, J. L. (Eds.). (1990). *Handbook of numerical analysis* (Vol. 11). Gulf Professional Publishing.

[37] Farhat, C., Geuzaine, P., Grandmont, C. (2001). The discrete geometric conservation law and the nonlinear stability of ALE schemes for the solution of flow problems on moving grids. *Journal of Computational Physics*, 174, 669–694.

[38] Fernández, M. A., Moubachir, M. (2005). A Newton method using exact Jacobians for solving fluid–structure coupling. *Computers & Structures*, 83(2–3), 127–142.

[39] Fortin, M., Glowinski, R. (1983). *Augmented Lagrangian methods: Applications to the numerical solution of boundary-value problems*. Elsevier Science Publishers B.V., North-Holland.

[40] Formaggia, L., Quarteroni, A., Veneziani, A. (Eds.). (2010). *Cardiovascular mathematics: Modeling and simulation of the circulatory system*. Springer.

[41] Galdi, G. P. (2014). *Fluid–structure interaction and biomedical applications*. Advances in Mathematical Fluid Mechanics Series. Springer Basel AG.

[42] Gerbeau, J.-F., Vidrascu, M. (2003). A quasi-Newton algorithm based on a reduced model for fluid–structure interaction problems in blood flows. *Mathematical Modelling and Numerical Analysis*, 37(4), 631–647.

[43] Girault, V., Raviart, P.-A. (1979). *Finite element approximation of the Navier–Stokes equations*. Springer-Verlag.

[44] Girault, V., Raviart, P.-A. (1986). *Finite element methods for Navier–Stokes equations: Theory and algorithms*. Springer Series in Computational Mathematics. Springer-Verlag.

[45] Gotoh, H., Khayyer, A. (2018). On the state of the art of particle methods for coastal and ocean engineering. *Coastal Engineering Journal*, 60, 79–103.

[46] Griffith, B. E. (2020). Immersed boundary methods. *Annual Review of Fluid Mechanics*, 52, 421–448.

[47] Hamdan, F. H., Dowling, P. J. (1995). Fluid–structure interaction: Application to structures in an acoustic fluid medium. Part 2: Literature review on near-field and far-field fluid formulations. *Engineering Computations*, 12, 759–772.

[48] He, Y. (2003). Two-level method based on finite element and Crank–Nicolson extrapolation for the time-dependent Navier–Stokes equations. *SIAM Journal on Numerical Analysis*, 41, 1263–1285.

[49] Jasak, H., Weller, H. G. (2000). Application of the finite volume method and unstructured meshes to linear elasticity. *International Journal for Numerical Methods in Engineering*, 48(2), 267–287.

[50] Kara, M., Mesbahi, S., Angot, P. (2021). The fictitious domain method with sharp interface for elasticity systems with general jump embedded boundary conditions. *Advances in Applied Mathematics and Mechanics*, 13, 119–139.

[51] Kausel, E. (2010). Early history of soil–structure interaction. *Soil Dynamics and Earthquake Engineering*, 30(9), 822–832.

[52] Kechkar, N., Louaar, M. (2022). Stabilized–penalized collocated finite volume scheme for incompressible biofluid flows. *Journal of the Korean Mathematical Society*, 59(3), 519–548.

[53] Kuan, J., Tawri, K. (2024). Existence of weak martingale solutions to a stochastic fluid–structure interaction problem with a compressible viscous fluid. *arXiv preprint arXiv:2409.16513 [math.AP]*.

[54] Kukavica, I., Tuffaha, A., and Ziane, M. (2009). Strong solutions to a nonlinear fluid–structure interaction system. Journal of Differential Equations, 247(5), 1452–1478. https://doi.org/10.1016/j.jde.2009.05.012

[55] Kukavica, I., Tuffaha, A., and Ziane, M. (2011). Strong solutions to a Navier–Stokes–Lamé system on a domain with a non-flat boundary. Nonlinearity, 24(1), 159–176. https://doi.org/10.1088/0951-7715/24/1/009

[56] Landau, L. D., Lifshitz, E. M. (1986). *Theory of elasticity* (Vol. 7). Pergamon Press.

[57] Layton, W., Labovschii, A., Manica, C. C., Neda, M., Rebholz, L. (2006). The stabilized, extrapolated trapezoidal–Galerkin finite element method. Technical Report, Department of Mathematics, University of Pittsburgh.

[58] Layton, W. (2008). *Introduction to the numerical analysis of incompressible viscous flows*. Society for Industrial and Applied Mathematics.

[59] Leal, L. G. (2007). *Advanced transport phenomena: Fluid mechanics and convective transport processes*. Cambridge University Press.

[60] Leung, J. H., Wright, A. R., Cheshire, N., Crane, J., Thom, S. A., Hughes, A. D., Xu, Y. (2006). Fluid–structure interaction of patient-specific abdominal aortic aneurysms: A comparison with solid stress models. *BioMedical Engineering OnLine*, 5(33).

[61] Lions, J. L., Magenes, E. (1961). Problèmes aux limites non homogènes. II. *Annales de l'Institut Fourier*, 11, 137–178.

[62] Lions, J. L. (1969). *Quelques méthodes de résolution des problèmes aux limites non linéaires*. Dunod, Gauthier-Villars.

[63] Lions, J. L., Magenes, E., Kenneth, P. (1972). *Non-homogeneous boundary value problems and applications*. Springer.

[64] Lopes, D. S., Silva, L., & Sequeira, R. (2016). Comparison of finite element and finite volume methods for fluid–structure interaction problems. *Computational Methods in Applied Sciences*, *41*, 275–294.

[65] Mannes, Y. (2024). *Derivation, mathematical and numerical analysis of models for blood flow in arteries*. General Mathematics. Université de Toulon. English. ffNNT : 2024TOUL0006ff. fftel-05004495.

[66] Marsden, J. E., Hughes, T. J. R. (1983). *Mathematical foundations of elasticity*. Prentice-Hall, New Jersey.

[67] Martínez-Ferrer, D., Aguado-Sierra, J., Vázquez, M. (2018). A finite volume solver for fluid–structure interaction in cardiovascular flows. *Journal of Computational Physics*, 374, 512–535.

[68] Medvedev, A. E., Fomin, V. M., Samsonov, V. I. (2012). Mathematical modeling of the blood flow in blood vessels. *Circulatory System and Arterial Hypertension: Experimental Investigation, Mathematical and Computer Simulation*, 55–114.

[69] Mitra, S. (2020). Local existence of strong solutions of a fluid–structure interaction model. *Journal of Mathematical Fluid Mechanics*, 22, 60.

[70] Moubachir, M. (2006). *Moving shape analysis and control: Applications to fluid–structure interactions*. Monographs and Textbooks in Pure and Applied Mathematics, Vol. 277. Chapman & Hall/CRC.

[71] Moukalled, F., Mangani, L., Darwish, M. (2016). *The finite volume method in computational fluid dynamics*. Springer, Cham.

[72] Muha, B., Canić, S. (2013). Existence of a weak solution to a nonlinear fluid–structure interaction problem modeling the flow of an incompressible, viscous fluid in a cylinder with deformable walls. *Archive for Rational Mechanics and Analysis*, 207, 919–968.

[73] Muha, B., Canić, S. (2015). Existence of a weak solution to a fluid–elastic structure interaction problem with the Navier slip boundary condition. *arXiv preprint arXiv:1505.04462 [math.AP].*

[74] Nicaise, S. (2000). *Analyse numérique et équations aux dérivées partielles: Cours et problèmes résolus.* Sciences SUP. Mathématiques, Dunod.

[75] Nobile, F., Vergara, C. (2008). An effective fluid–structure interaction formulation for vascular dynamics by generalized Robin conditions. *SIAM Journal on Scientific Computing*, 30(2), 731–763.

[76] Peskin, C. S. (1972). Flow patterns around heart valves: A numerical method. *Journal of Computational Physics*, 10, 252–271.

[77] Pramanik, S. (2024). Computational methods for fluid–structure interaction in biology: A review. *Biomechanics and Modeling in Mechanobiology*, 23(2), 305–329.

[78] Quarteroni, A., Tuveri, M., Veneziani, A. (2009). Computational vascular fluid–structure interaction: Problems, models and methods. *Computers & Visualization in Science*, 11, 227–239.

[79] Quarteroni, A., Manzoni, A., Negri, F. (2017). *Reduced basis methods for partial differential equations: An introduction.* Springer.

[80] Ramière, I., Angot, P., Belliard, M. (2007a). A fictitious domain approach with spread interface for elliptic problems with general boundary conditions. *Computer Methods in Applied Mechanics and Engineering*, 196(4–6), 766–781.

[81] Ramière, I., Angot, P., Belliard, M. (2007b). A general fictitious domain method with immersed jumps and multilevel nested structured meshes. *Journal of Computational Physics*, 225(2), 1347–1387.

[82] Rudin, W. (1976). *Principles of mathematical analysis* (3rd ed.). McGraw–Hill.

[83] Showalter, R. E. (1997). *Monotone Operators in Banach Space and Nonlinear Partial Differential Equations*, Mathematical Surveys and Monographs, Vol. 49, American Mathematical Society, Providence, RI.

[84] Sigrist, J. F. (2015). *Fluid–structure interaction: An introduction to finite element coupling*. New York Academy of Sciences Series. John Wiley & Sons.

[85] Simo, J. C., Armero, F., Taylor, C. A. (1995). Stable and time-dissipative finite element methods for incompressible Navier–Stokes equations in advection dominated flows. *International Journal for Numerical Methods in Engineering*, 39, 1475–1506.

[86] Temam, R. (1977). *Navier–Stokes equations: Theory and numerical analysis*. North-Holland, New York.

[87] Temam, R. (1995). *Navier–Stokes equations: Theory and numerical analysis*. AMS Chelsea Publishing.

[88] Temam, R. (2010). *Navier–Stokes equations: Theory and numerical analysis*. Studies in Mathematics and Its Applications, Vol. 2. North-Holland.

[89] Tewodros, Y. Y., Chen, F., Faller, K. R., Kim, S., Stolle, C. S. (2024). Simulating dynamic thin-walled structure–soil interaction under vehicular impacts using coupled FEM–ALE approach. *Engineering Structures*, 316, 118588.

[90] Tewodros, Y. Y., Fang, C., Faller, R. K., Kim, S., Alomari, Q. A., Bahar, M. A., Kumar, G. S. (2025). A review of soil constitutive models for simulating dynamic soil–structure interaction processes under impact loading. *Geotechnics*, 5(2), 40.

[91] Tezduyar, T. E. (2018). *Frontiers in computational fluid–structure interaction and flow simulation: Research from lead investigators under forty*. Modeling and Simulation in Science, Engineering and Technology. Springer International Publishing.

[92] Trimarchi, D., Turnock, S. R., Chapelle, D., Taunton, D. (2009). Fluid–structure interactions of anisotropic thin composite materials for application to sail aerodynamics of a yacht in waves. In *Proceedings of the 12th Numerical Towing Tank Symposium*, Cortona, Italy, 6 pp.

[93] Trifunović, S., Wang, Y. G. (2020). Existence of a weak solution to the fluid–structure interaction problem in 3D. *Journal of Differential Equations*, 268, 1495–1531.

[94] Vassilevski, Y., Simakov, S., Salamatova, V., Ivanov, Y., Dobroserdova, T. (2011). Vessel wall models for simulation of atherosclerotic vascular networks. *Mathematical Modelling of Natural Phenomena*, 6(7), 82–99.

[95] Woods, B. K. S., Dayyani, I., Friswell, M. I. (2015). Fluid/structure–interaction analysis of the Fish-Bone Active-Camber morphing concept. *Journal of Aircraft*, 52, 307–319.

[96] Xu, D., Kaliviotis, E., Munjiza, A., Avital, E., Ji, C., Williams, J. (2013). Large-scale simulation of red blood cell aggregation in shear flows. *Journal of Biomechanics*, 46, 1810–1817.

[97] Zhang, H., Liu, L., Dong, M., Sun, H. (2013). Analysis of wind-induced vibration of fluid–structure interaction system for isolated aqueduct bridge. *Engineering Structures*, 46, 28–37.

ملخص

تتناول هذه الأطروحة دراسة مسائل التفاعل المرن–المرن والتفاعل بين المائع والبنية في إطار شروط واجهة معمّمة تتجاوز القوانين الكلاسيكية للاستمرارية والتوازن. تم تطوير إطار وظيفي صارم يتيح صياغات ضعيفة وإثبات نتائج الوجود والاستقرار للأنظمة التي تتضمن قوانين اقتران تحتوي على تأثيرات الممانعة أو الصلابة أو التخميد من خلال مؤثرات معرفة موجبة. تؤدي هذه الحدود الإضافية إلى تعديل التوازن الطاقي الطبيعي وتفرض شروطاًا جديدة لضمان حسن الوضعية الرياضية. من الناحية العددية، تم تصميم مخططات تعتمد على طريقة الحجوم المنتهية على شبكات مقبولة، مع إيلاء اهتمام خاص بالمعالجة المحافظة والمستقرة لشروط الواجهة. كما تم اعتماد تقنيات العقوبة لفرض شروط الواجهة المعمّمة، وأُثبت تقارب الحلول إلى النموذج الأصلي. وقد تم التحقق من النتائج النظرية عبر مجموعة من التجارب العددية التي أكدت التقارب، وأبرزت تأثير معاملات الواجهة، وكشفت دور الاقتران المعمّم في الاستجابة الديناميكية. بوجه عام، تربط هذه الأطروحة بين التحليل الرياضي الصارم والأساليب العددية الفعّالة، وتقترح إطاراً موحداً لتحليل ومحاكاة الأنظمة المقترنة المعقدة.

كلمات مفتاحية: ميكانيك الموائع ،التفاعل بين المائع والبنية، طريقة الحجوم المنتهية، ميكانيك الأوساط المتصلة، مسائل التفاعل.

Abstract

This thesis investigates elastic–elastic and fluid–structure interaction (FSI) problems under generalized interface conditions that extend beyond classical continuity and balance laws. The work develops a rigorous functional framework, establishing weak formulations, existence, and stability results for systems where coupling laws incorporate impedance, stiffness, or damping effects through positive definite operators. These additional terms modify the natural energy balance and lead to new conditions for well-posedness. On the computational side, finite volume schemes are designed on admissible meshes, with particular attention to conservative and stable treatment of interface terms. Penalization techniques are introduced to enforce generalized interface laws, and convergence to the original model is demonstrated. Theoretical findings are validated through a set of numerical experiments, which confirm convergence, illustrate the influence of interface parameters, and highlight the role of generalized coupling in dynamic responses. Overall, the thesis bridges rigorous mathematical analysis with efficient numerical strategies, offering a unified framework for analyzing and simulating complex coupled systems.
Keywords: Fluid Mechanics, Fluid–Structure Interaction, FVM (Finite Volume Method), Continuum Mechanics, Interaction Problems.

Résumé

Cette thèse étudie les problèmes d'interaction élastique–élastique et fluide–structure (FSI) dans le cadre de conditions d'interface généralisées qui vont au-delà des lois classiques de continuité et d'équilibre. Un cadre fonctionnel rigoureux est développé, permettant d'établir des formulations faibles, ainsi que des résultats d'existence et de stabilité pour des systèmes où les lois de couplage intègrent des effets d'impédance, de raideur ou d'amortissement via des opérateurs définis positifs. Ces termes supplémentaires modifient l'équilibre énergétique naturel et conduisent à de nouvelles conditions de bien-posé. Sur le plan numérique, des schémas volumes finis sont conçus sur des maillages admissibles, en accordant une attention particulière au traitement conservatif et stable des conditions d'interface. Des techniques de pénalisation sont introduites pour imposer les lois d'interface généralisées, et la convergence vers le modèle original est démontrée. Les résultats théoriques sont validés à travers une série d'expériences numériques, qui confirment la convergence, illustrent l'influence des paramètres d'interface et mettent en évidence le rôle du couplage généralisé dans la réponse dynamique. Globalement, cette thèse établit un lien entre analyse mathématique rigoureuse et méthodes numériques efficaces, et propose un cadre unifié pour l'analyse et la simulation de systèmes couplés complexes.
Mots Clée : Interaction fluide–structure (FSI), Interaction élastique–élastique, Formulation faible, Méthode des volumes finis, Estimations d'énergie.